Static and dynamic properties of attractive spheres. A numerical study

Sujin Babu

▶ **To cite this version:**

Sujin Babu. Static and dynamic properties of attractive spheres. A numerical study. Condensed Matter [cond-mat]. Université du Maine, 2008. English. NNT : . tel-00379956

HAL Id: tel-00379956
https://theses.hal.science/tel-00379956

Submitted on 29 Apr 2009

HAL is a multi-disciplinary open access archive for the deposit and dissemination of scientific research documents, whether they are published or not. The documents may come from teaching and research institutions in France or abroad, or from public or private research centers.

L'archive ouverte pluridisciplinaire **HAL**, est destinée au dépôt et à la diffusion de documents scientifiques de niveau recherche, publiés ou non, émanant des établissements d'enseignement et de recherche français ou étrangers, des laboratoires publics ou privés.

Propriétés statiques et dynamiques de sphères dures attractives. Etude par simulation numérique

THÈSE

présentée le 22/01/2008

pour l'obtention du

Doctorat de l'Université du Maine - Le Mans
(Spécialité Chimie et Physico-chimie des polymères)

par

Sujin BABU

Composition du jury

Monsieur Walter KOB : Université Montpellier II,	Rapporteur
Monsieur Piero TARTAGLIA : Università di Roma,	Rapporteur
Monsieur Antonio CONIGLIO : Università di Napoli Federico II,	Examinateur
Monsieur Julian OBERDISSE : Université Montpellier II,	Examinateur
Monsieur Taco NICOLAI : Université du Maine,	Directeur de thèse
Monsieur Jean-Christophe GIMEL : Université du Maine,	Directeur de thèse

Contents

1 Introduction **1**
1.1 Outline of the thesis 6

2 Overview of the structure and the dynamics of attractive spheres. **9**
2.1 Random hard spheres 11
2.2 Irreversible aggregation 12
2.2.1 Structure 12
2.2.2 Kinetics 14
2.2.3 Tracer diffusion 15
2.3 Reversible aggregation 17
2.3.1 Structure 17
2.3.2 Dynamics 19

3 Simulation Method **23**
3.1 Brownian cluster dynamics (BCD) 25
3.1.1 Random distribution of hard spheres 25
3.2 BCD and Thermodynamics 27
3.3 Square well potential (SW) 28
3.4 How does it work? 29
3.4.1 How do we represent space in computer? 29
3.4.2 Periodic boundary conditions 31
3.4.3 What does a monomer know? 32
3.4.4 What does a cluster know? 33
3.4.5 Cluster construction 34
3.4.6 Movement of spheres 34

4 Structure and kinetics of reversibily aggregating spheres with rigid bonds **39**
4.1 Flocculation and percolation in reversible cluster-cluster aggregation . 41
4.1.1 Introduction 42
4.1.2 Simulation method 43
4.1.3 Encounter versus collision 43
4.1.4 Flocculation 45

4.1.5 Percolation . . . 50
4.1.6 Conclusion . . . 56
4.1.7 Appendix 1 . . . 56
4.1.8 Appendix 2 . . . 56
4.2 Phase separation and percolation of reversibly aggregating spheres with a square-well attraction potential . . . 58
4.2.1 Introduction . . . 59
4.2.2 Simulation method . . . 61
4.2.3 Results and discussion . . . 63
4.2.4 Summary . . . 77

5 Self diffusion of reversibily aggregating spheres with rigid bonds 79
5.1 Self diffusion of reversibly aggregating spheres . . . 81
5.1.1 Introduction . . . 82
5.1.2 Simulation method . . . 84
5.1.3 Results . . . 85
5.1.4 Discussion . . . 92
5.1.5 Conclusion . . . 95

6 The influence of bond-rigidity and cluster diffusion on the self-diffusion of hard spheres with square-well interaction. 97
6.1 The influence of bond-rigidity and cluster diffusion on the self-diffusion of hard spheres with square-well interaction. . . . 99
6.1.1 Introduction . . . 100
6.1.2 Simulation method . . . 101
6.1.3 Results and discussion . . . 103
6.1.4 Summary . . . 110

7 Diffusion limited cluster aggregation with irreversible flexible bonds 111
7.1 Diffusion limited cluster aggregation with irreversible flexible bonds . 113
7.1.1 Introduction . . . 114
7.1.2 Simulation method . . . 115
7.1.3 Results . . . 115
7.1.4 Discussion . . . 129
7.1.5 Conclusion . . . 133

8 Tracer diffusion in colloidal gels 135
8.1 Tracer diffusion in colloidal gels . . . 137
8.1.1 Introduction . . . 138
8.1.2 Simulation method . . . 139
8.1.3 Results and discussion . . . 139
8.1.4 Conclusion . . . 148

9 Conclusion **151**

Acknowledgements

I am obliged to both my thesis advisors Taco Nicolai and Jean-Christophe Gimel for their guidance and continues encouragement during the time of my research. The results presented here would not have been possible without their expertise.

I would like to thank Physics department of University of La Sapienza Roma especially Francesco Sciortino for the discussions we had during my short stay in Rome. Special thanks goes to Cristaino De Michele for sharing his EDBD codes with me.

I would also like to thank the Marie Curie network On Dynamical arrest (MRTN-CT-2003-504712) for the financial support.

I would also like to thank everybody in my lab for providing me with a wonderful working enviroment and also for all the jokes at the coffee. Special thanks goes to C. Chassenieux for teaching me *How to prepare real French coffee*.

Most of all I would like to thank my family who has always supported me during the good and bad times.

Chapter 1

Introduction

Generally, matter exists in three forms: solid, liquid and gas although plasma is believed to be the fourth state of matter. Colloidal systems have attracted a lot of interest as models for the liquid. Colloidal suspensions consist of particles of sizes between $10nm - 10\mu m$ suspended in a liquid. Colloids are orders of magnitude bigger than atoms and molecules and may exhibit different behavior due to their large size. Their structural relaxation times are large, typically of the order of seconds. They are weak mechanically, and colloidal solids can be shear melted to form a metastable fluid just by shaking. Resolidification may take minutes hours or days giving time to study the crystallization and the meta stable liquid. The spatial scale of the colloids is comparable to the wavelength of light making light scattering an important tool to investigate the structure and dynamics of such systems. The interaction between colloidal particles can be tailored, by various means such as addition of free polymers or modification of the surface coating of the particles. These features allow one to perform experiments with colloidal systems which are not possible with atomistic systems.

Attractive particles diffuse through Brownian motion before they aggregate into clusters. If the attraction is very strong the aggregation process is irreversible. The clusters formed by aggregation are usually fractals as was observed experimentally for example for colloids [1] or proteins [2]. Fractal aggregates were simulated by Kolb et. al [3] and Meakin [4] using a cluster-cluster aggregation model called diffusion limited cluster aggregation (DLCA). Weitz et. al [1] showed that the DLCA model can indeed be used to explain the structure of real particle aggregates, in their case aggregated colloidal gold. Fig.(1.1) shows the structure formed by diffusion limited cluster aggregation (DLCA) from simulations and a aggregate formed by gold colloids. Another aggregation model is reaction limited cluster aggregation (RLCA) where the sticking probability at a collision goes to zero. Real systems are often closer to RLCA (slow aggregation) than DLCA (fast aggregation), but it is very difficult to simulate RLCA at low volume fraction because very long times are needed to form big clusters. Both simulations and experiments have shown that structures formed by both types of aggregation are fractals and have a very broad cluster size distribution. This will be discussed in more detail in *chapter* 2. The aggregates formed by RLCA are denser

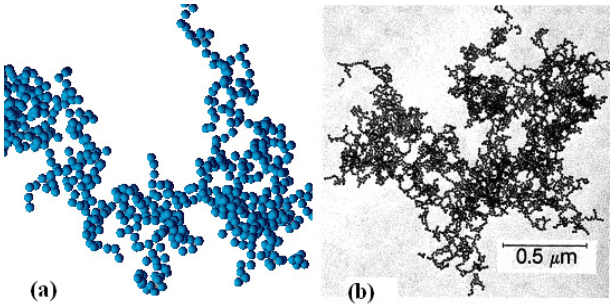

Figure 1.1: Example of DLCA clusters obtained (a) from an off-lattice computer simulation (present work), (b) from aggregation of gold colloids.

than the aggregates formed by DLCA as is apparent from fig(1.2).

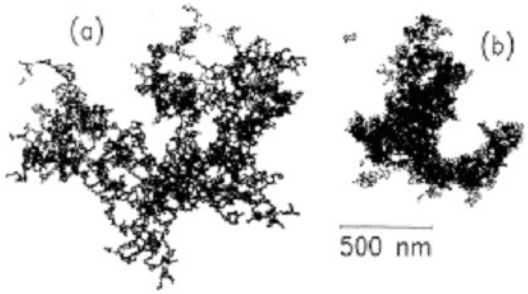

Figure 1.2: Gold colloid aggregates (a) DLCA, (b) RLCA obtained from experiments [1]

When the clusters start to inter penetrate their fractal dimension changes. After a cross-over the structure, cluster size distribution and fractal dimension is very well explained by the percolation model. The aggregation proceeds toward a point where a single cluster spans the whole space a phenomena referred to as gelation. Aggregates have a local structure determined by the initial stage of DLCA or RLCA and a large scale structure determined by the percolation process.

Reversible aggregation results in the formation of transient clusters, a phase separated system or a transient percolating cluster depending on the strength and range of attraction. A schematic diagram of these systems is shown in fig(1.3) in which four different regions are identified.

I Homogeneous system containing transient clusters.

II Homogeneous system containing a transient percolating network together with clusters.

III A phase separating system without the formation of a temporary percolating network.

IV A phase separating system with the formation of a temporary percolating network.

Colloidal suspensions show two types of behavior during phase separation in dilute solutions. Close to the binodal the colloids form a dense nucleus which grows in time called nucleation and growth. When the attraction is strong enough they form a tenuous system spanning structure usually referred to as spinodal decomposition. In fig(1.4) are shown examples of phase separation by nucleation and growth in (a) and spinodal decomposition (b) from experimental colloid-polymer mixtures. The nucleation and growth (c) and the spinodal decomposition (d) as obtained from computer simulations of attractive spheres are also shown. Colloidal suspensions show

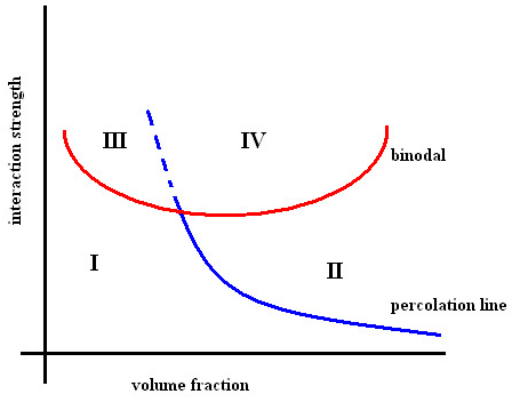

Figure 1.3: Schematic representation of the phase diagram indicating four different regions.

structural arrest above a particular volume fraction referred to as the glass transition.

Reversible aggregation is studied experimentally for instance with telechelic associative polymers. Telechelic associative polymers are soluble polymers with insoluble end groups. Above a critical associating concentration the end groups associate in multiplets forming flowerlike polymeric micelles as shown in fig(1.5) Bridging between micelles causes an effective attractive interaction which leads to reversible aggregation of the micelles [6]. They exhibit a variety of behaviors such as liquid-liquid phase separation, liquid-solid transition and gelation. When the micelles bridge they resemble soft spheres connected by springs. The interaction of such systems can be mimicked by a square well potential with very short range interaction as is schematically shown in fig(1.6). Assuming a square well potential and defining bonds between them with a probability P the liquid liquid phase separation was explained reasonably well. In these systems we can change the interaction depth by changing the ratio of the number of difunctional to monofunctional chains and the interaction range by varying the ratio of the length of the difunctional to monofunctional chains.

Another system of interest is spherical colloids dispersed in a solution of non adsorbing polymers [7]. The depletion of polymers from the colloid surface leads to an effective attraction between the spheres. Here we can control the strength of the interaction by the polymer concentration and interaction range by the length of the polymer chain. A schematic representation of this depletion interaction is shown in fig(1.7).

In this thesis we study the structure and the dynamics of attractive spheres using a novel simulation technique called Brownian Cluster Dynamics (BCD). With BCD we can relax the system by cooperative cluster motion and also study the effect of bond rigidity. More specifically a number of questions will be addressed:

1. For systems with zero interaction range what is the structure of clusters formed

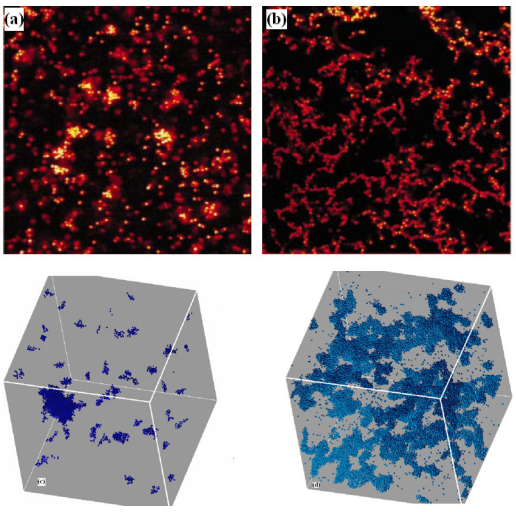

Figure 1.4: Confocal microscopy images of (a)nucleation and growth type phase separation and (b)spinodal decomposition in polymer colloid mixtures [5]. (c) Nucleation and growth and (d) spinodal decomposition obtained from computer simulations of attractive hard spheres.

by reversible aggregation?

2. What is the growth kinetics of such systems?

3. What determines the equilibrium state for such a system?

4. For finite interaction ranges, what is the relationship between the second virial coefficient and the structure and dynamics of the system?

5. What is the interplay between gelation and phase separation?

6. What is the effect of flexibility on the structure and kinetics of both reversibily and irreversibly aggregating spheres?

7. Can we quantify the heterogeneity of gels by measuring the tracer particle diffusion in these structures?

1.1 Outline of the thesis

Chapter 2 gives an overview of the structure and dynamics of attractive hard spheres.

In *chapter* 3 the simulation method called Brownian cluster dynamics is explained in detail. The method will be compared with Brownian dynamics simulations.

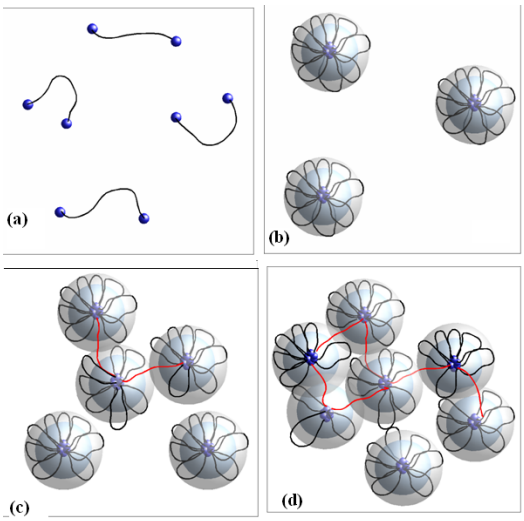

Figure 1.5: Schematic picture of (a)telechelic associative polymers. (b) The polymers forming micelles. (c) The micelles start to share arms. (d) The micelles forming a system spanning network.

Chapter 4 reports the structural properties of attractive spheres formed by rigid bonds for both finite (square well) and zero interaction range. In the case of finite interaction range a phase diagram for two well widths is presented which is compared to the equilibrium phase diagram obtained from Monte-Carlo simulations. Two kinds of percolation thresholds have been determined: the contact percolation and the bond percolation and differences will be detailed. In the case of zero interaction range, particles have only binary collisions so that no phase separation is observed and we only observed a percolation transition. The growth kinetics of these system is reasonably well explained by Smoluchowski's rate equation formalism at low concentrations. Here the relation between collisions and encounters is important and will be discussed in detail.

In *chapter* 5 the self diffusion of attractive spheres with rigid bonds is studied. It will be shown that the diffusion coefficient is determined by the second viral coefficient and has an Arrhenius dependence with temperature indicating that we have true dynamical arrest only at zero temperature.

In *chapter* 6 the effect of bond flexibility and collective motion on the structure and dynamics is presented. It will be shown that the equilibrium structure is the same but the diffusion is influenced in the homogenous regime.

In *chapter* 7 irreversible DLCA aggregation with rigid and flexible bonds is compared. It will be shown that when we allow flexibility of bonds the clusters prefer certain specific configurations. Aging and dynamics will also be addressed.

In *chapter* 8 a study is presented of the dynamical arrest of tracers in different frozen environments like gels formed by RLCA or DLCA and randomly distributed hard spheres. In all these systems the diffusion coefficient is nearly a universal function

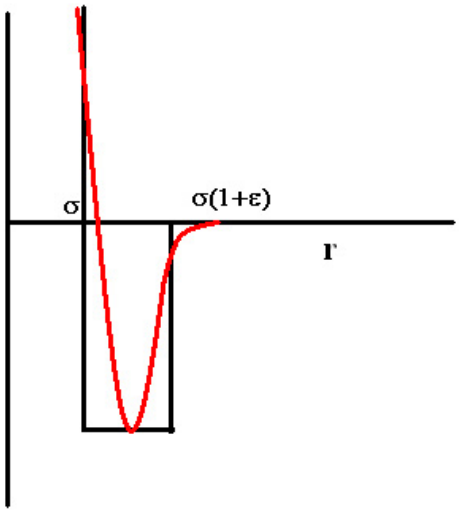

Figure 1.6: Schematic representation of the interaction potential between polymeric micelles (red) and between hard spheres with square well potential in (black). σ is the diameter of the hard sphere and ϵ is the well width.

of the volume accessible to the center of mass of the tracers independent of the size of the tracer. In any case the arrest transition takes place at nearly the same value of the accessible volume.

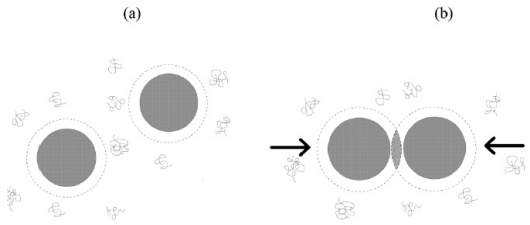

Figure 1.7: Schematic picture of 2 colloidal spheres in a polymer solution with non adsorbing polymers [7]. The depletion layers are indicated by short dashes. (a) When there is no overlap the osmotic pressure on the sphere is isotropic. (b) For overlapping depletion layers the osmotic pressure is unbalanced the excess pressure is shown by the arrow.

Chapter 2

Overview of the structure and the dynamics of attractive spheres.

2.1 Random hard spheres

The study of hard spheres has a long history from the time of Kepler when he predicted that the maximal packing of cannon balls cannot exceed a volume fraction (ϕ) of $\pi/\sqrt{18}$, known as Kepler's conjecture [8]. Hard spheres exhibit a liquid-solid transition when the volume fraction exceeds the freezing transition ($\phi_f = 0.494$). At higher volume fractions the liquid and the solid coexist up to the melting point ($\phi_m \approx 0.545$) after which only the solid is thermodynamically stable. This has been shown both by simulation [9] and experiments [10].

The phase diagram in the pressure-density plane shows that the thermodynamically stable liquid starts from zero volume fraction and extends up to the freezing point after which the phase diagram splits into two, see fig.2.1. One part is the ther-

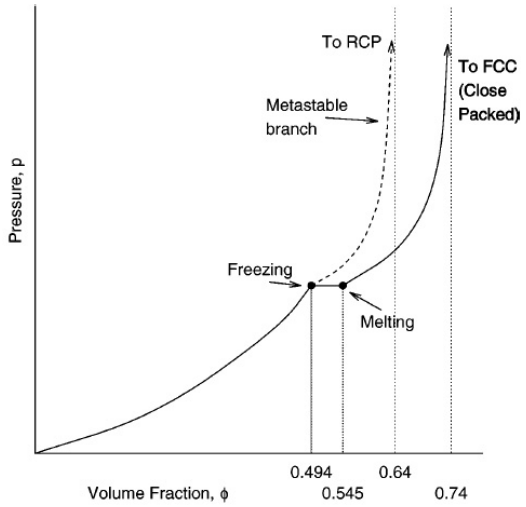

Figure 2.1: The schematic phase diagram for three dimensional hard sphere system [11]

modynamically stable solid and the other continues the metastable liquid up to the random close packing (RCP) ($\phi_c \approx 0.644$) [11, 12] where the pressure also diverges. It is observed in experiments on colloidal particles that close to RCP the system gets stuck in kinetic traps and the dynamics of the system slows down tremendously [13]. The system will still be a disordered liquid but will exhibit the mechanical properties of the solid. Such a system can be viewed as dynamically arrested. Dynamically arrested hard sphere liquids are known as a repulsive glasses. The glass transition takes place at a volume fraction of about $\phi_g \approx 0.58$ determined both by experiments[13] and simulation[14, 15]. Close to the glass transition one observes a steep decrease of the diffusion coefficient. A typical plot of the diffusion coefficient as a function of ϕ as obtained from experiments is shown in fig(2.2) [13]. The theoretical work by Tokuyama et. al [16] gives a fair predictions for the short time diffusion coefficient upto the glass transition. For the long time diffusion coefficient the work

by Tohuyama et.al and Mode Coupling Theory (MCT) [17] give a good discription close to the glass transition see fig(2.2) only if we use the value of ϕ_g as obtained from experiments. Close to the glass transition Tokuyama et. al [16]predicts a power law decrease of the long time diffusion coefficient: $(\phi_g - \phi)^\gamma$ with $\gamma = 2$ while MCT predicts a power law with $\gamma = 2.52$.

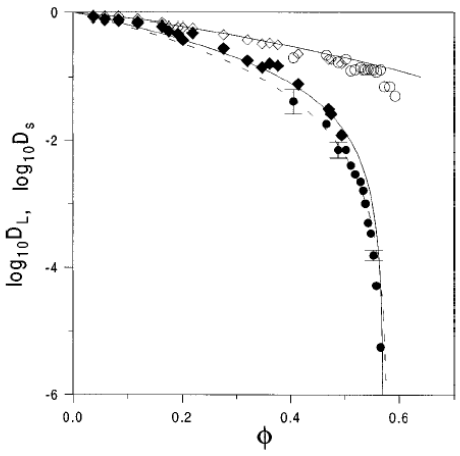

Figure 2.2: The short time diffusion coefficient (open symbols) and the long time diffusion coefficient (closed symbols) plotted as a function of the volume fraction as obtained from experiments [13]. The solid lines represent the prediction of Tokuyama et. al [16] and the dashed line represents the prediction from MCT.

Dawson et al. suggested that the so-called dynamical accessible volume was the parameter that determines the diffusion close to arrest [18, 19]. They tested these ideas for lattice models for which they found that the diffusion coefficient is indeed a universal function of dynamical accessible volume.

Introducing attraction leads to a variety of phenomena like aggregation, liquid-liquid phase separation, percolation and gelation just to name a few[5, 20]. Recently computer simulations have contributed a lot to the understanding of these phenomena. Generally in computer simulations two techniques are used Metropolis Monte-Carlo and Molecular Dynamics [21].

2.2 Irreversible aggregation

2.2.1 Structure

Irreversible aggregation leads to the formation of self similar clusters with aggregation number m and radius of gyration R_g. The relation between m and R_g is determined by the so-called fractal dimension d_f [3, 4, 22].

$$m \propto R_g^{d_f} \tag{2.1}$$

Two regions can be identified during irreversible aggregation: the flocculation region and the percolation region [23–27]. In the flocculation region the clusters are on average far apart while in the percolation region clusters strongly interpenetrate. For fractals the density decreases with increasing size of the clusters and irreversible aggregation always leads to the formation of a cluster that spans the whole space or in other words percolates. Thus beyond a critical time at least one cluster percolates forming a gel [24, 25, 27].

Two limiting types of aggregation can be distinguished: diffusion limited cluster aggregation (DLCA) [3, 22, 28] for which each collision leads to bond formation and reaction limited cluster aggregation (RLCA) [29–33] where on average a large number of collisions occur before the clusters bind. In the flocculation region DLCA is characterized by a fractal dimension around 1.8 [34] and RLCA is characterized by a fractal dimension around 2 [1]. Extensive computer simulation work has been done both on-lattice [3, 4, 23] and off-lattice [25, 26] in order to understand the structure and the aggregation kinetics of DLCA and RLCA. The experimental work on gold colloid solutions confirmed the values of the fractal dimension [1] found with simulations.

As the clusters grow they start to interpenetrate crossing over to the percolation regime which is charactarised by a higher fractal dimension of 2.5 [23, 25, 35]. It has been shown by computer simulations that the transition from flocculation to percolation happens at a characterastic mass (m_c) and size (R_c) [23, 25, 27] of the clusters related by eq.(2.1) with the fractal dimension of the flocculation regime.

The cluster size distribution ($N(m)$) of the aggregates may be written as

$$N(m) = m^{-\tau} f(m/m^*) \tag{2.2}$$

where τ is the polydispersity exponent and $f(m/m^*)$ is a cutoff function at a characteristic m^* that decreases faster than any power law and m^* increases with the time of aggregation. The flocculation region (DLCA $\tau = 0$ and RLCA $\tau = 1.5$) and the percolation region ($\tau = 2.2$) are characterised by different polydispersity exponents [23, 25]. A polydispersity index (K) may be defined as the ratio of the mass average aggregation number (m_w) to the number average aggregation number (m_n).

$$\begin{aligned} m_n &= \frac{\sum_{m=1}^{\infty} mN(m)}{\sum_{m=1}^{\infty} N(m)} \\ m_w &= \frac{\sum_{m=1}^{\infty} m^2 N(m)}{\sum_{m=1}^{\infty} mN(m)} \end{aligned} \tag{2.3}$$

In the flocculation regime $K = m_w/m_n$ is 2 for DLCA, while in the percolation regime K diverges because m_w diverges while m_n stays finite as was shown in simulations both on-lattice [23, 24] and off lattice [25].

Quite recently a new type of irreversible aggregation has been proposed [36] for particles with flexible bonds such as nano emulsions. This type of aggregation leads to quite a dense local structure but still preserves the same fractal dimensions at large lenght scales see fig.(2.3) and *chapter* 7.

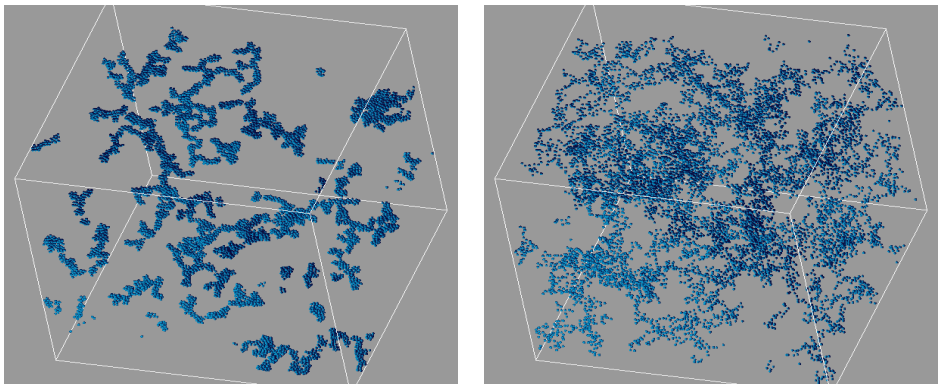

Figure 2.3: Snapshot of flexible DLCA (left) and rigid DLCA (right) at a low concentration as obtained from simulation.

2.2.2 Kinetics

Coagulation of colloidal particles can be schematically represented by the following reaction mechanism.

$$N(i) + N(j) \rightleftharpoons N(i+j) \tag{2.4}$$

Here $N(i)$ is the number of clusters with i monomers. The rate equation of coagulation and fragmentation of the clusters can be written as

$$\begin{aligned} \frac{\mathrm{d}N_m}{\mathrm{d}t} &= \frac{1}{2}\sum_{i+j=m}[K(i,j)N(i)N(j) - F(i,j)N(m)] \\ &\quad -\sum_{j}[K(m,j)N(m)N(j) - F(m,j)N(j+m)] \end{aligned} \tag{2.5}$$

The rate of formation of the clusters or alternatively the forward rate coefficient is represented by $K(i,j)$ and the fragmentation rate coefficient or the rate of the break up of clusters is represented by $F(i,j)$. This mean field approach [37] breaks down once correlation develops between the positions of the clusters. So eq(2.5) is valid only when the concentration of the system is extremely low.

For the case of irreversible aggregation the fragmentation rate is put to zero: $F(i,j) = 0$ [25, 38]. Smoluchowski has derived an analytical equation for $K(i,j)$ [39, 40] in the case of DLCA assuming that there is no positional correlation between clusters (very low concentration) [41].

$$K(i,j) = 4\pi(D_i + D_j)(R_{(col)i} + R_{(col)j}) \tag{2.6}$$

Here D_i is the diffusion coefficient of the cluster of mass i which is inversely proportional to the hydrodynamics radius of the cluster($R_{(h)i}$) by the relation of Stokes-Einstein $D_i = k_B T/(6\pi\eta R_{(h)i})$, where k_B is Boltzmann's constant, T is the absolute

temperature and η is the solvent viscosity. At short aggregation times when the fraction of clusters of mass greater than 2 is negligible we can write

$$\frac{\partial N(2)}{\partial t} = K(1,1)N^2(1)$$
$$\text{with } K(1,1) = 16\pi D_1 R_{(col)1}$$

where $N(1)$ is the fraction of monomers and $N(2)$ is the fraction of dimers. For a sphere of unit diameter the collision radius and the hydrodynamic radius are the same $R_{(h)1} = R_{(col)1} = 0.5$. At very low concentration the diffusion coefficient of a sphere is $D_1 = 1/6$ if we define the unit of time as the time needed for a sphere to diffuse its own diameter. The initial dependence of m_w is

$$m_w = 1 + 8\phi t \tag{2.7}$$

The Smoluchoskwi approach using $K(i,j) = K(1,1)$ seems to work well for DLCA at very low volume fractions up to fairly large cluster sizes [25].

The same approach was extended to RLCA aggregation using different kernels but with limited success [31]. One of the assumptions that went into the derivation of eq.(2.4) was that there exists no correlation between clusters in the system. The problem with RLCA is that there is strong correlation between clusters even in dilute solution. During RLCA aggregation two clusters have correlated collisions before they stick or diffuse apart to collide with a third cluster. To take this effect into account the idea of encounters was introduced. An encounter between two clusters starts from the first collision which may be followed by many collisions before a bond is formed between the clusters in which case it is called a successful encounter or before they diffuse apart in which case it is an unsuccessful encounter [42]. Empirical expressions like the sum kernel $K(i,j) = K(1,1)\left(i^\lambda + j^\lambda\right)/2$ [43] and the product kernel $K(i,j) = K(1,1)\,(ij)^{\lambda/2}$ [44] have been proposed where λ is the homogenity exponent. There have been also attempts to modify the kernel by introducing two probabilities: the probability to bind and the probability that the cluster does not bind but collides again with the same cluster[31].

2.2.3 Tracer diffusion

The final stage of any irreversible aggregation is the formation of one cluster called a chemical gel, which is completely arrested if the bonds are rigid. One way to study these gels is to measure diffusion of tracer particles placed in the gels. It turns out that we can map this physical situation on to a mathematically tractable percolation problem of an ant walking in a labrynith [35, 45]. There have been computer simulation studies of tracer diffusion in frozen hard spheres [46, 47] and in the so-called Lorentz gas [48–51] (randomly placed overlapping spheres). The tracer particle is trapped if there is no path between the opposite sides of the box or in other words if the volume available to the center of mass of the tracer, called accessible volume

(ϕ_a), does not percolate. It has been shown by simulations for a Lorentz gas that ϕ_a percolates only above a particular critical value $\phi_a^c \approx 0.0301$ [51]. For crystalline structures like FCC, simple cubic etc ϕ_a^c is also approximately 0.03 except for BCC where it is about 0.005 [52]. A typical picture of the accessible volume available for

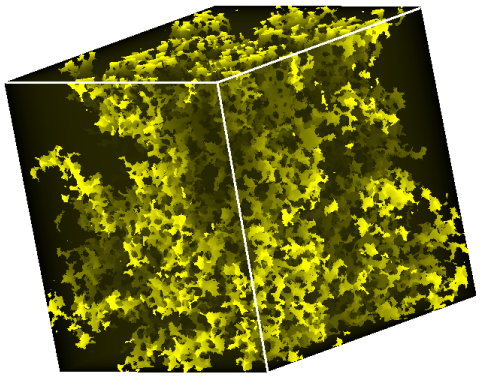

Figure 2.4: Picture of the accessible volume available for a tracer particle of the same size as the monomeric unit in a colloidal gel.

the center mass of a tracer is shown in fig(2.4). Computer simulations on frozen hard spheres as well as DLCA and RLCA also showed that the critical accessible volume fraction was around 0.03 [47] and that the mean square displacement at the critical point followed the scaling laws proposed by percolation theory. The diffusion coefficient of the tracer particles were found to be nearly a universal function of the accessible volume see *chapter* 8.

The diffusion of point tracers in a system of partially overlapping spheres was also simulated to study the conductivity in a random resistor network. A novel algorithm was proposed depending on the first passage time [53]. It was rigorously proved that the diffusion coefficient of a tracer of finite diameter b in a system of frozen hard spheres is completely equivalent to the diffusion of a point tracer in the same system after increasing the diameter of the spheres by a factor $1+b$ without changing their position and allowing them to overlap [46]. This idea was later extended to highly correlated irreversible colloidal gels where the diffusion coefficient of the tracer particles was found to be nearly universal when plotted as a function of the accessible volume see *chapter*8. A simple phenomenological equation was also put forward to relate dynamics of the tracer to the accessible volume.

In these simulations two populations of tracer particles were identified, tracer particles which get stuck in finite size pores and tracer particles which can diffuse through the percolating pores. The distribution of average distances traveled by all particles is initially gaussian as all the tracers perform Brownian diffusion [41].

However, after some time the distribution becomes bimodal as tracers in the finite pores cannot diffuse any further. The area under the curve for short distances gives the fraction of finite size pores, and the peak at larger distance, which keeps moving with time, represents the percolating fraction of the pores see *chapter* 8.

2.3 Reversible aggregation

Introducing reversibility in the system through a particular interaction potential like the square well [54–57] or Yukawa [58] potential produces a dramatic effect on the structure and the dynamics of the system. Depending on the strength and the range of the interaction the system will either be in the one phase fluid state, or crystallize or may be phase separated. In fig. (2.5) we show the phase diagram of hard spheres with short and long range attraction [10]. For the case of short range attraction the

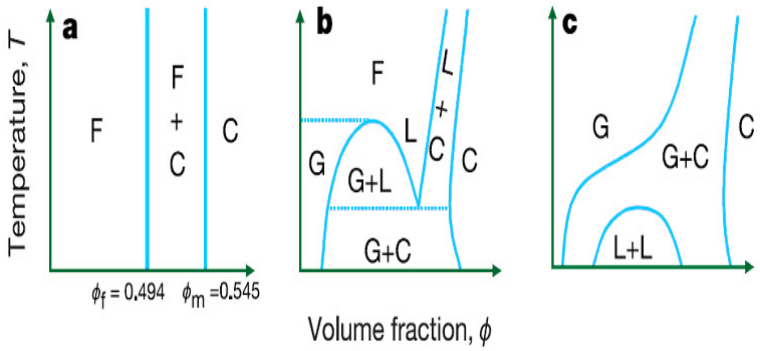

Figure 2.5: Schematic phase diagram[5] of hard spheres (a). For long range attraction there exists a triple point where all the three phases co-exist (b). For short range attraction the liquid and crystal phase coexist and the liquid-liquid phase separation becomes metastable (c). In the figure are indicated fluid (F), gas (G), liquid (L), fluid-crystal coexistence (F+C), gas-liquid coexistence (G+L), gas-crystal coexistence (G+C), and liquid-liquid coexistence (L+L).

liquid-liquid phase separation becomes metastable and the system always crystallizes. Such systems may exhibit diverging relaxation times which have been interpreted as a glass transition at high concentration and as a gel transition at low concentration [59].

2.3.1 Structure

For weak attraction, the aggregation of the particles leads to the formation of fractal aggregates. Contrary to irreversible aggregation where both flocculation and percolation can be observed, in reversible aggregation only percolation can be studied [54]. To observe large aggregates in the flocculation region (i.e. at low concentration)

strong attraction is needed which causes phase separation. At high concentrations the aggregates already starts to inter penetrate even when they are small. The systems percolates ie. forms a system spanning network above a critical interaction strength which is completely reversible (transient gels).

The phase diagrams of systems with different interaction range and strength are very close when plotted as a function of the second virial coefficient (B_2) [60] as long as the interaction range is short ($\epsilon < 0.1$). It was also reported that in the one phase regime the structure was very similar when plotted as a function of B_2 even for fairly large interaction range ($\epsilon = 0.5$) in the case of square well fluids [54], see *chapter* 4.

One may distinguish between 2 routes to phase separation: nucleation and growth and spinodal decomposition [5]. Typical pictures of nucleation and growth and spinodal decomposition are shown in fig(1.5). Close to the binodal the system forms fractal aggregates which are metastable till dense critical nuclei of rather well defined radius and mass is formed. The system phase separates into a low density liquid and a high density liquid by the growth of the nuclei. For strong attraction the aggregation kinetics of the system shows close resemblance to irreversible aggregation and may form a percolating network. The strands of the network become thicker over the course of time. This process is usually referred to as spinodal decomposition. The network is temporary and will eventually break up into individual spherical dense domains as has been shown on-lattice [61]. For short range interactions the transition from metastability close to the binodal to the spinodal behavior is gradual and nothing dramatic happens at a particular interaction strength[62] which makes it impossible to define a spinodal unambiguously. As mentioned above, decreasing the interaction range makes the liquid-liquid phase separation metastable and the system crystallizes when the spheres are monodisperse.

Much effort has been devoted to the study of the structure and dynamics of reversibly aggregating systems in the one phase regime. Many ways have been proposed and efficiently used in simulation and experiments to study glass transition without the hindrance of phase separation. As the glass transition is observed at relatively high density, crystallization was avoided by introducing polydispersity. Generally a binary system of spheres was used with a size difference of 10% [63]. Foffi et. al [58] tried to describe the structure of these systems using the Ornstein-Zernike approximation with various closure relations like the Percus-Yevick approximation (PY) or the mean spherical approximation. For non interacting hard spheres the PY closure together with an ad-hoc refinement describes the structure upto the freezing transition reasonably well, but for interacting systems the success was limited to weak short range attraction [64]. Introducing rigid bonds between spheres also suppresses crystallization. The reason being that when the bonds are rigid the pathway to crystalise is extremely improbable see *chapter* 4.

A way of avoiding liquid-liquid phase separation is to introduce discrete interaction sites [65–67]. It was shown that after introducing a maximum coordination below 6 the liquid-liquid phase separation line shifts towards lower concentrations opening up a homogeneous regime with strong interaction in the high concentration region.

Long range repulsive interaction may also suppress phase separation [68–71]. For some potentials the clusters stop growing when a critical size is reached which is known as the cluster phase [71]. The size of the clusters increase with ϕ and they may even percolate. The internal structure of such clusters in some cases resembles the so-called Bernal spiral.

A third way of avoiding the phase separation is to introduce directional interaction [72]. The coordination number as well as the angle of the patchy interactions may be fixed for example on a tetrahedron [66], icosahedron [72] etc.

A way to suppress phase separation completely is to reduce the interaction range to zero and make the bonds rigid so that we have only binary contacts or in other words aggregation due to non-slippery surface adhesion [73] see *chapter* 4 and 5. For this kinetically driven aggregation process one observes a flocculation-percolation transition in the steady state as a function of ϕ and the interaction strength, similar to that during irreversible aggregation as a function of time. The clusters in the steady state are characterised by a fractal dimension of $d_f = 2$ in the flocculation region and $d_f = 2.7$ in the percolation region [73]. The value of the fractal dimension in the percolation region is slightly higher than the value predicted by the random percolation model [35]. The size distribution is characterised by a polydispersity exponent $\tau = 1.5$ during flocculation and $\tau = 2.1$ during percolation. It was possible to understand the growth kinetics with the rate equation given in eq (2.5) in the low density limit. It was found that the parameter that determined the steady state was the encounter time, which is defined as the time needed for the monomer to become decorrelated from another monomer see *chapter* 4. The value of the encounter time depended both on the elementary stepsize (the maximum distance a monomer can move in one time step) and the sticking probability.

2.3.2 Dynamics

The long time self diffusion of non interacting hard spheres slows down at high concentrations due to the increased mutual hindrance, while locally the motion is free. This effect is known as caging. Above a critical volume fraction the diffusion coefficient becomes almost zero and such systems are called a glass. Mode coupling theory predicts a power law decay of the diffusion coefficient close to a critical volume fraction (ϕ_c) $D \sim (\phi_c - \phi)^\gamma$ with $\gamma = 2.52$ and $\phi_c = 0.516$ using the Percus-Yevick approximation for the structure factor of hard spheres[17]. This value is smaller than that observed from experiments [13] and simulations [14, 15, 74] which is $\phi_c \approx 0.58$. One of the reasons of the failure of the theory is attributed to its inability to take into account the hopping process.

Introducing short range attraction at high concentrations has a significant effect on the structure. Because of the attraction the system starts to form clusters. Within the clusters the spheres share common excluded volume which opens up space for other particles to diffuse. As a consequence the repulsive glass line moves to higher ϕ for lower temperatures see fig(2.6). Upon further increasing the attraction it is proposed

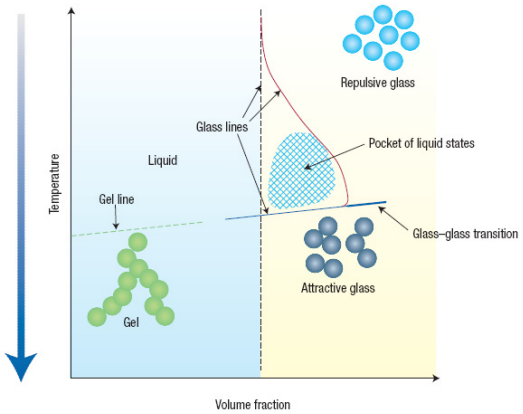

Figure 2.6: Schematic state diagram[17] at high concentrations indicating two kinds of glass.

that the system forms a new type of glass called the attractive glass. It was also proposed that contrary to the repulsive glass which happens only above a ϕ of 0.58, the attractive glass line extends to lower volume fractions as shown in fig(2.6). MCT predicts that $D \propto (T - T_c)^{\gamma}$ where T_c is the critical temperature where the arrest takes place. There is simulation[14, 15, 75] and experimental[59] work supporting the concept of attractive glasses.

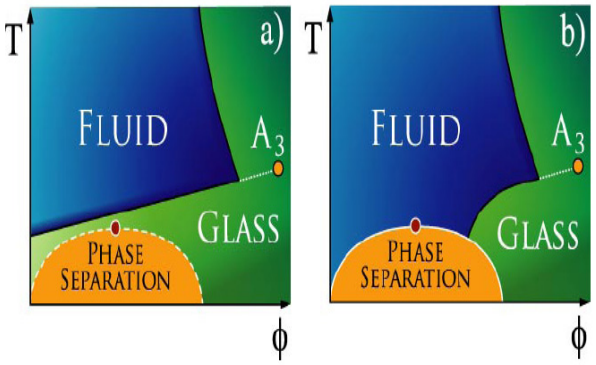

Figure 2.7: Schematic phase diagram[76] with the attractive glass line crossing the binodal or staying in the homogeneous phase.

From fig.(2.6) we can expect two scenarios: either the attractive glass line crosses the liquid-liquid binodal or it stays in the homogeneous regime, as shown schematically in fig(2.7). Foffi et.al [76] concluded that the scenario of the glass line going into the binodal was the right one. It was proposed that phase separation was arrested due to glass formation, but from this study it is not very clear what happens to the particles at the surface. The open question being whether the particles at the surface still have a dynamical exchange with the surrounding. Another important result that came out from this study was that the diffusion coefficient in the homogeneous regime

was the same when plotted as a function of the second virial coefficient [76] for short range attractive interactions. This supported the idea put forward earlier that the structural properties of the system are very close when plotted as a function of second virial coefficient for short range potentials [60].

Based on simulation work we have argued against the existence of attractive glasses see *chapter* 5. The argument is that introducing attraction opens up more free space for monomers to diffuse before they bind again. The increase of the free space can be shown by calculating the accessible volume [47] available to a sphere see *chapter* 8. This effect leads to an increase of D when the attraction is weak as observed in experiments [59] and simulation [14, 69] see *chapter* 6. The decrease of D at strong attraction is caused by the increase of the bond lifetime but only diverges for strictly irreversible aggregation ($T = 0$) [72, 77] see *chapter* 6.

There has been a recent attempt with well defined analytical models to quantify the dynamical heterogeneity at short times considering that particles belonging to the percolating cluster are localised while the rest of the particles consisted only of monomers diffusing [78] freely. The effect of dynamical heterogeneities is observed only during the initial time in these reversible systems. With time the immobile particles liberate themselves from the percolating network and start to diffuse, while the fast moving ones attach to the percolating network so that after a long time on average all the particles have traveled the same distance with a well defined diffusion coefficient. Using the same kind of argument we have shown that the diffusion coefficient can be calculated from the cluster distribution of the non percolating fraction at equilibrium, and that it is inversely proportional to the number average aggregation number of the system [77] see *chapter* 5. The difference between the two approaches is that we considered the contribution of all the clusters to the diffusion while in ref.[78] the authors considered that the non percolating fraction consisted of monomers and thus the diffusion of clusters was neglected.

Chapter 3

Simulation Method

Statistical mechanics predicts the equilibrium properties of the system through the knowledge of the partition function, even though it does not describe how a system approaches equilibrium. Computer simulation helps in understanding equilibrium phenomena such as pressure, chemical potential and non equilibrium phenomena such as irreversible aggregation and glasses. Two widely used simulation techniques are molecular dynamics (MD) [79] and Monte Carlo (MC) [21, 80]. To study the equilibrium phenomena Monte Carlo techniques are a better choice because of the relatively simple implementation and faster performance. Their drawback is the unphysical representation of the trajectory in the phase space which makes it a poor candidate to study the kinetics. With molecular dynamics one resolves the equations of motion yeilding a physical interpretation of time that can be used to directly compare the evolution of the system with experiments, even though it is much slower than the conventional Monte Carlo techniques.

3.1 Brownian cluster dynamics (BCD)

BCD is an algorithm which works on the principle of Metropolis Monte Carlo with the dynamical predictions of molecular dynamics.

3.1.1 Random distribution of hard spheres

In the simulation of liquids most of the time the initial configuration is randomly distributed hard spheres (RHS). To create a random distribution of hard spheres first we define the unit of length in terms of the diameter of the sphere. We create a box of size L and distribute the centers of mass of N_{tot} spheres in that box, so that the number concentration is $C = N_{tot}/L^3$ and the volume fraction is $\phi = C\pi/6d^3$ where d is the diameter of the sphere generally $d = 1$. After this step we give a random displacement to each sphere with a constant step size s and we relax the system. Whenever there is hard core overlap between the spheres we either reject the movement or will move it only up to contact. It is very important to keep the step size s small enough (three times smaller than the average distance between nearest neighbors [81]) so that there is no difference if we truncate the movement at conctact with other sphere or simply reject the movement. During this process we keep track of the distance between the centre of mass (CM) of the nearest neighbors (Δ) and the process is continued till the steady state is reached. In the steady state Δ is equal to that predicted by Torquato [8] for random distributions of hard spheres see fig(3.1). For this equilibrium distribution of hard spheres we calculated the excess chemical potential compared to the ideal case using Widom's particle insertion [21] method and compared it with the Carhanan and Starling equation [82] of state.

$$\mu_{HS}^{ex} = \frac{3-\phi}{(1-\phi)^3} - 3 \tag{3.1}$$

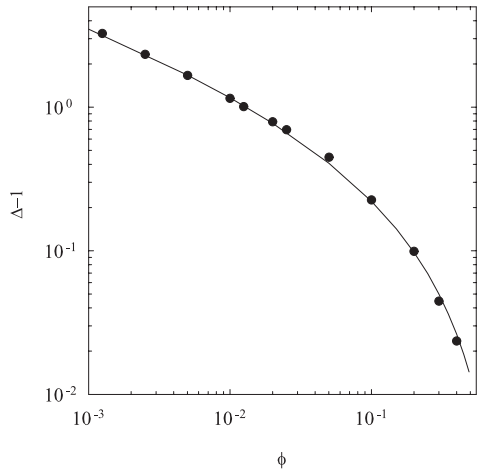

Figure 3.1: The average distance between nearest neighbors is plotted as a function of the volume fraction. The solid line represents the values predicted by Torquato.

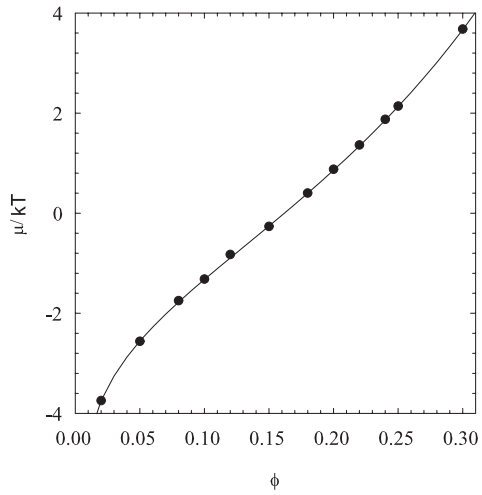

Figure 3.2: The excess chemical potential is plotted as a function of the volume fraction. The solid line represents the Carnahan-Startling equation (eq(3.1)) for the excess chemical potential.

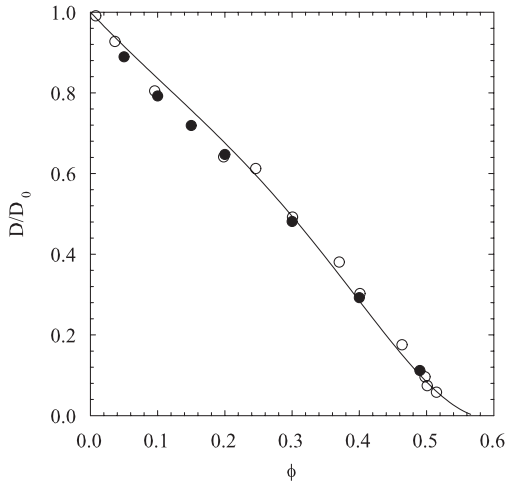

Figure 3.3: Comparison of the decrease of the diffusion coefficient with increasing volume fraction for non-interacting hard spheres obtained with BCD (filled symbols) and EDBD (open symbols)[83]. Solid line is the empirical equation given by Speedy [84].

A close agreement was found as shown in fig(3.2).

With this algorithm we perform a random walk of the center of mass of the spheres. If we have only one sphere in the box then the average mean squared displacement performed by the CM of the sphere is given by ($\langle r^2 \rangle = Ns^2$) where N is the number of steps taken by the CM of the sphere and is also the number of MC time steps. For a particle undergoing Brownian motion it has to satisfy the equation $\langle r^2 \rangle = 6D_0 t$ in 3 dimensions (3D), which gives $Ns^2 = 6D_0 t$, here we define $D_0 = 1/6$ ($\langle r^2 \rangle = 1$ when $t = 1$), thus $t = Ns^2$. We determined the diffusion coefficient of RHS as $D = \langle r^2 \rangle / (6t)$ as a function of ϕ and compared it with the results obtained from event driven Brownian dynamics (EDBD) [83] and the phenomenological equation from Speedy [84] also based on molecular dynamics simulations:

$$\frac{D}{D_0} = \frac{1}{C}\left(1 - \frac{1}{C}\right)\left(1 - C^2\left[0.4 - 0.83C^2\right]\right] \tag{3.2}$$

Identical results are obtained for D/D_0 versus ϕ, see fig(3.3).

3.2 BCD and Thermodynamics

Interaction between the spheres is introduced by defining a probability P by which particles in contact are bound. The ratio of the number of bound (ν_b) to free contacts (ν-ν_b) is given by the Boltzmann distribution: $\nu_b/(\nu - \nu_b) = \exp(-\Delta H)$, where ΔH is the enthalpy difference between bound and free contacts and is expressed in units

of kT. The formation of ν_b randomly distributed bonds over ν contacts leads to a decrease of the free energy equal to u per contact. This decrease may be written as the sum of the decrease of the enthalpy and the gain of the entropy: $\nu u = \nu_b \Delta H - \Delta S/k$ where u is expressed in units of kT. The latter is determined by the number of ways ν_b bonds can be distributed over ν contacts: $\Delta S/k = \ln(\nu!/[\nu_b!(\nu - \nu_b)!])$. Noticing that P=$\nu_b/\nu$, we can express P in terms of u using the Sterlings formula:

$$P = 1 - \exp(u) \tag{3.3}$$

3.3 Square well potential (SW)

For a SW interaction potential, particles are in contact when the distance between the monomers is less than $1 + \epsilon$ where ϵ is the well width. A bond is formed with probability α and an already existing bond is broken with probability β so that the average probability a bond exists is $P = \alpha/(\alpha+\beta)$. Alternativly one can bind spheres within each others interaction range with probability P independent of the previous state.Clusters are defined as collections of bound spheres. In this way N_c clusters are formed with varying aggregation numbers m.

We have used three kinds of movement steps.

BCD1- We pick N_0 monomers randomly and give them a displacement s in a random direction. All movements leading to bond breaking or overlap with other spheres are rejected. If s is small compared to ϵ and $\Delta - 1$ then the diffusion coefficient of the centre of mass of the clusters is proportional to the inverse of m.

BCD2- We pick N_c clusters randomly except the percolating cluster and give a random displacement s/R_h to each cluster where R_h is the radius of the cluster. All movements leading to overlap with other clusters are truncated at contact or rejected. As a consequence the diffusion coefficient is inversly proportional to the diameter of the clusters.

BCD3- First we perform a BCD1 movement and calculate the distance moved by the CM of each cluster and its resultant direction. We then perform a BCD2 movement, i.e. cluster motion, in the resultant direction previously calculated with a stepsize s/R_h minus the distance moved during the BCD1 movement.

One or more movement steps are followed by a cluster construction step and this procedure is repeated until steady state is obtained which is the same with all three movement steps. Reducing both α and β while keeping the ratio α/β constant the same equilibrium structure but with slower kinectics.

BCD1- Simulates Brownian motion of flexible bonds with a friction coefficient proptional to m (Rouse dynamics).

BCD2- Simulates Brownian motion of rigid bonds with a friction coefficient proptional to d (Zimm dynamics).

BCD3- Simulates Brownian motion of flexible bonds with a friction coefficient proptional to d (Zimm dynamics).

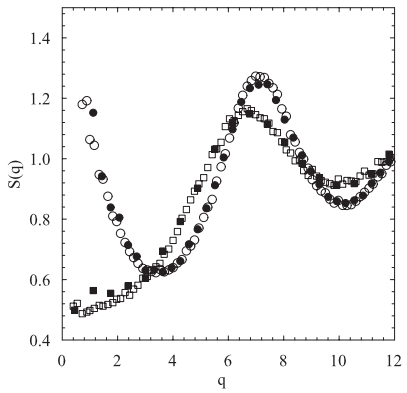

Figure 3.4: Comparison of the structure factor of equilibrium systems at $\phi = 0.15$ and $\epsilon = 0.1$ obtained by BCD (filled symbols) and EDBD (open symbols) with $B_2 = 2$ (squares) or $B_2 = -2$ (circles).

In fig(3.4) we have compared the structure factor obtained from EDBD and BCD for $\phi = 0.15$ at $\epsilon = 0.1$ at different second virial coefficients (B_2), showing that the results are the same. The diffusion coefficient D obtained with the two methods shows that the movement step of EDBD is equivalent to BCD1, see fig(3.5). We find that the step size s has to be quite small to obtain the same results with BCD1 and EDBD.

For strong attraction we observe a liquid-liquid phase separation if the bonds are rigid (BCD2) and crystalization if the bonds are flexible. We have compared the liquid-liquid binodal for $\epsilon = 0.5$ with that obtained from the Gibbs ensemble Monte Carlo technique [55]. Fig(3.6) shows that the Gibbs ensemble Monte Carlo technique and BCD are in fairly good agreement.

3.4 How does it work?

According to Einstein *Research is* 1% *inspiration and* 99% *prespiration* for the case of programming we have to say that *Programming is* 1% *writing and* 99% *debugging.* The language I used is C, with extensive use of *pointers* and *structure*. With the algorithm described here we perform $3D$ off-lattice simulation of attractive spheres.

3.4.1 How do we represent space in computer?

We create a box of size L in 3 dimensions divided into L^3 small lattices. In order to have periodic boundary conditions we have to declare a bigger box, $LL = L+2*GAP$ where GAP is kept 2 which is sufficient if the maximum step size is less than unity. Each lattice has 8 *pointers* which point to a monomer if it is present or else it is just a null pointer. If we know the lattice number of a monomer (a) in the box L it can easily be converted into that of the bigger box LL as $tran(a) = (GAP * ((1 + LL +$

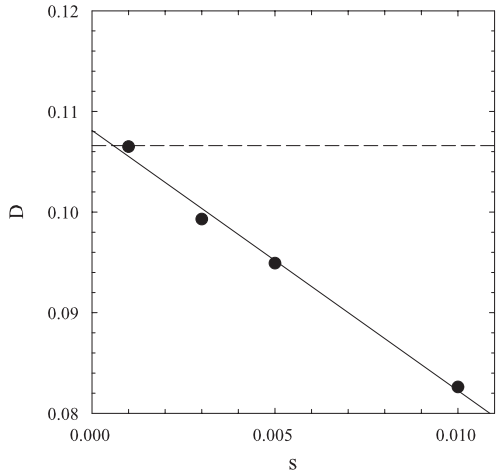

Figure 3.5: Dependence of the diffusion coefficient simulated using BCD1 on the step size ($\phi = 0.49$, $B_2 = -2$, $\epsilon = 0.1$). The dashed line represents the result from EDBD.

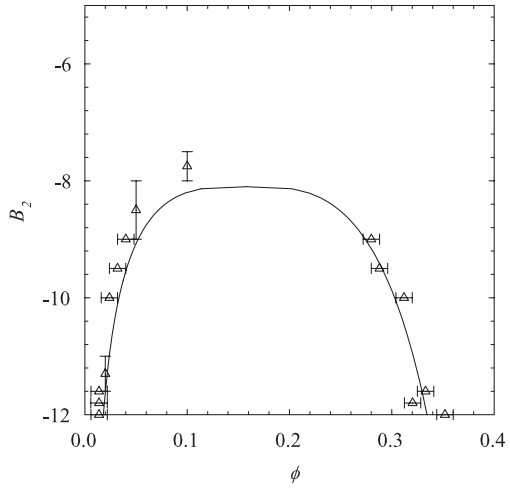

Figure 3.6: The phase diagram obtained from BCD (triangles) and Gibbs Ensemble Monte Carlo simulations (solid line) for $\epsilon = 0.5$

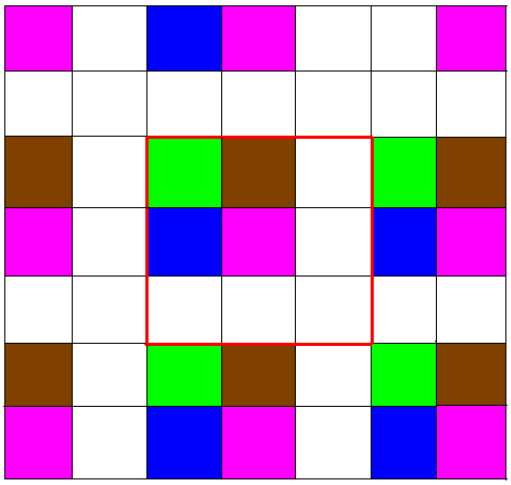

Figure 3.7: Schematic diagram of how we create a periodic boundary condition.

$LL * LL) + 2 * (((a)/L) + ((a)/(L * L)) * LL)) + (a))$ which returns an integer. Once the position of the monomer defined by (x, y, z) has been updated in the computer memory we assign the corresponding lattice number and one *pointer* out of 8 to each monomer.
$j = trans(x1 + y1 * L + z1 * L * L)$; /* index of the lattice in space */
$m = 0$;
$while(lat[j].ptm[m])$/*m is the first zero pointer ptm[8] */
$m + +$;
$lat[j].ptm[m] = ptmono + i$;
where $x1 = (unsignedlongint)floor((double)x)$; is the integer value of the coordinate x, lat is the $structure$ assigned to the lattice.

3.4.2 Periodic boundary conditions

In fig(3.7) we show a schematic representation of periodic boundary conditions in $2D$ which is trivially extended to $3D$. Here the box with $L = 3$ is shown in red and the bigger box with $LL = L + 4$ is shown in black. The colors in the red box are reproduced in the bigger lattice exactly the same way as is done in the program. Thereby we define a torus. Usually in simulations the entire box is reproduced in all directions once for periodic boundry conditions, which takes 27 times more computer space. As we do not reproduce the entire box we can work with bigger simulation boxes. The computer time taken to perform one complete cycle (1 movement step + 1 cluster construction step) for 10^5 particles is $1.5s$ in a 64 bit processor with a frequency of $2400Hz$.

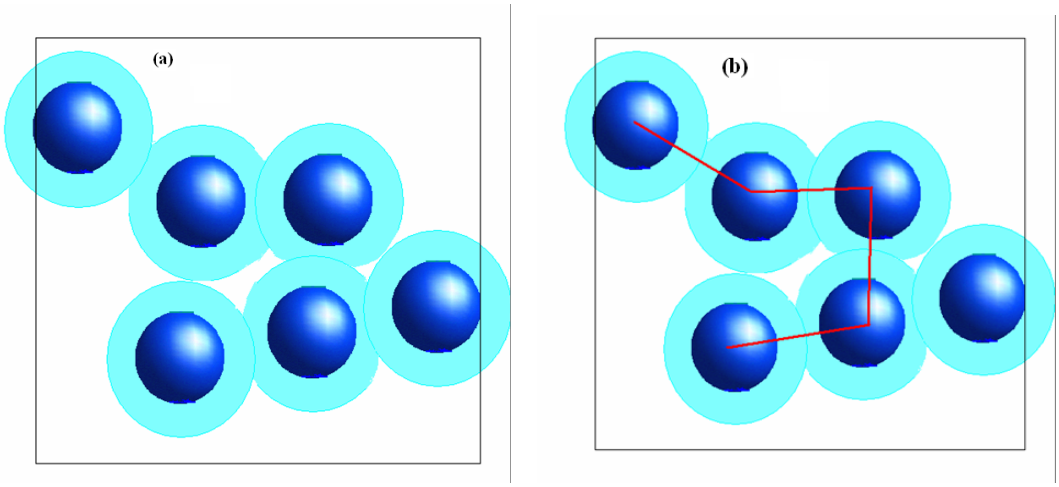

Figure 3.8: (a) P1 construction and (b) when bonds are distributed following the P construction.

3.4.3 What does a monomer know?

The *structure* defined for the monomer contains all the relevent information: to which cluster it belongs, to which neighbors it is bonded, its position coordinates in the box, and with how many monomers it is in contact and bonded.

$structmono$

{

$doublex, y, z, dx, dy, dz, dxP1, dyP1, dzP1;$

$floatx0, y0, z0, xreal, yreal, zreal;$

$charcellposition, Nneighb, Nconnect;$

$structmono * pt_next, *pt_nextP1;$

$structmono * ptlinks[40];$

$structcluster * pt - father, *pt - fatherP1;$

};

As explained before, 2 spheres at a distance of $1 + \epsilon$ may be bonded or free. We define 2 kinds of clusters: clusters formed by all spheres within a distance $1 + \epsilon$ called the $P1$ construction, and clusters of bonded particles called the P construction. As an example fig(3.8) shows a single cluster with the $P1$ construction (a) and 2 clusters with P construction (b). The monomer knows its initial position $(x0, y0, z0)$ and its current position $(xreal, yreal, zreal)$ so that at any time the displacement is given by $\sqrt{[(xreal - x0)^2 + (yreal - y0)^2 + (zreal - z0)^2]}$. It also knows the lattice site to which it belongs ($cellposition$) and the number of monomers connected to each monomer both by $P1$ ($Nneighb$) and P ($Nconnect$) construction. We keep track of the monomers to which each monomer is connected with the P construction ($*ptlinks[40]$) with a maximum of 40 connected neighbors. The monomers also know

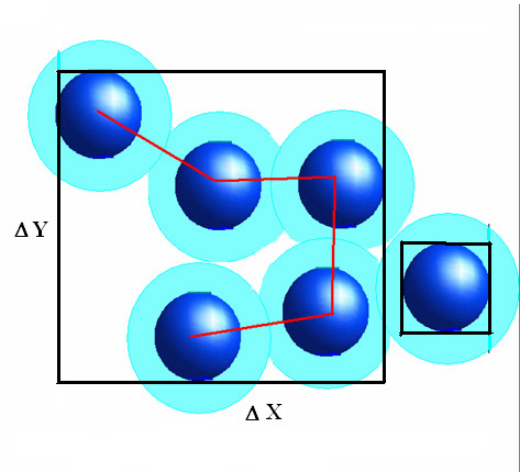

Figure 3.9: Calculation of the extend of the cluster.

to which cluster they belong by having a *pointer* to the cluster *structure*. *pt_next* gives the next monomer in the cluster list and (dx, dy, dy) gives the distance to the header monomer in the cluster *structure*. The use of these variables will be explained below.

3.4.4 What does a cluster know?

structcluster
{
$double Xmin, Xmax, Ymin, Ymax, Zmin, Zmax, Dl;$
$double xcm0, ycm0, zcm0, xcm1, ycm1, zcm1;$
$unsigned long int mass;$
$struct mono * pt_first, *pt_last;$
};
The cluster knows its extent in all three directions for example $\Delta X = Xmax - Xmin$ see fig(3.9) and Dl gives the maximum of the three directions. Because we use periodic boundary conditions some parts of the cluster will be broken but $\Delta X, \Delta Y, \Delta Z$ are recalculated after each cluster construction step. For this reconstruction we keep track of the distance of the monomer of a cluster from its header which can be any arbitrarily choosen monomer of the cluster. With respect to the header we reconstruct the entire cluster as shown in fig(3.10). We also keep track of the CM of the cluster after each cluster movement and construction step (xcm,ycm,zcm). The cluster also knows it mass and all the information available to its monomers.

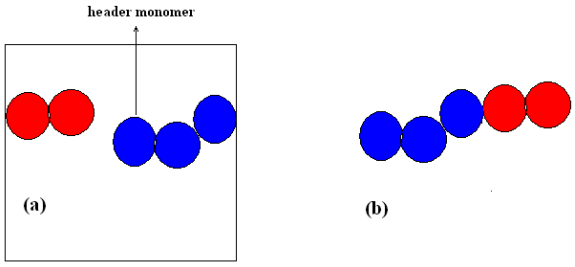

Figure 3.10: Reconstruction of clusters to calculate the extend.

3.4.5 Cluster construction

We sweep the big box in descending order of the lattice number. We check if the distance between monomers in the lattices is less than $1 + \epsilon$, if a bond was already formed in the last step we take a random number between 0 and 1. If the random number is less than β we break the already formed bond if not the bond is kept intact. If the bond is not formed before, we check it with α and if the random number is less than α we create a bond. If the bond formation connects two clusters, we merge the cluster. Alternately we can create a bond with probability P independent of the previous state.

Merging or scission of clusters

Figure(3.11a) shows a schematic representation of the state before merging in a simple case with 3 monomers and 2 clusters. The 4 pointers described above are represented with 4 different colors as indicated in the figure. Merging 2 clusters using this representation is very simple: it is done by appending the smallest list to the biggest one and adjusting the pointers correctly: Figure(3.11b) shows a schematic representation of the state after cluster number 2 has moved 1 site to the right and merged with cluster number 1. After the merging procedure, the structure of cluster number 2 is not used anymore. For the scission we break a clusters and all the new clusters are assigned a pointer which was initially zero.

The efficiency of the algorithm is due to the double representation of data in the computer memory: the list of the monomers with their coordinates, and a complete description of the space with the content of each site. At any time we know where a given monomer is, to which cluster it belongs and what is its neighborhood without scanning the complete monomer list. The cost is, of course random access memory but it saves a lot of computation time. Such a representation of data is possible nowadays because modern computers have a large memory capacity.

3.4.6 Movement of spheres

As explained before we can have three kinds of movement steps.

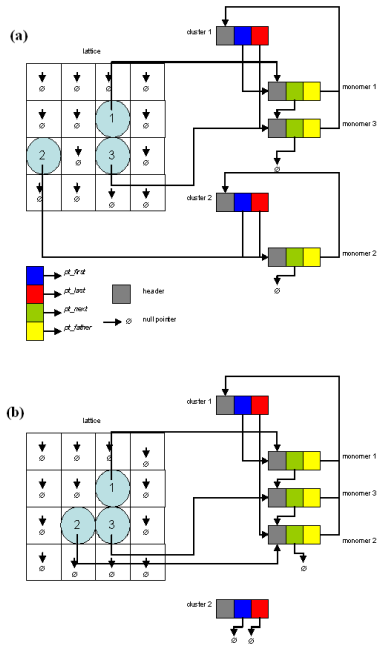

Figure 3.11: (a)Clusters before merging and (b) after merging.

Direction In the program we pre calculate 3156 different directions which are distributed uniformly over a sphere of unit diameter. The directions are stored in an array, so that to choose a random direction we need to pick only one random number instead of 3 for the 3 dimensions.

Collision We define a cylinder through which the monomer moves and then with help of simple geometry we detect a collision as shown in fig(3.12). Here the moving sphere is shown in red and the neighbor with which it will colloide is shown in blue. In the program we explore the region shown in black and whenever a sphere is found in this region we reject the movement or move it upto contact.

If we want to move the sphere up to contact we have to do a simple calculation. Let the new position of the CM of the moving monomer be **NCM1**, as shown in fig(3.13). The distance from the collison point **NCM1** to **I** can be calculated from the Pythogorean theorem for right triangles as the distance between **NCM1** and **CM2** is the diameter of the sphere. This is reduced to a simple geometrical problem of a line cut into two uneven lengths at **NCM1** and thus we can get the coordintes of **NCM1**.

$xcontact = (((e-d)*xa)+(d*x))*inv.e-x;$
$ycontact = (((e-d)*ya)+(d*y))*inv.e-y;$
$zcontact = (((e-d)*za)+(d*z))*inv.e-z;$

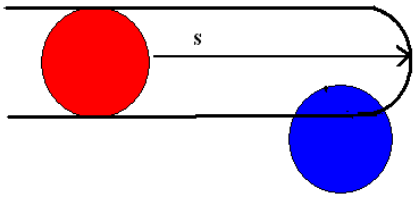

Figure 3.12: Schematic representation of the region explored for collision.

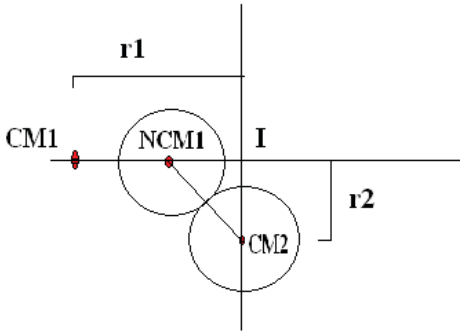

Figure 3.13: Schematic representationof the position of a particle intially at (CM1) from where it has moved up to contact with a particle at CM2 and reached position NCM1.

BCD1- Here we pick N_0 number of monomers randomly and give them a displacement in a random direction with magnitude s. Then we check for collision if we detect a collision we reject the movement or truncate it at contact. If the spheres stays in the same lattice after the movement only the position is adjusted but if the spheres moves to another lattice one of the 8 *pointers* which belong to the sphere is made a null pointer and the first free *pointer* of the new lattice is assigned to the sphere. Then we increment the physical time by s^2 as explained before.

BCD2- Here we have defined the diffusion coefficient of the cluster proportional to the cluster size with diffusion coefficient $d = \frac{3}{\Delta X+\Delta Y+\Delta Z}$ which is 1 for monomers. We randomly choose all N_c clusters and displace them in a random direction with step size $s/\sqrt{d}$. This ensures that the diffusion is inversely proportional to the diameter.

BCD3-Here we perform both BCD1 and BCD2 in succession. After BCD1 we calculate the CM of the clusters. Then we move the N_c clusters as explained in BCD2, but instead of choosing a new direction we calculate the direction of displacement of the cluster due to the BCD1 movement and move the cluster up to $s/\sqrt{d}$ as explained before. If the resultant displacement of any cluster is zero by chance then we take a random displacement and move the cluster a distance $s/\sqrt{d}$.

It is important to pick each cluster in one movement step as picking randomly N_c clusters results in many spheres moving more than s in one movement step. After one or more movement steps we proceed with a cluster construction step yielding a different configuration of clusters and the CM of the clusters are recalculated. After the cluster movement step the physical time is incremented with s^2.

The general algorithm using BCD3 can be represented as shown in fig(3.14)

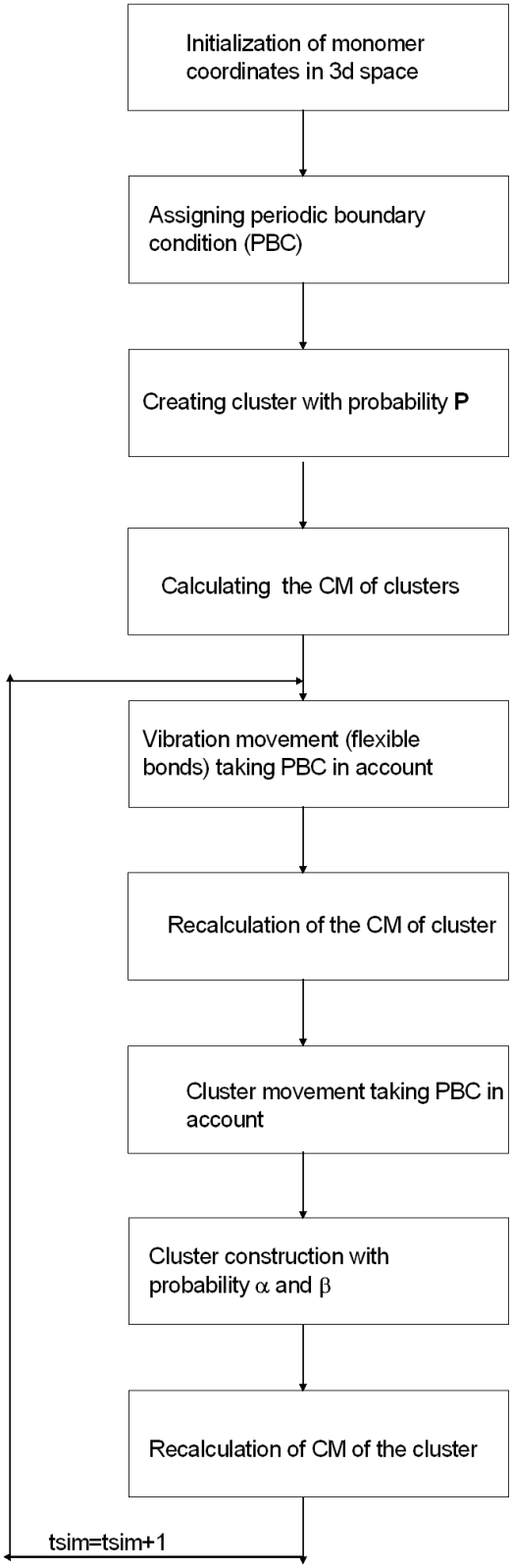

Figure 3.14: Algorithm of BCD3.

Chapter 4

Structure and kinetics of reversibily aggregating spheres with rigid bonds

[4.1] S. Babu, M. Rottereau, T. Nicolai, J. C. Gimel and D. Durand, J. Eur. Phys. E, **19** 203-211 (2006).
[4.2] S. Babu, J. C. Gimel and T. Nicolai, J. Chem. Phys., **125** 184512-1-10 (2006).

4.1 Flocculation and percolation in reversible cluster-cluster aggregation

Abstract

Off-lattice dynamic Monte-Carlo simulations were done of reversible cluster-cluster aggregation for spheres that form rigid bonds at contact. The equilibrium properties were found to be determined by the life time of encounters between two particles (t_e). t_e is a function not only of the probability to form or break a bond, but also of the elementary step size of the Brownian motion of the particles. In the flocculation regime the fractal dimension of the clusters is d_f=2.0 and the size distribution has a power law decay with exponent τ=1.5. At larger values of t_e transient gels are formed. Close to the percolation threshold the clusters have a fractal dimension d_f=2.7 and the power law exponent of the size distribution is τ=2.1. The transition between flocculation and percolation occurs at a characteristic weight average aggregation number that decreases with increasing volume fraction.

4.1.1 Introduction

Random aggregation of small particles is a commonly observed phenomenon and may lead to the formation of gels [85–88]. The initial stage of the aggregation process in dilute systems has been extensively studied using computer simulations [3, 4, 30, 89, 90]. Kinetic equations with the appropriate kernels have been used to model the growth [30, 31, 90]. Much less attention has been given to the situation where the clusters can no longer be considered dilute [23, 24, 91, 92]. As the clusters grow their cumulated volume fraction increases and at some point they will start to interpenetrate. Eventually irreversible aggregation leads to gelation at any concentration. If the aggregation process is reversible a steady state will be reached at a more or less advanced stage depending on the ratio of the aggregation and fractionation rate [42, 61, 93–100]. Also in this case the clusters may percolate the system, but now the gel is only transient [61, 96, 101–103].

In recent work we have simulated irreversible diffusion limited cluster-cluster aggregation (DLCA) from the initial state of monomers to the final state where all particles form a single percolating cluster [25, 26]. We have shown that as long as the average distance between the clusters is large (flocculation regime) they have a self-similar structure characterized by a fractal dimension d_f=1.8. With increasing cluster size the average distance between the clusters decreases and at a characteristic aggregation number ($m = m_c$) and radius of gyration ($R_g = R_c$) they fill up the whole space and start to interpenetrate. The aggregation of clusters larger than R_c, which leads to gelation, can be described by the percolation model [23–25, 35]. As a consequence the structure of the clusters on length scales larger than R_c is characterized by d_f=2.5. Also the size distribution changes from relatively monodisperse for clusters formed in the flocculation regime, i.e. $m < m_c$, to the power law size distribution for clusters formed in the percolation regime: $N(m) \propto m^{-2.2}$ for $m > m_c$.

This paper reports a study of the effect of bond breaking on the aggregation of spheres. The clusters stick at collision with probability α, and break at each diffusion step with probability β. The two limiting cases of diffusion (DLCA) and reaction limited (RLCA) cluster aggregation are obtained by setting α=1 and $\alpha \ll 1$, respectively. If α/β is small the equilibrium state contains essentially monomers, while if it is large most particles will be part of a single percolating cluster. The fact that the particles stick only at contact implies that solely binary collisions occur. Therefore the average number of neighbours per particle cannot exceed two as the bonds are rigid. This means that reversibility does not lead to densification and phase separation. The latter does occur if the interaction range is finite or if the bonds are not rigid [60, 98, 101, 104]. The present model of cluster-cluster aggregation is thus probably the simplest one that includes reversibility. We note that for lattice simulations more than one contact can be formed per collision so that densification and phase separation do occur [61, 105].

The paper is organized as follows. We will first explain the off-lattice simulation method used for this study and discuss the distinction between encounters and colli-

sions. This distinction was discussed earlier by Odriozola et al. [31, 42] in the context of irreversible RLCA and reversible DLCA. During one encounter the particles may have many correlated collisions before they move apart. In order to model the early stage of irreversible RLCA or reversible aggregation it is necessary to account for the number of collisions per encounter. It will be shown that the important parameter in the simulations is not the life time of a single bond, but the life time of an encounter (t_e). t_e is a function both of α/β and the number of collisions per encounter. The latter increases when the step size of the Brownian motion (s) is decreased. However, the simulations are independent of s if α/β is chosen in such a way that t_e is constant.

Next we will discuss the results obtained in the flocculation regime in terms of mean field theory using kinetic equations containing both an aggregation and a fragmentation kernel. These results will be compared with earlier simulations of reversible DLCA reported by Odriozola et al. [42]. Finally, we will show that if the fragmentation rate is decreased transient gels are formed and that the sol-gel transition can be described by the percolation model.

4.1.2 Simulation method

A cluster is chosen randomly and is moved with step size s in a random direction. The movement of a cluster occurs with a probability inversely proportional to its diameter which simulates Brownian motion. If the displacement of a cluster leads to overlap between two spheres or the wall it is truncated at contact. The displacement procedure is repeated a number of times equal to the total number of clusters in the box. Then bonds are formed with probability α between spheres in contact and bonds are broken with probability β. This cluster formation procedure defines the clusters that are moved in the subsequent displacement procedure. After these two procedures the simulation time (t_{sim}) is incremented by 1 and the whole process is repeated until equilibrium is reached. Contrary to Odriozola et al [42]. we do not move the clusters automatically apart when the bond is broken. If the clusters have not moved apart in the following movement procedure the bonds will be formed again with probability α in the next cluster formation procedure.

The starting configuration consists of N randomly positioned spheres with unit diameter in a box with size L at volume fraction ϕ. The physical time (t) is defined as the time needed for an individual sphere to diffuse a distance equal to its diameter: $t = s^2 \cdot t_{sim}$. For example the time unit would be $0.4s$ for spheres with a diameter of 1μm in water at 20°C. The effect of finite box size was studied and is negligible as long as the largest cluster in the box is smaller than L. The results shown in this paper are not influenced by finite size effects.

4.1.3 Encounter versus collision

Two initially decorrelated spheres that collide will have on average N_{col} collisions before they move apart and their positions become decorrelated again. The number

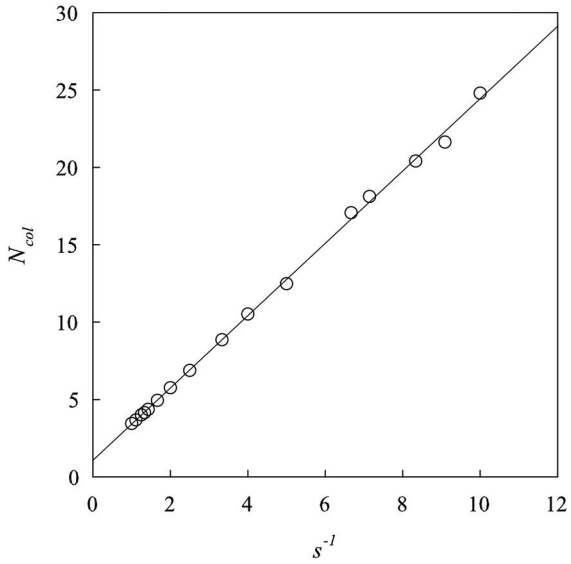

Figure 4.1: Dependence of the number of correlated collisions on the step size. The straight line represents a linear least square fit : $N_{col} = 1 + 2.36/s$.

of collisions per encounter is, of course, independent of α and β, but does depend on s. We have done simulations following the diffusion of two spheres that collide at $t = 0$. They show that N_{col} increases linearly with s^{-1}: $N_{col} = 2.36/s + 1$, see Fig.4.1. Here, we also count as a collision the event when two unbound spheres at contact move into each others direction and therefore remain at contact after the displacement procedure. This event will account on average for halve of the collisions. Each collision leads to a delay of the diffusion process proportional to α/β corresponding to the average time during which the particles are bound per collision. We will call the average time that the particles are bound during an encounter the life time of an encounter, which is a linear function of α/β and s, see appendix 1:

$$t_e = (2.36 + s) \cdot \alpha/\beta \cdot s \tag{4.1}$$

The distinction between collisions and encounters is important, because the properties of the system are not determined by the life time of a single bond, but by the total time that two spheres are bound during an encounter. We have verified that the same simulation results are obtained for different values of s and α/β if t_e remains the same. However, s needs in any case to be much smaller than the average distance between the surfaces of the spheres in order to assure Brownian motion between encounters as was discussed elsewhere for the case of irreversible aggregation [81].

In RLCA, encounters between larger clusters occur, which may have a larger number of correlated collisions before they move apart. In this case the bonds are permanent and the clusters retain their integrity during diffusion. In reversible aggregation, however, the clusters are transient and it is in our opinion more useful to consider encounters between larger clusters as a collection of a number of individual

sticky spheres. At any time an encounter may involve many clusters, contrary to the assumption of Odriozola et al. [42] who just considered encounters between only two stable clusters. At each simulation step any of the bonds in the cluster has probability β to break. As a consequence, the average life time (t_l) of a cluster with aggregation number m before any of its bonds breaks, decreases rapidly with increasing m and is proportional to s^2, see appendix 2. Large clusters can only diffuse a mean square distance of $< r^2 >= s^2/(\beta \cdot m^{1+1/d_f})$, before one of the bonds breaks. For a given t_e, $\beta \propto s$ (see Eq.4.1) so that $< r^2 > \propto s$. It follows that when a cluster fragments each of the parts will itself fragment before the parts have diffused apart by a significant distance.

4.1.4 Flocculation

Fig.4.2 shows the time dependence of the number averaged (m_n) and the weight averaged (m_w) aggregation number of the clusters for different values of t_e at $\phi = 0.5\%$ using $\alpha = 1$, i.e. reversible DLCA. The initial growth of m_n and m_w follows that of irreversible DLCA ($t_e = \infty$) as long as relatively few bonds are broken. At later times the growth of m_n slows down rapidly, while m_w continues to increase, which means that the polydispersity increases. Finally also the growth of m_w slows down until equilibrium values are obtained for $t \gg t_e$. Similar behaviour is seen at all volume fractions.

The effect of varying α for the same t_e is shown in Fig.4.3. Decreasing α slows the aggregation down, but does not modify the equilibrium structure. We have verified for different values of ϕ and t_e that the equilibrium structure is independent of α at fixed t_e. There is thus no distinction between reversible DLCA and RLCA at equilibrium. Therefore we have generally used $\alpha = 1$ for which equilibrium is reached quickest.

The size distribution and the structure of the clusters were determined at equilibrium for a range of t_e. Fig.4.4 shows that m has a power law dependence on R_g, which means that the clusters have a self similar structure with $d_f = 2.0$. The same value was found by Odriozola et al. from simulations of reversible DLCA. A fractal dimension of 2 is expected if each configuration has equal probability [106–108], which is the case for reversible aggregation where the clusters restructure rapidly compared to their diffusion rate. Fig.4.5 shows that the size distributions at different values of t_e, can be well described by a power law decay with an exponential cut-off at a characteristic aggregation number $m^* \propto m_w$:

$$N(m) = \kappa \cdot m^{-\tau} \cdot \exp(-m/m^*) \tag{4.2}$$

where $N(m)$ is the fraction of clusters with aggregation number m and $\tau = 1.5$. κ is related to m^* by the condition of mass conservation $\sum_m m \cdot N(m) = 1$, which gives $\kappa = (m^{*(2-\tau)} \cdot \Gamma(2-\tau))^{-1}$ for $m^* \gg 1$. It follows that:

$$m_w = \frac{1}{2\pi \cdot \kappa^2} \quad m_w \gg 1 \tag{4.3}$$

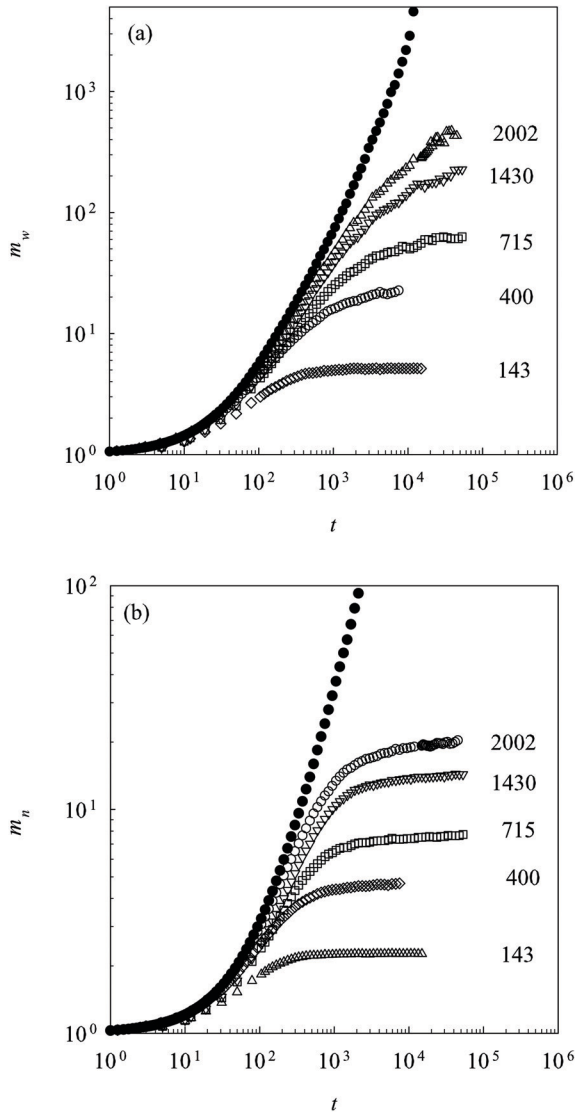

Figure 4.2: Time dependence of the weight averaged (a) and the number averaged (b) aggregation number for $\phi = 0.5\%$ at different values of t_e indicated in the figure. the closed symbols represent the result of irreversible DLCA.

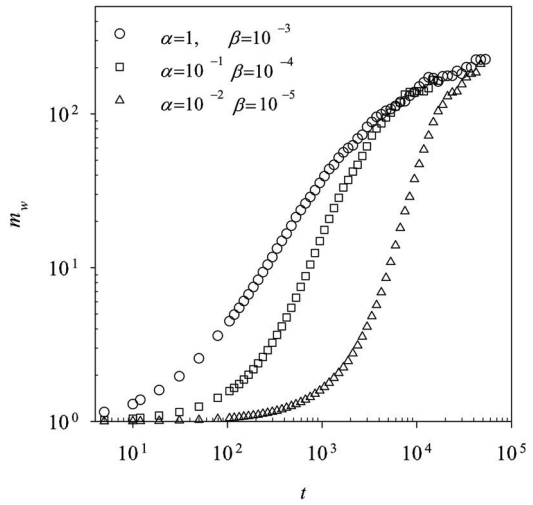

Figure 4.3: Comparison of the evolution of M_w of different values of α for the same value of t_e=1430.

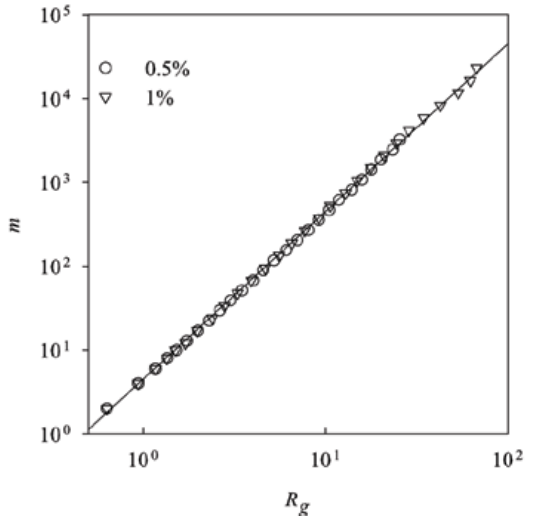

Figure 4.4: Dependence of the aggregation number on the radius of gyration for $\phi = 0.5\%$ and 1%. The straight line represents a linear least square fit and has a slope of 2.0.

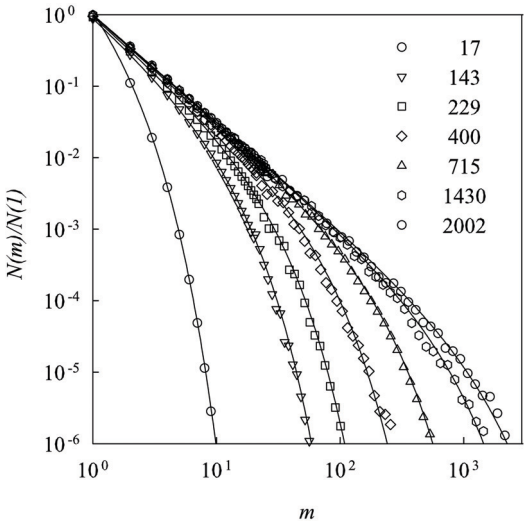

Figure 4.5: Cluster size distribution for $\phi = 0.5\%$ at different values of t_e indicated in the figure. The solid lines represent the fits to Eq.4.2.

$$m_n = \frac{1}{2\kappa} \quad m_n \gg 1 \tag{4.4}$$

If aggregation and fragmentation of the clusters does not depend on the position of the clusters, the time dependence of $N(m)$ can be written as [93]

$$\begin{aligned} \frac{dN(m)}{dt} &= \frac{1}{2}\sum_{i+j=m}[K(i,j)N(i)N(j) - F(i,j)N(m)] \\ &\quad -\sum_{j}[K(m,j)N(m)N(j) - F(m,j)N(j+m)] \end{aligned} \tag{4.5}$$

where $K(i,j)$ is the mean rate with which a cluster with size i binds to a cluster with size j, and $F(i,j)$ is the mean rate with which a cluster breaks up into two clusters with size i and j. In equilibrium the number of clusters of a given size stays constant and the condition of detailed balance gives:

$$K(i,j)\cdot N(i)\cdot N(j) = F(i,j)\cdot N(m) \tag{4.6}$$

If the collisions between the particles are uncorrelated the collision rate can be described by the Brownian kernel [41]:

$$K(i,j) = 4\pi\cdot(R_{col,i} + R_{col,j})\cdot(D_i + D_j) \tag{4.7}$$

where $R_{col,i} \propto i^{1/d_f}$is the collision radius and $D_i \propto i^{-1/d_f}$ is the diffusion coefficient of clusters with size i. At each collision the clusters form a bond with average life time: $s^2\cdot\alpha/\beta$, see appendix 1.

For $m_w \ll 1$ the average molar aggregation number is determined essentially by the monomer-dimer equilibrium. The concentration of encounters between two

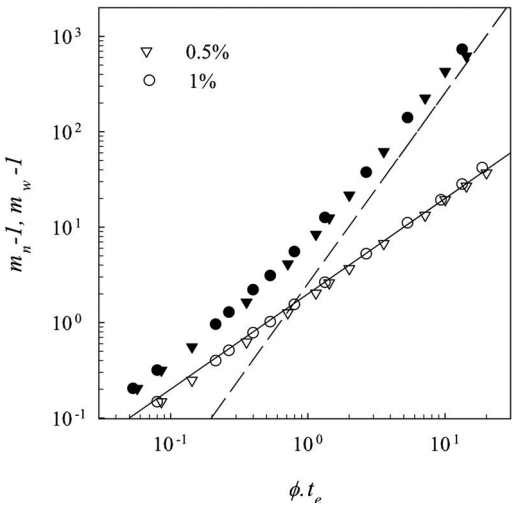

Figure 4.6: Dependence of the weight (open symbols) and the number averaged (closed symbols) aggregation number as a function of $\phi \cdot t_e$ for $\phi = 0.5\%$ and 1%. The solid line represents $m_n = 2.2\phi \cdot t_e$ and the dashed line $m_w = 3.0(\phi \cdot t_e)^2$.

spheres, C_e, is a function of the rate of formation and the rate of break-up of an encounter: $C_e = C \cdot K(1,1)/F(1,1)$, considering that the number concentration of spheres ($C = 6\phi/\pi$) is much larger than C_e. $K(1,1)$ is the collision rate of uncorrelated spheres, which is $4\pi/3$ in our simulations, because the spheres have radius 0.5 and diffusion coefficient 1/6. $F(1,1)$ is the rate at which the two monomers become decorrelated, which is equal to the inverse of the life time of an encounter (t_e). The fraction of dimers ($N(2)$) is proportional to the number of encounters: $N(2) \propto \phi \cdot t_e$. It follows that:

$$m_n - 1 = \frac{(m_w - 1)}{2} \propto \phi \cdot t_e \quad m_w - 1 \ll 1 \tag{4.8}$$

The dependence of $m_n - 1$ and $m_w - 1$ on $\phi \cdot t_e$ is shown in Fig.4.6 for 0.5% and 1% and is well described by Eq.4.8 for $m_w - 1 \ll 1$ using a proportionality factor of 2.2.

Remarkably, m_n has the same dependence on $\phi \cdot t_e$ also for large values, while m_w has a steeper dependence. The same dependence of m_n on $\phi \cdot t_e$ is only obtained for $m_n \gg 1$ if κ in Eq. 4.4 is equal to $0.23(\phi \cdot t_e)^{-1}$, which means:

$$m_n = 2.2\phi \cdot t_e \text{ and } m_w = 3.0(\phi \cdot t_e)^2 \quad m_w \gg 1 \tag{4.9}$$

The dashed line in Fig.4.6 shows that the simulation results for m_w approach the power law dependence asymptotically. Unfortunately, we are at the present stage not able to use box sizes with $L > 200$ that are necessary to simulate equilibrium states with even larger m_w.

For $m_w >> 1$ the cluster size distribution in equilibrium is given by Eq.4.2 if $K(i,j)$ and $F(i,j)$ are homogeneous ($K(ai,aj) = a^\lambda \cdot K(i,j)$ and $F(ai,aj) = a^\theta \cdot$

$F(i,j)$) and if the fragmentation kernel may be written as [109]:

$$F(i,j) = \kappa \cdot K(i,j) \cdot (i^{-1} + j^{-1})^{\tau} \tag{4.10}$$

The implication is that $\tau = \lambda - \theta$. For the Brownian collision kernel $\lambda = 0$ so that $\theta = -\tau$.

The clusters have a self similar structure and contain no loops. This would suggest that the number of bonds (e_{ij}) that connect a cluster with size i to a cluster with size $j = m - i$ is proportional to $m \cdot i^{-1}$ for $m \gg 1$ and choosing $i < j$. Odriozola et al. [42] found using computer simulations : $e_{i,j} = 0.439m \cdot (i^{-1} + j^{-1}) \cdot (i \cdot j)^{-0.136}$. The term $(i \cdot j)^{-0.136}$ is not expected for self similar clusters without loops if each bond has the same probability to break. If each bond breaking leads to decorrelation of the fragments then the fragmentation kernel would be: $F(i,j) \propto \beta/(s^2 \cdot \alpha) \cdot i^{-1}$.

However, the fragments become decorrelated only if they diffuse apart without colliding again. In our simulations monomers move at each step, but the probability of relative movement for two larger clusters is equal to $(D_i + D_j)$. Even if the fragments move apart they have a high probability to collide again. If we assume that the number of correlated collisions between the two fragments is equal to that found for two monomers ($N_{col}(i,j) = N_{col}(1,1)$), then the average total bond life time between the fragments is proportional to $t_e/(D_i + D_j)$. One may thus attempt to account for the correlation between collisions by writing the fragmentation kernel as:

$$F(i,j) \propto \frac{(D_i + D_j)}{t_e \cdot i} \tag{4.11}$$

The homogeneity exponent of this kernel is $\theta = -(1 + d_f^{-1}) = -1.5$, which is consistent with the simulation results.

Odriozola et al. [42] have deduced the number of correlated collisions explicitly as a function of i and j from computer simulations of RLCA. They obtained: $N_{col}(i,j) = N_{col}(1,1) \cdot (i \cdot j)^{0.35}$, but it is unclear why this result obtained on irreversibly bonded clusters is relevant for transient clusters with a very short life time compared to their diffusion rate. Nevertheless, they found that the fragmentation kernel obtained in this way could well describe the evolution of m_w in reversible DLCA. We note that the homogeneity exponent of their fragmentation kernel is very close to that of Eq.4.11: $\theta = -1.49$. However, neither the fragmentation kernel proposed by Odriozola nor Eq.4.11 is consistent with the condition of detailed balance (Eq.4.6) if the Brownian kernel is used to describe the collision rate. One may even wonder whether using a mean field theory (Eq.4.5) is justified for the case of reversible aggregation where collisions are highly correlated. In addition, as we have discussed above, the fragments can only move a very small distance before they break again.

4.1.5 Percolation

Flocculation describes the aggregation process of highly diluted systems when the clusters are on average far apart although the collisions may still be highly correlated,

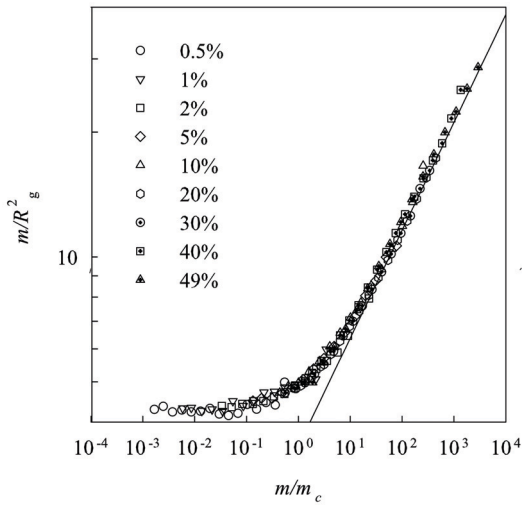

Figure 4.7: Dependence of m/R_g^2 as a function of m/m_c for different volume fractions indicated in the figure. The solid line has a slope of 0.37.

as we have seen in the previous section. However, for any given volume fraction the average distance between the clusters decreases with increasing t_e, because the size of the clusters increases and their density decreases. The cumulated volume fraction of the clusters can be calculated as:

$$V_{cum} = N \cdot \sum_{m=1}^{\infty} \frac{N(m)}{L^3} \cdot \frac{4\pi}{3} \cdot R_g^3(m) \tag{4.12}$$

In the flocculation regime Eq.4.12 becomes:

$$V_{cum} \propto \phi \cdot \kappa \int_1^{\infty} m^{\frac{3}{d_f}-\tau} \cdot \exp(-m/m^*)\, dm \tag{4.13}$$

where we have used Eq.4.2. It follows that $V_{cum} \propto \phi \cdot \sqrt{m_w}$ for $m_w \gg 1$ because $m_w \propto m^*$. At any volume fraction a transition from flocculation to percolation occurs when the clusters start to overlap, i.e. when V_{cum} is of order unity. As a consequence of this transition the structure and the size distribution of clusters change for clusters with m larger than a characteristic value $m_c \propto \phi^{-2}$.

The change in the fractal structure between flocculated clusters and percolated clusters is seen in Fig.4.7. In order to demonstrate the universality of the cross-over at m_c we have plotted m/R^2 as a function of m/m_c. This representation also allows for an accurate determination of the fractal dimensions in the limiting regimes of flocculation ($m \ll m_c$) and percolation ($m \gg m_c$) ($m/R^2 = (m/m_c)^{1-2/d_f}$). In the flocculation regime $d_f = 2.0$, while in the percolation regime $d_f = 2.7$, which is slightly above the value found for random percolation [35, 110] on lattices and irreversible aggregation ($d_f = 2.5$) [23–25]. The dependence of m_c on the volume fraction is compatible with $m_c \propto \phi^{-2}$, see Fig.4.8.

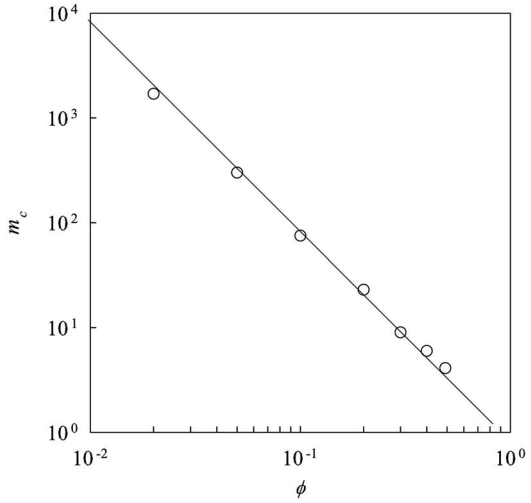

Figure 4.8: Dependence of m_c on the volume fraction. The solid line has a slope -2.

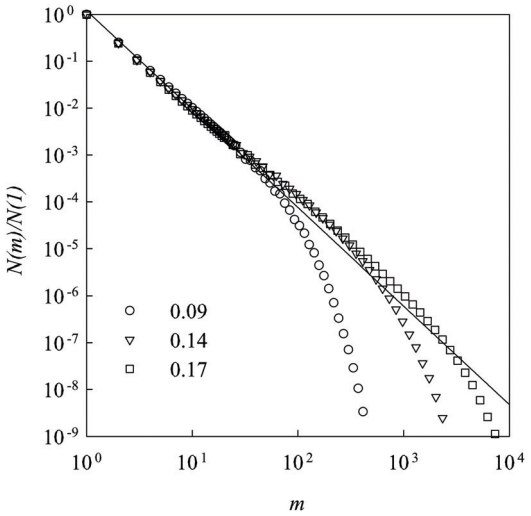

Figure 4.9: Cluster size distributions at different values of t_e indicated in the figure for $\phi = 49\%$. The solid lines has a slope of -2.1.

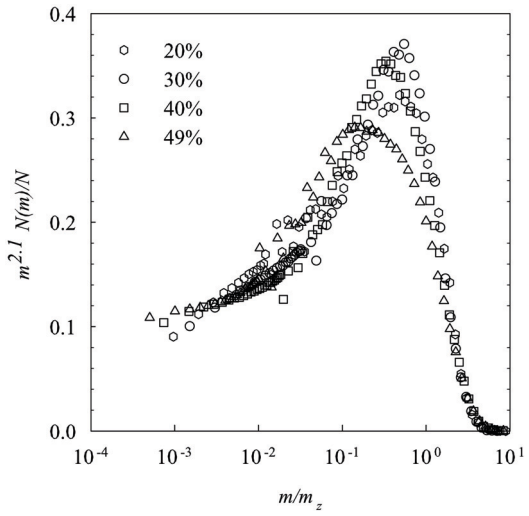

Figure 4.10: Cut-off functions of size distributions close to the gel point at different volume fractions indicated in the figure.

The number of percolating clusters with size m decreases with m following a power law as in the flocculation regime, but the exponent τ increases from the flocculation value 1.5 for $m \ll m_c$ to a larger value for $m \gg m_c$. In addition, the cut-off function at $m = m^*$ is no longer a simple exponential. For percolating clusters τ and d_f are related by the so-called hyper scaling law: $d_f = d/(\tau - 1)$, with d the spatial dimension. Simulations of site percolation on a cubic lattice gave $\tau = 2.2$ consistent with the hyper scaling law [35, 110]. The percolation regime is best observed for simulations at high volume fractions where m_c is small. Fig.4.9 shows cluster size distributions at different t_e for $\phi = 0.49$ where $m_c = 3.3$. For comparison a line representing $\tau = 2.1$ is shown, which is the value predicted by the hyper scaling law using $d_f = 2.7$. The power law decrease of $N(m)$ is observed only in a relatively narrow region, because finite size effects limit the exploration of very large clusters. At intermediate concentrations a cross-over between $\tau = 1.5$ and $\tau = 2.1$ occurs at $m \approx m_c$.

Assuming that $\tau = 2.1$ we can obtain the cut-off function of the size distribution by plotting $m^{2.1} \cdot N(m)/N$ as a function of m/m_z for $m \gg m_c$, where $m_z \approx m^*$ is the z-average aggregation number. Fig.4.10 shows the cut-off functions of size distributions close to the percolation threshold for a few high volume fractions. For static percolation on a cubic lattice a Gaussian cut-off function was found [35, 110]. In the present case the cut-off function has again the form of a Gaussian, but not with the same numerical constants. In addition, the shape of the cut-off function depends slightly on the volume fraction. It thus appears that the structure and the size distribution of percolating clusters obtained from reversible off-lattice simulations is slightly different from those obtained random percolation on a cubic lattice. The fractal dimension of percolating clusters obtained for on- and off-lattice simulations

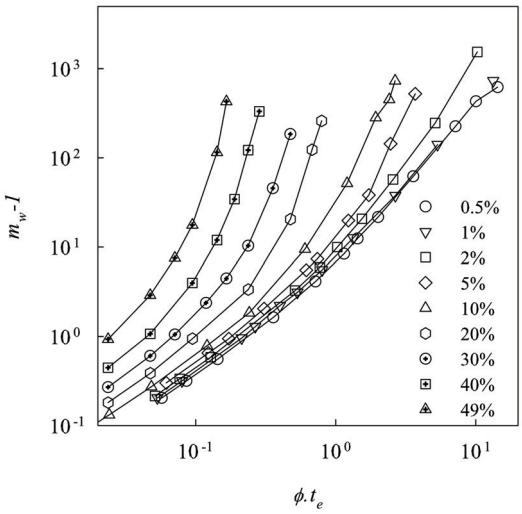

Figure 4.11: Dependence of the weight average aggregation number on $\phi \cdot t_e$ for different volume fractions indicated in the figure.

of irreversible DLCA is the same as found for random percolation. Unfortunately, these simulation results were not sufficiently precise to distinguish between $\tau = 2.2$ and $\tau = 2.1$.

For irreversible aggregation the transition from flocculation to percolation causes an acceleration of the growth rate [24, 25]. Fig.4.11 shows that also for reversible aggregation the transition causes an increase of the dependence of m_w on t_e for $m_w > m_c$. At each volume fraction m_w diverges at a critical value of $t_e = t_e^*$ where the system percolates, while m_n remains finite. If the flocculation-percolation transition is universal then m_w/m_c should be a universal function of t_e/t_e^* for $m_w \gg 1$, as was reported earlier for lattice and off-lattice simulations of irreversible aggregation [24, 25]. Fig.4.12 shows that a universal transition is also found for reversible aggregation.

The dependence of t_e^* on ϕ is shown in Fig.4.13. In the flocculation regime, i.e $m_w/m_c \propto (t_e/t_e^*)^2$, which implies that $t_e \propto \phi^{-2}$, because $m_w \propto \phi^2$ and $m_c \propto \phi^{-2}$. A line with slope -2 is drawn for comparison in Fig.4.13. Of course, this behaviour is only expected if the concentration is low enough so that the initial growth occurs in the flocculation regime.

In this work reversible aggregation of spheres was studied for the case that the bonds are rigid and formed only at contact. As mentioned in the introduction this implies that only binary collisions are possible and no densification can occur. We verified that in all cases each sphere was bound to on average $2 \cdot (1 - 1/m_n)$ neighbors. Therefore phase separation does not occur at any bond-breaking probability. Elsewhere we will show that if bond formation may occur not only at contact, but also if the particles are within a finite attraction range then a square well potential is mimicked and phase separation is observed if the attraction is sufficiently strong.

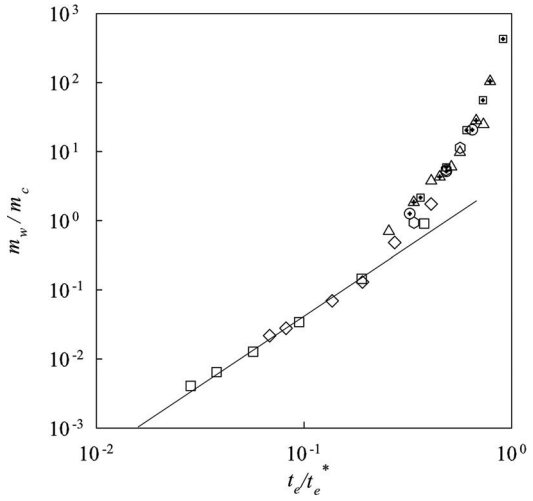

Figure 4.12: Representation of the data shown in Fig.4.11 for $\phi \geq 2\%$ and $m_w > 10$ in terms of the reduced parameters m_w/m_c and t_e/t_e^*. The solid line has a slope of 2.

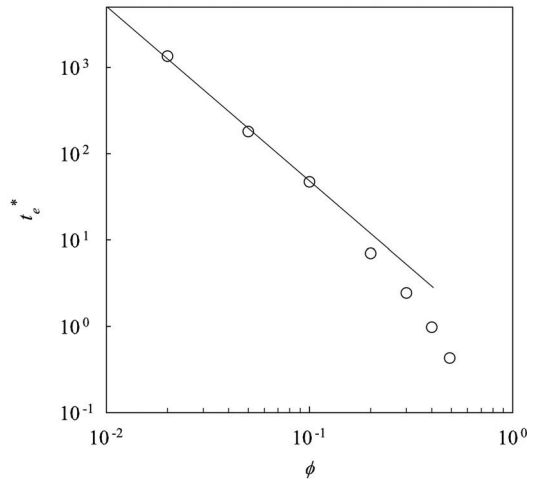

Figure 4.13: Dependence of the critical life time on the volume fraction. The solid line has a slope of -2.

4.1.6 Conclusion

The equilibrium properties of clusters formed by reversible aggregation are determined by the average life time of an encounter between two particles (t_e). The latter is not only a function of the bond formation (α) and break-up (β) probabilities, but also of the elementary step size (s) of the Brownian motion of the particles. At the same value of t_e the equilibrium state is the same both in the diffusion controlled limit ($\alpha = 1$) and in the reaction controlled limit ($\alpha \ll 1$). If the clusters are on average far apart, i.e. in the flocculation regime, then $d_f = 2.0$ while the size distribution has a power law decay with exponent -1.5 and an exponential cut-off. A transition to the percolation regime occurs with increasing t_e when the clusters start to overlap. At each volume fraction a transient gel is formed above a critical life time t_e^*. t_e^* decreases with increasing volume fraction and is proportional to ϕ^{-2} for small ϕ. Close to the percolation threshold the clusters have a fractal dimension $d_f = 2.7$ while the size distribution has power law decay with exponent $\tau = 2.1$ and a Gaussian cut-off. The transition between flocculation and percolation occurs at a characteristic weight average aggregation number that decreases with increasing volume fraction: $m_c \propto \phi^{-2}$.

4.1.7 Appendix 1

The probability that two monomers that collide form a bond is α. After the bond is formed it is broken with probability β at each simulation step.

The probability that the bond lifetime is $0, 1, 2$ or i simulation steps is: $P_0 = 1-\alpha$, $P_1 = \alpha \cdot \beta$, $P_2 = \alpha \cdot \beta \cdot (1-\beta)$ or $P_i = \alpha \cdot \beta \cdot (1-\beta)^{i-1}$ respectively. The average bond life time per collision in simulation steps is $\sum_i i \cdot P_i$, which gives:

$$\alpha \cdot \beta \cdot \sum_{i=1}^{\infty} i \cdot (1-\beta)^{i-1} = \frac{\alpha}{\beta}$$

The average physical life time (t_e) is thus:

$$t_e = N_{col} \cdot s^2 \cdot \frac{\alpha}{\beta}$$

4.1.8 Appendix 2

The probability that at least one of the bonds of a cluster of size m breaks in a single simulation step is:

$$1 - (1-\beta)^{m-1}$$

The probability that at least one bond breaks after i simulation steps is:

$$P(i) = [1 - (1-\beta)^{m-1}] \cdot (1-\beta)^{i \cdot (m-1)}$$

The average number of simulation steps during which they remain intact is:

$$\sum_{i=1}^{\infty} i \cdot P(i) = \frac{(1-\beta)^{m-1}}{1-(1-\beta)^{m-1}}$$

The average life time of a cluster (t_l) is thus:

$$t_l = s^2 \cdot \frac{(1-\beta)^{m-1}}{1-(1-\beta)^{m-1}}$$

Large clusters with $m \gg 1$ can only be formed for $m \cdot \beta \ll 1$ which gives:

$$t_l = \frac{s^2}{m \cdot \beta}$$

The average distance a cluster diffuses during that time is:

$$< r^2 >= \frac{t_l}{m^{1/d_f}}$$

4.2 Phase separation and percolation of reversibly aggregating spheres with a square-well attraction potential

Abstract

Reversible aggregation of spheres is simulated using a novel method in which clusters of bound spheres diffuse collectively with a diffusion coefficient proportional to their radius. It is shown that the equilibrium state is the same as with other simulation techniques, but with the present method more realistic kinetics are obtained. The behaviour as a function of volume fraction and interaction strength was tested for two different attraction ranges. The binodal and the percolation threshold were determined. The cluster structure and size distribution close to the percolation threshold were found to be consistent with the percolation model. Close to the binodal phase separation occurred through the growth of spherical dense domains, while for deep quenches a system spanning network is formed that coarsens with a rate that decreases with increasing attraction. We found no indication for arrest of the coarsening.

4.2.1 Introduction

The structure of a wide range of complex liquids is determined by the aggregation of small particles such as colloids [1, 85, 86, 111], protein [2, 87, 112], micelles [6, 113], or oil droplets [88]. Depending on the concentration, the range and strength of the attraction, stable cluster dispersions, transient gels or phase separated systems can be formed. In order to better understand these processes computer simulations have been done of model systems.

When the attraction is infinitely strong, irreversible aggregation occurs, which in theory always leads to percolation in the thermodynamic limit, however small the concentration. Of course, in practice gravity may cause precipitation before a space filling network is formed. Irreversible aggregation has been studied in detail using lattice and off-lattice numerical simulations [3, 4, 23–25, 27, 31, 37, 38, 89, 91, 114–124]. In the case of diffusion limited cluster aggregation (DLCA) particles form a bond with probability $\alpha = 1$ at each collision, while in the case of reaction limited cluster aggregation (RLCA) $\alpha \to 0$. Reversible aggregation has also been simulated, by introducing a probability (β) that the bond breaks [27, 42, 61, 73, 94–96, 102, 103, 105, 125–128]. In this way, systems in equilibrium are formed that are either a collection of transient clusters or a transient gel. The average probability that particles in contact are bound is $P = \alpha/(\alpha + \beta)$.

Here, we present off-lattice numerical simulations of reversible aggregation of hard spheres with a finite interaction range. Rigid bonds are formed and broken with probabilities α and β if the spheres are situated at a distance between 1 and $1 + \varepsilon$ in units of the diameter of the spheres. The interaction is thus equivalent to that of a hard spheres with a square-well potential with depth u in units of $k \cdot T$ and width ε. Particles that are within the interaction range are able to move independently only when their bonds are broken, which occurs with probability:

$$1 - P = \exp(u) \tag{4.14}$$

For square-well interactions it is straightforward to define bound particles as those that are at distances smaller than $1 + \varepsilon$ from each other. In this way clusters can be defined as ensembles of bound particles. With increasing volume fraction or interaction energy the average cluster size increases. The percolation threshold is defined as the point where a cluster spans the whole volume and has been determined for a limited number of cases [101, 129].

For the case of reversible aggregation, particles are bound only with probability P if they are within each others interaction range. As a consequence there are two different ways to define clusters: either as collections of particles that are within the interaction range or as collections of bound particles. We will call percolation in the first case contact percolation and in the second case bond percolation. The situation is analogous to that of site-bond percolation on lattices. Obviously, contact percolation occurs at lower volume fractions and weaker interactions than bond percolation as was shown in [105] for lattice simulations.

The equilibrium properties of spheres with square-well interaction have been obtained using various simulation techniques for a range of widths [14, 55–57, 63, 76, 101, 129–150]. Phase separation is found if the attraction exceeds a critical value depending on the volume fraction (ϕ) and ε. Coexistence curves have been determined for a number of well widths including the case $\varepsilon \to 0$ but with constant second virial coefficient (B_2) [151, 152], i.e the Baxter model [151–159]. The results are strongly dependent on ε, if expressed in terms of the interaction energy. However, they are close if expressed in terms of B_2. In fact, it turns out that the coexistence curves of any short range interaction potential are similar if expressed in terms of B_2 [60, 160].

In this paper we will show that the simulation of reversible aggregation leads to the same equilibrium properties as obtained from Monte-Carlo simulations, although not as efficiently. However, the method presented here allows one to study the development of the system. This is especially important for the detection of temporary gel formation during phase separation. The dynamics of spheres with a square-well interaction have been extensively investigated using molecular dynamics, but with this method the non-draining Brownian motion of the clusters is not correctly simulated. In addition, no distinction was made between contact and bond percolation.

The method employed here ensures that the diffusion coefficient of the clusters is inversely proportional to their radius. We have shown that this method leads to the correct aggregation kinetics for DLCA [25]. As mentioned above we simulate the situation that the bonds are rigid so that bound particles cannot move relative to each other. We are currently working on a modification of the method in which the particles within the clusters are free to move as long as no bonds are broken, which is the case in most molecular dynamics simulations.

We have done a systematic study for systems with $\varepsilon = 0.5$ and 0.1. We will present the results in terms of the second virial coefficient normalized by the particle volume (B_2), because, as mentioned above, the properties for different interaction ranges are close if the interaction is expressed in terms of B_2. B_2 is the sum of the excluded volume repulsion and the square well attraction: $B_2 = B_{rep} - B_{att}$. $B_{rep} = 4$ and B_{att} can be expressed in terms of P and ε [161]:

$$B_{att} = \frac{4P}{1-P}[(1+\varepsilon)^3 - 1] \tag{4.15}$$

where we have used eq. 4.14 to relate u and P. We will discuss first the phase behaviour and compare the binodal with Monte-Carlo simulations reported in the literature. Then we will discuss contact and bond percolation. By an analysis of the structure and the size distribution of clusters we will show that they have the well-known properties of percolating clusters. As far as we know, an analysis of the cluster structure during reversible aggregation using off-lattice simulation has not been reported earlier. Elsewhere, we will discuss the pair correlation function, the static structure factor, and the dynamical properties. We have checked that the initial concentration dependence of the pressure and the susceptibility was consistent with

the virial development using the analytical expressions for the second and third virial coefficient [161].

Recently, we reported a detailed study of the structure and size distribution of clusters formed by off-lattice reversible aggregation with zero interaction range [73]. The differences with results obtained here for non-zero interaction range will be discussed.

4.2.2 Simulation method

The simulations were done in a cubic box of size L with or without periodic boundary conditions. The unit of length is given by the diameter of the spheres. The starting configuration consists of N randomly positioned non-overlapping spheres in a box with size L so that the volume fraction is $\phi = (\pi/6) \cdot N/L^3$. The starting configuration is obtained either by a random insertion procedure or by equilibrating an initially non-random distribution by repeatedly moving the spheres a distance s in a random direction. If the displacement of a particle leads to overlap it is truncated at contact. The average distance between centers of mass of nearest neighbours is defined as $(1 + \Delta)$. In the initial state it is equal to the theoretical values obtained by Torquato [162] as long as s is significantly smaller than Δ.

After the random starting configuration is reached, clusters are formed in a cluster formation procedure by creating bonds with probability P between spheres that are at a distance between 1 and $1 + \varepsilon$. Then, in a displacement procedure, clusters (including monomers) are chosen randomly and attempted to be moved with step size s in a random direction. It is important to choose small step sizes, because the kinetics of the aggregation process is influenced if s is larger than about $\Delta/3$ [81]. In addition, the pair correlation function of the systems is influenced by the use of a finite step size for distances between 1 and $1 + s$ [81]. The displacement occurs with a probability inversely proportional to the radius of gyration of the cluster, which simulates Brownian motion for non-draining clusters [163]. If the displacement of a cluster leads to overlap between two spheres (or the wall for fixed boundary conditions) it is truncated at contact. During a single displacement procedure each cluster is on average chosen once. Thus the monomers have on average moved a distance s and the clusters a distance s divided by their radius. After the displacement procedure the simulation time (t_{sim}) is incremented.

The physical time is defined as the time needed for an individual sphere to diffuse a distance equal to its diameter: $t = s^2 \cdot t_{sim}$. For example, the time unit would be $0.4s$ for spheres with a diameter of $1\mu m$ in water at $20°C$. After the displacement procedure has been repeated n times the cluster formation procedure is run. Bonds are thus formed and broken with attempt frequency $f = 1/(n \cdot s^2)$ in physical time units. Instead of forming bonds with probability P irrespective of history one can break existing bonds with probability β and make new bonds with probability α during the cluster formation procedure. We have verified that this method gives the same equilibrium results if $P/(1 - P) = \alpha/\beta$. Reducing the attempt frequency is

equivalent to reducing both the bond formation and bond breaking probability by the same factor.

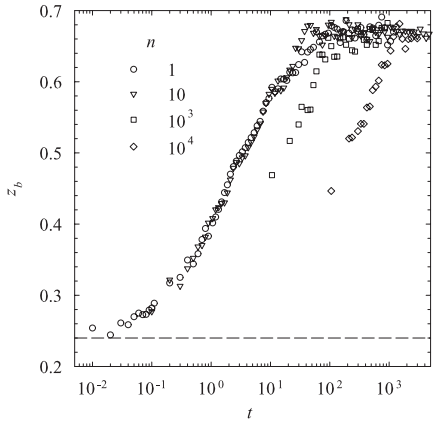

Figure 4.14: Time dependence of the bond coordination number (z_b) at different ratios of the movement procedure to the cluster formation procedure (n) indicated in the figure ($\phi = 2\%$, $\varepsilon = 0.5$, $B_{att} = 15$, and $s = 0.1$). The dashed line represents the value of z_b at $t = 0$ after the initial construction procedure.

Fig. 4.14 shows an example of the evolution of the average bond coordination number (z_b) of the particles for $\phi = 2\%$, $\varepsilon = 0.5$ and $B_{att} = 15$ using different attempt frequencies. As expected, the same equilibrium state is reached independently of the attempt frequency, but the time to reach equilibrium increases if n is large. $n = 1$ corresponds to diffusion limited aggregation, while $n \to \infty$ corresponds to reaction limited aggregation. Since the CPU time of the cluster formation procedure is longer than the displacement procedure it is favourable to increase n. The kinetics in terms of the physical time will be influenced up to at least $n \cdot s^2$. In practice the gain of increasing n becomes negligible for $n > 10$ and we have used $n = 10$ in most of the simulations presented here.

For reversible aggregation with $\varepsilon = 0$ and finite step size it was shown that the equilibrium properties are not determined by the average life time of a bond, but by the average life time of an encounter between two spheres. The second is longer than the former, because two spheres can have many correlated collisions. It was shown [73] that the number of correlated collisions is inversely proportional to s. The (physical) life time of an encounter is proportional to the number of correlated collisions and thus for a given attempt frequency it increases linearly with the step size.

For finite interaction ranges with $s < \varepsilon$ the encounter life time is longer, because the spheres have to diffuse out of each others interaction range. Since the particles can only move if they are not bound the average diffusion coefficient within the well is multiplied by $(1 - P)$ compared to diffusion outside the well. The life time of an encounter is determined by the physical time it takes to diffuse out of the well, which

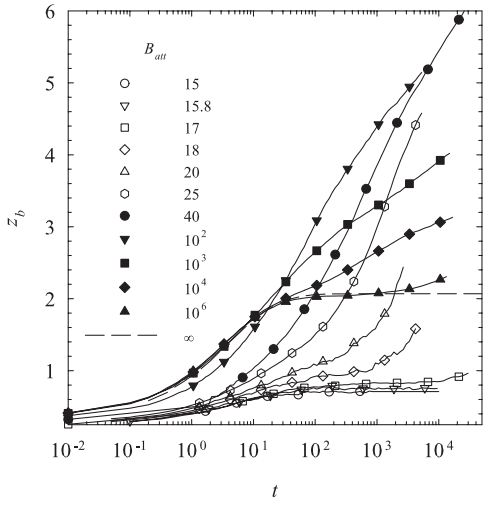

Figure 4.15: Time dependence of the bond coordination number (z_b) at different values of B_{att} indicated in the figure ($\phi = 2\%$ and $\varepsilon = 0.5$). The dashed line indicates the evolution for irreversible DLCA.

becomes independent of the step size for $s \ll \varepsilon$. We verified that the influence of the step size on the equilibrium results is negligible for $s < \varepsilon/5$. In our simulations we have used step sizes that were smaller than $\min(\Delta/3, \varepsilon/5)$. It is clear that very small step sizes need to be used at high concentrations or small interactions ranges, which limits the physical time that can be explored.

The effect of finite box size was studied and is negligible as long as the largest cluster in the box is smaller than L. The results shown in this paper are not influenced by finite size effects unless specified explicitly. Both fixed and periodic boundary conditions have been used with the same results.

4.2.3 Results and discussion

Phase behaviour

Fig. 4.15 shows the evolution of the average bond coordination number, z_b, for different values of B_{att} at $\phi = 2\%$ and $\varepsilon = 0.5$. For B_{att} smaller than about 16, z_b increases monotonically and then stabilizes when equilibrium is reached. For B_{att} larger than 16, however, z_b continues to increase and shows no sign of stabilizing within the duration of the simulation. The reason is that for B_{att} larger than 16 the system phase separates into a phase with low density (gas phase) and one with high density (dense phase). For $B_{att} > 10^3$ the initial increase is close to that of irreversible aggregation ($B_{att} = \infty$), but it deviates after a time that increases with increasing B_{att}. A second metastable state is observed very close to the binodal, because a certain time is needed to create large enough nuclei to initiate growth of the dense

phase.

Fig. 4.16 shows images of the system during phase separation for two values of B_{att}. Very close to the binodal ($B_{att} = 17$), phase separation occurs by the formation of a dense domain that grows with time. In order to observe the formation of the dense cluster more clearly in the sea of small clusters we show only clusters containing more than 20 particles. It can be seen that most large clusters have an open ramified structure. Only when by chance one of these clusters obtains a denser structure does it serve as a seed for further growth. Clearly, for nucleating a dense liquid it is not enough that the cluster reaches a critical size, but in addition it needs to have a dense structure.

With increasing attraction the fractal clusters grow larger and the density of nuclei increases. The critical size of the nuclei is much smaller than the radius of the larger clusters. Therefore phase separation occurs as densification of fractal clusters, which is in competition with the growth of the clusters. The strands of the clusters thicken progressively and the clusters become progressively more spherical. Above a critical value of B_{att} a space filling ramified structure is formed that coarsens. The dense phase is initially a percolating structure of increasingly thicker strands in equilibrium with a gas phase of small clusters that retain their fractal structure. In the long run, coarsening leads to break-up of the system spanning structure. With increasing B_{att} the coarsening process slows down until in the limit of irreversible aggregation only the initial process of the formation of the percolating structure is observed.

Similar features have been shown and discussed earlier for lattice simulations [105]. These characteristic features are generally called nucleation and growth, and spinodal decomposition, respectively. We stress, however, that there is no unambiguous signature to distinguish nucleation and growth from spinodal decomposition. We have not seen crystallisation during the duration of the simulations, even though in some situations the crystal phase is most stable. The reason is that the pathway to create crystals is highly improbably when only rigid bonds are formed.

Very recently, molecular dynamics simulations of spheres with a very narrow square well interaction ($\varepsilon = 0.005$) were reported [63]. For a quench at $B_{att} = 48$ they observed slow coarsening of the percolated structure similarly to the results obtained here and the earlier lattice simulations. However, for a very deep quench of $B_{att} = 2.9 \times 10^7$ they found no sign of ripening of the network within the duration of the simulations. This situation corresponds to the metastable state that is reached when the bond breaking probability is very low. The percolated structure obtained by molecular dynamics at very large B_{att} shows thicker strands than obtained by the present simulation method and z_b is larger. The reason is that with the former method particles can move freely within the interaction range without breaking bonds. With the present method the bonds are rigid so that even for relative movements within the interaction range bonds need to be broken.

It was suggested that the absence of ripening for large B_{att} was caused by glass formation of the dense phase [63, 104]. Clearly, glass formation will impede further densification so that the dense phase may not reach it equilibrium density. However,

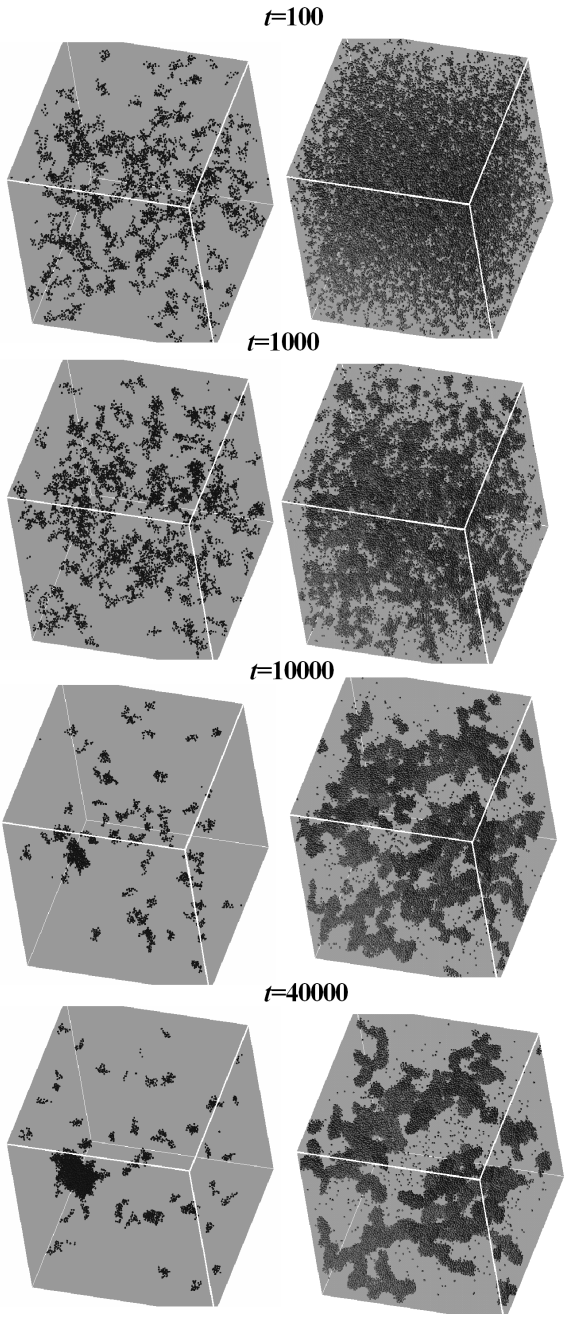

Figure 4.16: Images of attractive spheres ($\phi = 2\%$, $L = 100$, and $\varepsilon = 0.5$) taken at different times indicated in the figure. For $B_{att} = 17$ (left panel) the phase separation occurs through nucleation and growth, while for $B_{att} = 40$ (right panel) a network structure is formed that coarsens. For clarity, only clusters containing more than 20 particles are shown for $B_{att} = 17$.

bulk vitrification does not stop coarsening through a process of evaporation and condensation, since the particles at the surface are not in the glassy state. In our view the coarsening is simply too slow at very large B_{att} to be observed due to the very small probability to break bonds.

Just below the phase boundary z_b levels-off for some duration. The reason is that just below the phase boundary the system is meta-stable until a dense nucleus of sufficient size and density is formed by random fluctuations. The duration of the meta-stable state increases with decreasing B_{att} and diverges at the binodal. As mentioned before, a second metastable state is observed for very large values of B_{att} during which the coarsening of the network is not yet significant. The properties of this meta-stable state are the same as those obtained by irreversible aggregation. Only for these cases can cluster growth be distinguished in time from phase separation. At intermediate values of B_{att} the two occur simultaneously.

One way to determine the binodal is to increase B_{att} progressively until an upturn is observed for z_b as a function of time. Obviously, the value of B_{att} at the binodal will be overestimated in this way to an extent that depends on the total duration of the simulation. Alternatively, one can determine the value of B_2 at the binodal by decreasing B_{att} starting from a phase separated system until the dense phase melts completely. Combining the two methods it can be verified that a system is in true equilibrium. In this way we found that the system at $B_{att} = 15.8$ is in fact meta-stable, while the system at $B_{att} = 15$ is stable, see Fig. 4.17. At $B_{att} = 15.8$ the dense phase formed at larger B_{att} initially evaporates partially, but some of it remains to serve as a nucleus for further long time growth. At $B_{att} = 15$ the dense phase evaporates completely.

For a given value of B_{att} in the two phase regime, one can estimate the densities of the two phases by measuring the local density distribution. This was done by placing randomly a sphere with diameter D and counting the number of particles in this sphere. D has to be chosen large enough so that the fluctuations within each phase are not too big, but significantly smaller than the domain size of the dense phase. We have found that D between 5 and 6 constitutes a good compromise.

Fig. 4.18 shows an example of the evolution of the density distribution during phase separation at $B_{att} = 16$, $\phi = 5\%$ and $\varepsilon = 0.5$. Initially, one observes broadening of the distribution and a shift of the peak position to smaller densities. After some time the position stabilizes and a separated peak representing the dense phase develops as the dense domains grow. The broad range of intermediate values between the two peaks is caused by the surface of the dense domains. The high density peak will continue to grow and become better separated from the low density peak as the coarsening process continues. After completion of the coarsening process the relative amplitudes of the peaks depend on the concentration, but their positions are the same for a given B_{att}. Unfortunately, since the simulation took already several weeks it is not possible to extend it to much longer times with the current generation of computers. The peak position of the low density peak stabilizes relatively quickly, but for the high density peak long simulation times are needed to approach its equilibrium

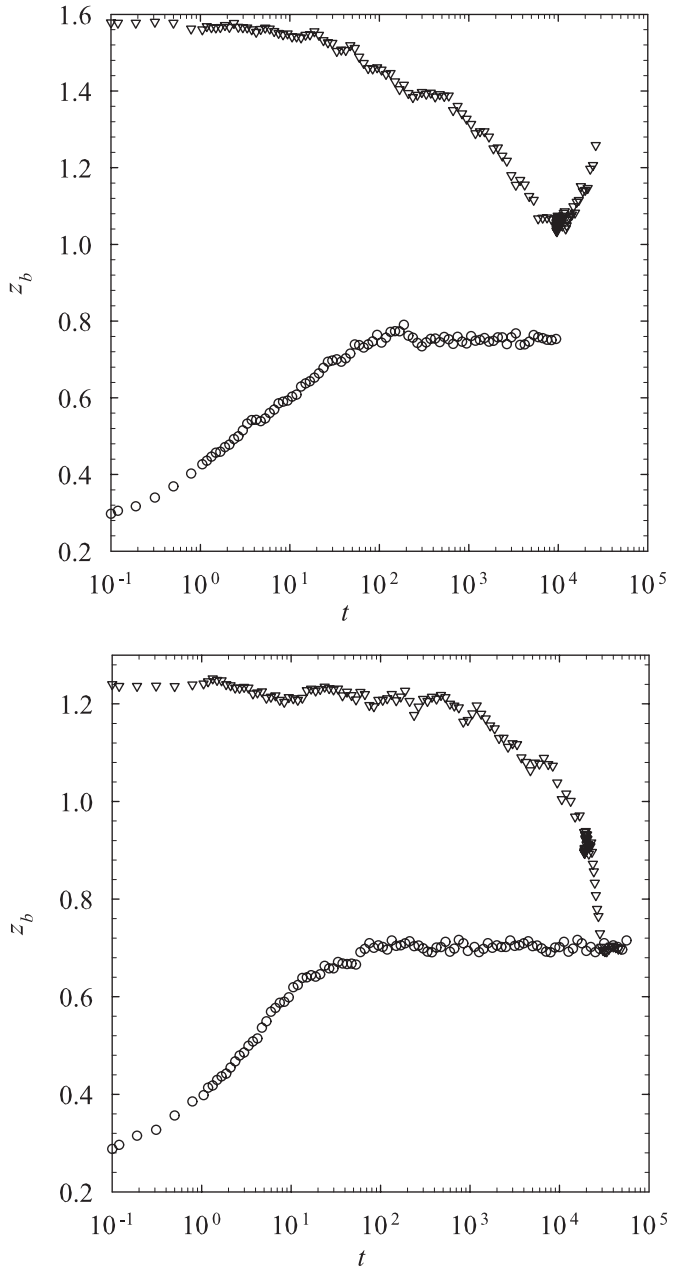

Figure 4.17: Time dependence of the bond coordination number (z_b) at $B_{att} = 15.8$ (top) or $B_{att} = 15$ (bottom) starting from a random distribution of particles (circles) or from a phase separated system (triangles) formed at larger B_{att} ($\phi = 2\%$ and $\varepsilon = 0.5$). For $B_{att} = 15$ the system reaches the same equilibrium state independent of the starting configuration. For $B_{att} = 15.8$ the system phase separates and the apparent steady state does not represent an equilibrium, but a meta-stability.

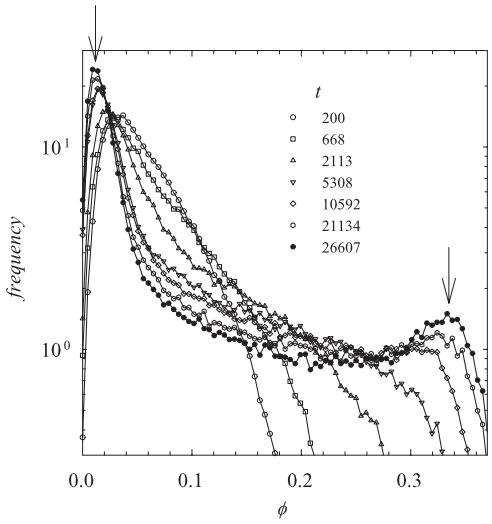

Figure 4.18: Example of the evolution of the density distribution during phase separation ($\phi = 5\%$, $\varepsilon = 0.5$, and $B_{att} = 16$). The arrows indicate approximately the average equilibrium densities of the gas and the dense phase.

value.

Examples of density distributions at long times are shown in Fig. 4.19 at different values of B_{att} for $\phi = 5\%$ and $\varepsilon = 0.5$. In Fig. 4.19 the peak positions, but not their shapes, are close to equilibrium. In the one phase regime a single peak is observed that broadens with increasing B_{att}. For phase separated systems one observes two peaks representing the densities of the two phases.

Using a combination of methods we have estimated the binodal for $\varepsilon = 0.5$ and $\varepsilon = 0.1$, see Fig. 4.20. The results for $\varepsilon = 0.5$ are compared with Monte-Carlo simulations reported in the literature [55]. The results obtained by the present simulation method are consistent with earlier results albeit not as accurate especially concerning the dense phase. However, the objective of the simulation method presented here was not to obtain an accurate description of the binodal, but to obtain realistic kinetics of the evolution of the system. For $\varepsilon = 0.1$ we have already reached the limit of very small interaction range and the results are close to those of the Baxter model reported in [152].

Interestingly, the equilibrium values of z_b in the one-phase regime increase linearly with B_{att} until the binodal is approached for $\phi < 10\%$ or the percolation threshold for $\phi > 10\%$, see Fig. 4.21. The slope is proportional to the concentration and we find $z_b = 2 \cdot B_{att} \cdot \phi$ both for $\varepsilon = 0.1$ and $\varepsilon = 0.5$. z_b is equal to the average contact coordination number (z_c) multiplied with the probability that a bond is formed: $z_b = P \cdot z_c$. The average bond energy per particle (E) is u times the number of contacts per particle, i.e $E = 1/2 \cdot z_c \cdot u$. Since $u = \ln(1-P)$ it follows that: $E = 1/2 \cdot z_b \cdot \ln(1-P)/P$. In the mean field approximation the decrease of the free energy per particle caused by

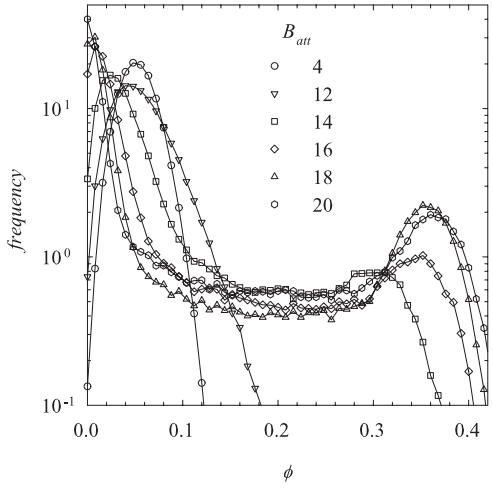

Figure 4.19: Density distributions obtained at long times of systems at different B_{att} indicated in the figure ($\phi = 5\%$ and $\varepsilon = 0.5$). For $B_{att} > 12$ the system phase separates and the peak positions indicate approximately the average equilibrium densities of the gas and the dense phase.

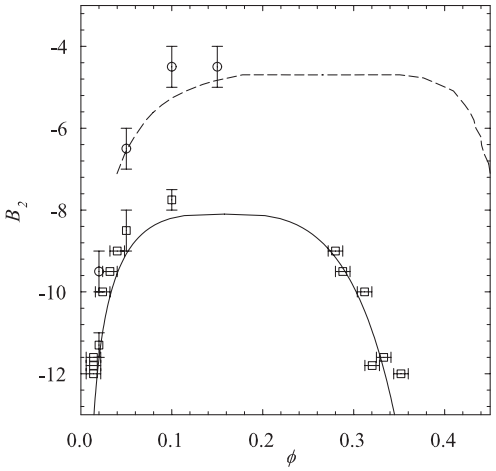

Figure 4.20: Phase diagram in terms of the second virial coefficient (B_2) and the volume fraction (ϕ) for $\varepsilon = 0.1$ (circles) and $\varepsilon = 0.5$ (squares). The dashed and solid line represent the binodal for $\varepsilon = 0$ and $\varepsilon = 0.5$, respectively, obtained from other types of simulations taken from the literature [55, 152]. The vertical error bars represent the difference between the lowest value of B_2 tested for which the system remained homogeneous and the highest value of B_2 where the system phase separated. Horizontal error bars represent the uncertainty in determining the peak position of the density distributions of phase separated systems.

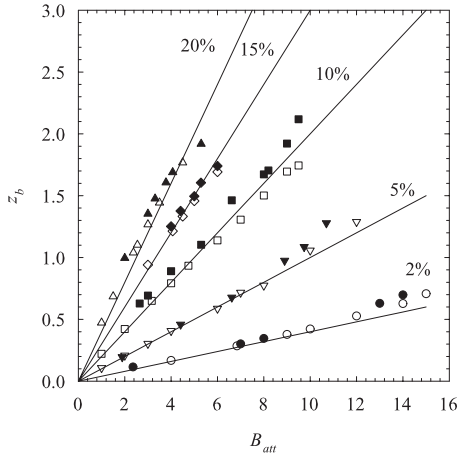

Figure 4.21: Dependence of the equilibrium bond coordination number (z_b) as a function of B_{att} at different values of ϕ indicated in the figure for $\varepsilon = 0.1$ (filled symbols) and $\varepsilon = 0.5$ (open symbols). Solid lines represent $z_b = 2B_{att} \cdot \phi$.

bond formation may be written as $E = -B_{att} \cdot \phi$ if we consider only binary contacts. It follows that in this approximation $z_b = -2 \cdot B_{att} \cdot \phi \cdot P/\ln(1-P)$, which is equal to $z_b = 2 \cdot B_{att} \cdot \phi$ for small values of P and thus small values of B_{att}. However, the latter relation is observed also for larger values of P. Apparently, the effect of finite P is compensated by the loss of configurational entropy, which is ignored in the mean field approximation.

Percolation

The percolation threshold was defined as the point where a system spanning cluster is first observed. It was reported earlier [157, 158] that the percolation threshold was not very sensitive to finite size-effects for $L > 10$. Fig. 4.22 shows an example of the probability to percolate as a function of ϕ for $B_{att} = 10$ and $\varepsilon = 0.5$. There is a small, but significant finite size effect even for $L > 10$. Finite size effects are perhaps not very important when determining the percolation threshold, but it is clear that for a proper analysis of the structure and the size distribution of the clusters, shown below, large box sizes are necessary. We have used $L = 100$ for $\phi = 10\%$ and $L = 50$ for higher volume fractions.

In the two phase regime only the dense phase percolates at equilibrium, with the exception of a very small regime close to the critical point where both phases percolate, because the percolation line crosses the binodal below the critical concentration. However, as the system evolves starting from a random distribution, the whole system may percolate temporarily. An example of percolation during phase separation is shown in Fig. 4.16 for $B_{att} = 40$. Break-up of the percolation due to coarsening was not yet observed during the simulation, but it has been shown to occur in lattice

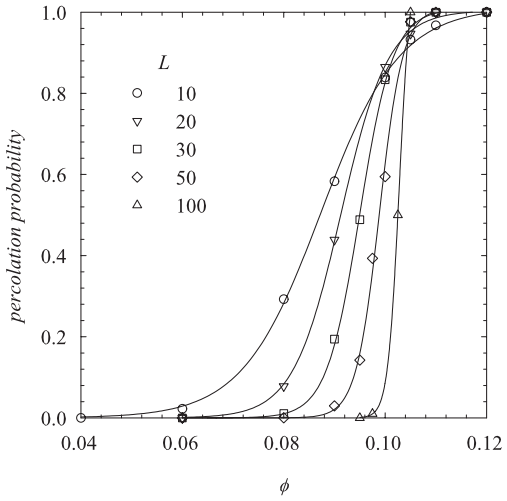

Figure 4.22: Example of the percolation probability as a function of the concentration for different box sizes indicated in the figure ($\varepsilon = 0.5$ and $B_{att} = 10$). Solid lines are guides to the eye.

simulations of reversible aggregation [105].

Fig. 4.23 shows that the percolation thresholds expressed in terms of $B_2 = 4 - B_{att}$ are close for $\varepsilon = 0.5$ and 0.1. For $\phi < 10\%$ the percolation is temporary since the system phase separates. Simulations of the Baxter model, i.e. $\varepsilon = 0$ and $u = -\infty$, [152] gave a percolation threshold at a slightly higher concentration for a given value of B_2, see solid line in Fig. 4.23. These results were, however, obtained for very small box sizes ($L < 10$). Note that the adhesiveness parameter used in the Baxter model (written as τ) is equal to B_{att}^{-1}. The results may also be compared with the percolation threshold of randomly distributed spheres, i.e. the system at the start of the simulation. This process is called static percolation in distinction with the present case where the particles diffuse that we call dynamic percolation. In [164] results were reported for static percolation of randomly distributed hard spheres with different interaction ranges. The percolation thresholds could be described analytically in terms of the free volume. The results are reproduced in Fig. 4.23 for $\varepsilon = 0.5$ and 0.1 in terms of B_2. At high volume fractions the static percolation thresholds are very close to the ones for dynamic percolation implying that Brownian motion does not lead to strong modification of the relative positions of the particles and that the percolation process is essentially random distribution of bonds. The reason is that for high concentrations $\Delta < \varepsilon$ and the interaction range of the particles is already strongly overlapping at t=0. As a consequence, the percolation threshold becomes independent of ε and depends only on P. Thus for large ϕ when $\Delta < \varepsilon$ the percolation threshold is not independent of ε when expressed in terms of B_2 even for small ε. At low volume fractions the randomly distributed system cannot percolate even for $P = 1$

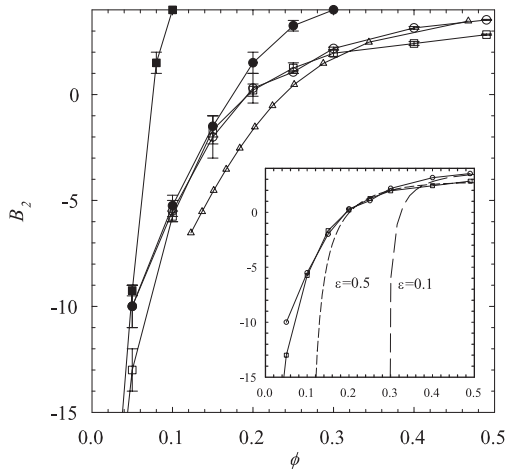

Figure 4.23: Comparison of the contact (filled symbols) and bond (open symbols) percolation thresholds obtained at $\varepsilon = 0.1$ (circles) and $\varepsilon = 0.5$ (squares). The triangles represent the result for $\varepsilon = 0$ taken from the literature [152]. The solid lines are guides to the eye. The insert shows a comparison of the dynamic bond percolation thresholds with the values for static bond percolation taken from [164] indicated by dashed lines.

($B_2 \to -\infty$) and Brownian motion is necessary for percolation to occur.

So far we have considered bond percolation, but the same can be done for contact percolation. As mentioned above, for $\varepsilon \to 0$ contact and bond percolation are the same ($P \to 1$). The contact percolation thresholds for $\varepsilon = 0.1$ and 0.5 are close to those obtained from Monte-Carlo simulations [101, 129]. Contact percolation is obtained for smaller B_{att} than bond percolation, see Fig. 4.23, but they become close at low concentrations for which P approaches unity at the percolation threshold. For contact percolation attraction is not a necessary condition. Static contact percolation occurs even for randomly distributed hard spheres without attraction (P=0) for $\phi >$ 10% at $\varepsilon = 0.5$ and for $\phi > 28\%$ at $\varepsilon = 0.1$ [164].

Cluster structure and size distribution

Fig. 4.24 shows the dependence of the aggregation number (m) of the clusters on their radius of gyration (R_g) obtained at different volume fractions close to the percolation threshold. For self-similar clusters m has a power law dependence on R_g:

$$m \propto R_g^{d_f} \tag{4.16}$$

where d_f is the so-called fractal dimension. The solid lines have slopes 2.5 and 2.6, which shows that the fractal dimension of the clusters is compatible with the percolation model. For a given value of R_g, m is slightly bigger at higher concentrations,

because $\Delta < \varepsilon$ at the start of the simulation. For more dilute systems the distance between nearest neighbours is controlled by the diffusion process and therefore close to ε, which explains why the clusters are slightly denser using $\varepsilon = 0.1$ than using $\varepsilon = 0.5$.

We have determined the number of clusters with aggregation number m ($N(m)$) at equilibrium. $N(m)$ decreases with m following a power law with a cut-off at a characteristic size m^*:

$$N(m) \propto m^{-\tau} \cdot f(m/m^*) \tag{4.17}$$

The cut-off function has the properties of becoming a constant for $m \ll m^*$ and decreases more rapidly than a power law for $m > m^*$. Fig. 4.25 shows examples of $N(m)$ for different values of B_{att} at $\phi = 10\%$ and $\varepsilon = 0.5$. Similar results are obtained for other volume fractions and for $\varepsilon = 0.1$. $N(m)$ broadens with increasing B_{att} until the system percolates and a space filling network is formed. If B_{att} is further increased the clusters size distribution splits up between a gel and sol fraction. In the thermodynamic limit ($L \to \infty$) the molar mass of the percolating cluster diverges, but for finite box sizes it cannot exceed the total number of particles used in the simulation.

At the percolation threshold $N(m)$ is expected to follow a power law decay for large m: $N(m) \propto m^{-\tau}$. We find for all concentrations and both interaction ranges $\tau = 2.15 \pm 0.05$, which is compatible with the percolation model [35].

We have calculated the weight average aggregation number of the clusters as: $m_w = \sum m^2 \cdot N(m)/N$. The dependence of m_w on B_{att} at equilibrium is shown in Fig. 4.26. In this representation the results for $\varepsilon = 0.1$ and 0.5 are close. With increasing B_{att}, the size of equilibrium clusters grows and m_w diverges at the percolation threshold. For volume fractions below approximately 10% the binodal is reached before the system percolates and the value of m_w at the binodal decreases strongly with further decrease of the concentration. Beyond the percolation threshold the gel fraction increases and m_w of the sol fraction decreases with increasing B_{att}.

Fig. 4.27 shows that m_w plotted as a function of z_b is independent of ϕ and ε for small z_b. We found the same initial dependence of m_w on z_b also for on-lattice simulations and off-lattice simulations with $\varepsilon = 0$. The average number of bonds per particle at the percolation threshold is close to two at lower concentrations, and decreases weakly with increasing ϕ. If the aggregates contain no loops then $z_b = 2(1-1/m_n)$ where m_n is the number average aggregation number: $m_n = N/\sum N(m)$. The fraction of loops is calculated as $1-2(1-1/m_n)/z_b$. In the homogeneous regime it is less than 0.2 up to the percolation threshold. For the same ϕ and B_{att}, the fraction of loops is somewhat smaller when $\varepsilon = 0.5$ than when $\varepsilon = 0.1$.

Comparison with reversible aggregation with zero interaction range

Recently, we reported a detailed study of the structure and size distribution of clusters formed by off-lattice reversible aggregation with zero interaction range [73]. These simulations are different from the Baxter model for which the interaction range also

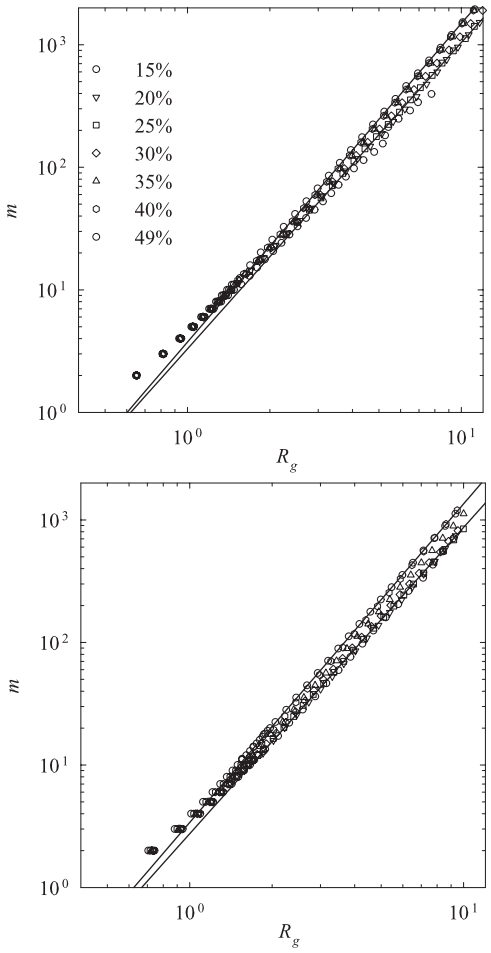

Figure 4.24: Double logarithmic representation of the dependence of the aggregation number (m) on the radius of gyration (R_g) for clusters formed at different concentrations indicated in the figure with $\varepsilon = 0.1$ (top) or $\varepsilon = 0.5$ (bottom). The solid lines in each figure have slopes 2.5 and 2.6.

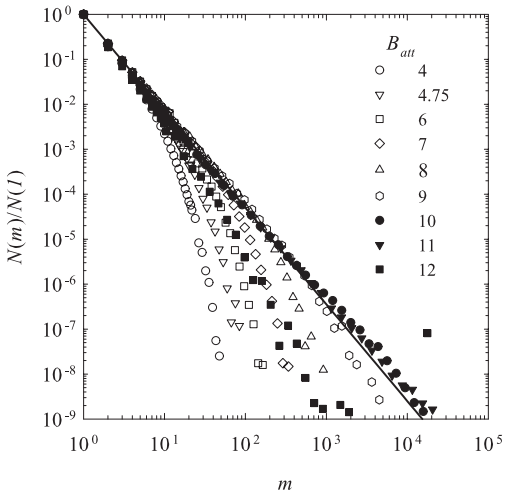

Figure 4.25: Double logarithmic representation of the cluster size distribution ($N(m)$) normalized with the number of monomers ($N(1)$) at different values of B_{att} indicated in the figure. The solid line has a slope of -2.15. At $B_{att} = 12$ the distribution is split into a sol phase and a gel phase.

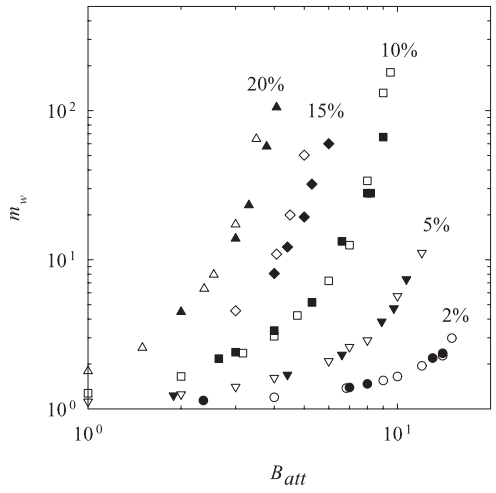

Figure 4.26: Weight average aggregation number (m_w) at equilibrium as a function of B_{att} at different values of ϕ indicated in the figure. Filled symbols represent $\varepsilon = 0.1$ and open symbols $\varepsilon = 0.5$.

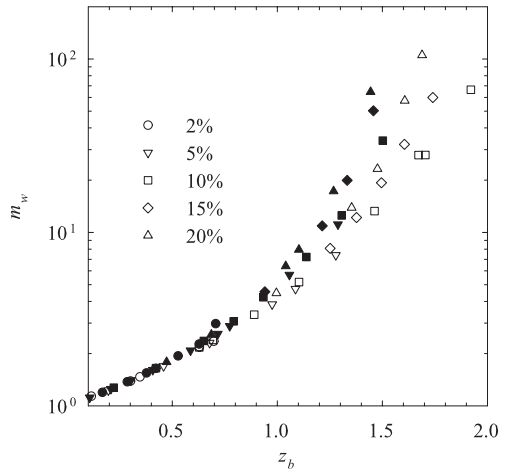

Figure 4.27: Weight average aggregation number (m_w) at equilibrium as a function of z_b at different values of ϕ indicated in the figure. Filled symbols represent $\varepsilon = 0.1$ and open symbols $\varepsilon = 0.5$.

approaches zero, because the aggregation is kinetically driven and the bonds are rigid. The equilibrium properties of the system depend on the life time of an encounter between particles, which is a function both of P and the attempt frequency to form and break bonds. Since the bonds are rigid the average coordination number, z_c, is at most two so that there is no densification and phase separation. This means that, contrary to the present simulations, homogenous systems containing large aggregates or a percolating network could be formed at equilibrium even at low volume fractions.

During the aggregation process up to the gel point, two regimes could be distinguished: the so-called flocculation regime when the clusters were on average well separated and the percolation regime close to the gel point when the clusters were highly interpenetrated. In both regimes large clusters had a self-similar structure and a power size distribution. In the percolation regime we found $d_f = 2.7$ and $\tau = -2.1$, while in the flocculation regime we found $d_f = 2.0$ and $\tau = -1.5$. The crossover between the two regimes occurs at characteristic aggregation number (m_c) that decreases with increasing volume fraction. The two different regimes were also observed for irreversible aggregation [24, 25, 27]. For reversible aggregation with a finite interaction range, one cannot create stable systems with large clusters at small ϕ. A percolated system is formed at equilibrium only for volume fractions above about 10% for which m_c is small. Therefore the two regimes cannot be distinguished and essentially only the percolating clusters are observed.

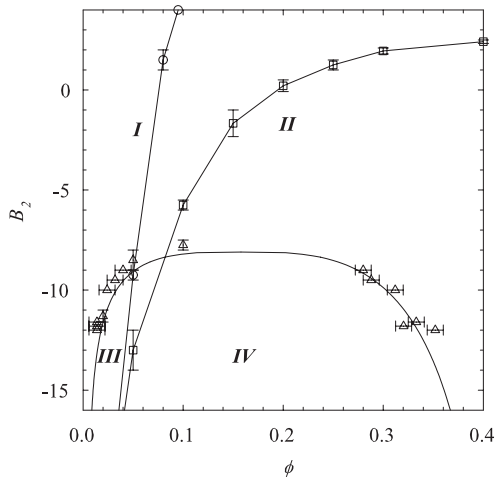

Figure 4.28: State diagram for $\varepsilon = 0.5$ indicating four different states of the systems delimited by the contact (circles) or bond (squares) percolation threshold and the binodal (triangles), see text.

4.2.4 Summary

Reversible aggregation with finite interaction range leads to four different situations depending on B_2 and ϕ, see Fig. 4.28: I) a homogeneous system containing transient clusters; II) a homogeneous system containing a transient percolating network together with clusters; III) a phase separating system without formation of a temporarily percolating network; IV) a phase separating system with formation of a temporarily percolating network. In addition to these domains the system may show transient contact percolation without bond percolation.

For given values of B_2 and ϕ the size of the equilibrium clusters is little dependent on the interaction range as long as the latter is smaller than the average distance between the random distributed spheres.

Close to the binodal, phase separation occurs through nucleation and growth of spherical dense domains. Systems that are quenched deeper in the two phase regime, phase separate through coarsening of large fractal clusters or the percolated network. This ripening process leads finally to the break-up of the temporary network and the formation of spherical dense domains.

Chapter 5

Self diffusion of reversibily aggregating spheres with rigid bonds

[5.1] S. Babu, J. C. Gimel and T. Nicolai, J. Chem. Phys., **127** 54503-1-7 (2007).

5.1 Self diffusion of reversibly aggregating spheres

Abstract
Reversible diffusion limited cluster aggregation of hard spheres with rigid bonds was simulated and the self diffusion coefficient was determined for equilibrated systems. The effect of increasing attraction strength was determined for systems at different volume fractions and different interaction ranges. It was found that the slowing down of the diffusion coefficient due to crowding is decoupled from that due to cluster formation. The diffusion coefficient could be calculated from the cluster size distribution and became zero only at infinite attraction strength when permanent gels are formed. It is concluded that so-called attractive glasses are not formed at finite interaction strength.

5.1.1 Introduction

Reversible aggregation of small particles in solution is a common phenomenon. It leads to different equilibrium states depending on the volume fraction (ϕ) of the particles and the strength of the interaction energy (u). Weak attraction results in the formation of transient aggregates at low ϕ and a transient percolating network at high ϕ, while strong attraction may drive phase separation into a high and a low density liquid [14, 54–57, 63, 76, 101, 130–152]. The strength of the interaction and thus the equilibrium properties are determined by the ratio of the bond formation (α) and the bond breaking (β) probability [27, 42, 61, 73, 94–96, 102, 103, 105, 125–128], while the kinetics of such systems depend on the absolute values of α and β. Two limiting cases may be distinguished: diffusion limited cluster aggregation (DLCA) for which a bond is formed at each collision ($\alpha = 1$) and reaction limited cluster aggregation (RLCA) for which the probability to form bonds goes to zero ($\alpha \to 0$).

The average long time self diffusion coefficient (D_l) of non-interacting hard spheres decreases with increasing volume fraction [74, 84, 165–167] and the system forms a glass above a volume fraction of about 0.585. For a recent review of theories and experiments on the glass transition in colloids see Sciortino and Tartaglia[17]. Mode coupling theory predicts that D_l goes to zero at a critical volume fraction $\phi_c = 0.516$ following a power law:

$$D_l \propto (\phi_c - \phi)^\gamma \tag{5.1}$$

The pictorial view is that particles become trapped in cages formed by neighbouring particles. Experiments [13] and computer simulations [14, 15] confirmed this behaviour over a range of ϕ though with a larger value of ϕ_c (0.585). However, the diffusion coefficient is not truly zero at ϕ_c, and some mobility is still possible between ϕ_c and the volume fraction of random close packing ($\phi_{cp} = 0.64$). The reason is that fluctuations of the cage size around the average value, allow particles to "hop" from one cage to another. Mode coupling theory uses the static structure factor as input and therefore cannot include the effect of fluctuations and heterogeneity.

Introducing reversible bond formation between the hard spheres has two consequences. Firstly, the structure factor is modified, because on average more particles will be within each others bond range. Secondly, the diffusion of bound particles becomes correlated for some duration that is related to the bond life-time. Obviously, the latter effect leads to a decrease of D_l, because clusters of bound particles move more slowly than individual spheres and not at all in the case when they form a percolating network. However, modification of the structure may also lead to an increase of D_l compared to the hard sphere case [14, 69, 143], because the accessible volume for a particle in which it can move increases. In other words, the average cage size increases. This effect can be clearly seen for the self diffusion of tracer particles in a medium of fixed spherical obstacles. For a given volume fraction of obstacles, D_l is smaller when the obstacles are randomly distributed than when they form a percolating network [47].

An increase of D_l with increasing attraction has actually been observed for con-

centrated suspensions of hard spheres with weak short range attraction where the particles can freely move within the attraction range. With further increase of the interaction energy the effect on the structure weakens, but the bond life-time increases so that D_l decreases again. These effects have also been found in molecular dynamics simulations of such systems [14, 69, 143]. Mode coupling theory describes this behaviour purely on the basis of the changes in the static structure factor and predicts complete arrest at finite interaction strength even at low volume fractions [75]. Systems arrested by attraction are called attractive glasses [59] to distinguish them from the ordinary repulsive glasses [13].

Obviously, irreversible aggregation, i.e. infinite attraction strength, leads to arrest at any volume fraction when all spheres become part of the percolating network [25]. Generally, arrested systems at low volume fractions due to irreversible aggregation are called gels. In analogy, percolated systems with finite interaction strength may be called transient gels, though in practice one would only do that only if the bond life-time is very long so that the system flows very slowly. The issue addressed here is how D_l varies with increasing attraction strength and specifically whether D_l becomes zero in transient gels with a finite bond life-time. In other words, whether transient gels can be attractive glasses. Even if, as for repulsive glasses, D_l does not truly become zero due to hopping processes, the question remains whether D_l can be usefully described as going to zero at a finite critical interaction energy following a power law over a broad range of D_l:

$$D_l \propto (u - u_c)^\gamma \tag{5.2}$$

as was suggested in the literature [65, 69] (u_c).

As mentioned above, phase separation occurs when the attraction is strong, and needs to be avoided if one wishes to study the effect of strong attraction on D_l at low volume fractions. This can be done to some extent by limiting the maximum number of bound neighbours below 6 [65, 168] or by introducing a correlation between the bond angles with different neighbours [72]. One can also introduce a long range repulsive interaction to push phase separation to lower concentrations [69, 100, 169]. Phase separation disappears completely if the bonds are rigid and the bond range is zero, because only binary collisions can occur so that the average coordination number cannot exceed two [73]. For this model D_l can be studied at any interaction strength and volume fraction without the interference of phase separation.

An extensive study of the structural properties of such systems was published earlier [73]. It was shown that the equilibrium properties depend on the ratio α/β and the elementary step size s of the Brownian motion. As long as s is much smaller than the average distance between the particles, the equilibrium properties are determined by a single parameter called the escape time (t_e) that is a combination of s, α and β. t_e is defined as the excess time it takes for two particles at contact to become decorrelated compared to the situation where no bonds are formed ($\alpha = 0$). If the interaction range is finite and if s is much smaller than the interaction range, then the escape time becomes independent of s and the equilibrium properties are the same

as for spheres interacting with a square-well potential.

Here we present results of the mean square displacement (MSD) of the particles as a function of the interaction strength for systems forming rigid bonds with zero and finite interaction strength. The main conclusion of this work is that introducing attraction leads to a decrease of D_l without any sign of arrest at finite interaction strength. As mentioned above, there are two different mechanisms for slowing down: one is controlled by the bond life-time and the other is controlled by crowding. We show here that for rigid bond formation with $\alpha = 1$ the two mechanisms are independent and can be factorized. Since the first mechanism leads to complete arrest only for irreversible aggregation, we propose that the expression "attractive glass" is abandoned in favour of the expression "gel" that is commonly used to describe irreversibly bound percolating networks. The results presented here resemble to some extent those obtained recently by Zaccarelli et al.[65] for attractive spheres with limited valency. The main difference is that in those simulations the bonds were not rigid and localized motion was possible even at infinite bond strength. We will briefly discuss the effect of bond flexibility.

5.1.2 Simulation method

The simulation method for aggregation with zero interaction range has already been detailed elsewhere [73]. Initially, N non-overlapping spheres with unit diameter are positioned randomly in a box with size L, using periodic boundary conditions, so that $\phi = (\pi/6)N/L^3$. Different sizes between $L = 10$ and $L = 50$ were used, and the results shown here are not influenced significantly by finite size effects. N times a particle is chosen and moved a distance s in a random direction. When the movement leads to overlap with another sphere it is truncated at contact. After this movement step all spheres in contact are bound with probability α leading to the formation of N_c clusters that are defined as sets of bound particles. In the next movement step, N_c times a cluster is chosen and moved a distance s in a random direction with a probability that is inversely proportional to the diameter of the cluster, thus simulating non-draining within the clusters. In the following cluster construction step, all bound particles are broken with probability β and bonds are formed for new contacts with probability α. Movement and cluster formation steps are repeated until all particles have formed a single cluster for irreversible aggregation or until equilibrium is reached for reversible aggregation.

The diffusion coefficient was calculated as $\langle r^2 \rangle/(6t)$ and the time unit was defined as the time needed for a single particle to diffuse its own diameter so that the diffusion coefficient at infinite dilution is $D_0 = 1/6$. In this article we will present diffusion coefficients normalized by D_0. For the case of irreversible ($\beta = 0$) diffusion limited ($\alpha = 1$) aggregation, the kinetics of cluster growth were the same as predicted from the Smolechowski equations for DLCA if s was chosen sufficiently small[25]. As mentioned in the introduction, the equilibrium properties for reversible aggregation

with zero interaction range are determined by the escape time [73]:

$$t_e = (2.37s + s^2)\frac{\alpha}{\beta} \tag{5.3}$$

At equilibrium, a distribution of self-similar transient clusters is formed together with a transient percolating network if t_e and ϕ are sufficiently large.

Reversible aggregation with finite interaction range ε was simulated by forming bonds with probability α when the centre to centre distance between particles is less than $1 + \varepsilon$ [54]. Bonds were again broken with probability β. In this case the equilibrium properties are independent of the step size if $s \ll \varepsilon$. The system is equivalent to particles interacting through a square well attraction with interaction energy $u = \ln(1 - P)$, where P is the probability that particles within each others interaction range are bound: $P = \alpha/(\alpha+\beta)$. u is given in units of the thermal energy and is equivalent to the inverse temperature that is sometimes used to express the interaction strength. The equilibrium properties of systems with different interaction range are close if they are compared at the same second virial coefficient (B_2)[60]. B_2 is the sum of the excluded volume repulsion and the square well attraction: $B_2 = B_{rep} - B_{att}$. $B_{rep} = 4$ and B_{att} is determined both by the interaction strength and the interaction range [161]:

$$B_{att} = 4[(1 + \varepsilon)^3 - 1][\exp(-u) - 1] \tag{5.4}$$

in units of the particle volume

5.1.3 Results

Zero interaction range

Fig. 5.1 shows the mean square displacement, i.e. $\langle r^2 \rangle$, of spheres at $\phi = 0.49$ for different values of t_e with $\alpha = 1$, starting from a random distribution. Initially, the particles move freely until they begin colliding with other particles. This leads to slowing down of the MSD even in the absence of attraction ($t_e = 0$). At long times $\langle r^2 \rangle$ is again proportional to t, but the long time diffusion coefficient (D_l) is smaller. Fig. 5.2 shows that the dependence of the normalized diffusion coefficient of hard spheres in the absence of attraction (D_{hs}) on ϕ is in good agreement with literature results [74, 84, 165–167].

Introducing attraction slows down the MSD, because transient clusters are formed that move more slowly and above a critical value of t_e a transient percolating network is formed. Particles that are part of the transient network are immobile and need to break bonds before they can diffuse. In the limit of $t_e = \infty$, corresponding to irreversible DLCA, all particles are permanently stuck when they become part of the percolating network. Naturally, the value of $\langle r^2 \rangle$ where the particles get stuck decreases with increasing volume fraction, see Fig 5.3.

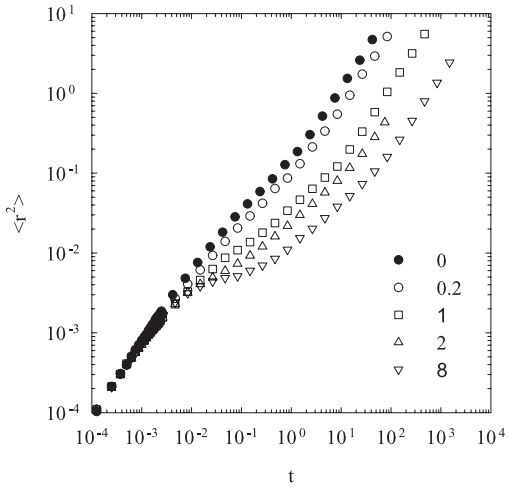

Figure 5.1: MSD of spheres starting from a random position at $\phi = 0.49$ for different t_e as indicated in the figure.

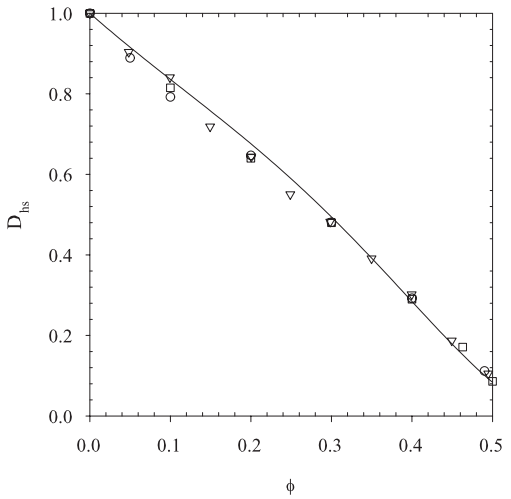

Figure 5.2: Dependence of the self diffusion coefficient of randomly distributed hard spheres on the volume fraction obtained from computer simulations: present work (circles), [84] (solid line), [166] (squares) and [167] (triangles).

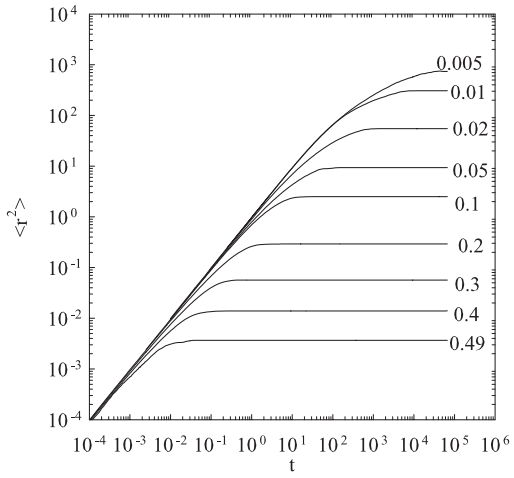

Figure 5.3: MSD of spheres during irreversible aggregation (DLCA) for different volume fractions as indicated in the figure.

Once the system has reached equilibrium one can start again measuring the MSD. Fig. 5.4*a* shows the MSD for the same systems as in Fig 5.1, but starting from the equilibrium state. In this case the initial diffusion is slower than that of individual spheres, since the system contains clusters and for $t_e > 0.43$ a percolating network. After some time the clusters collide causing a further slowing down of the MSD, but simultaneously, for $\alpha = 1$, bonds are formed and broken. Of course, for $t \gg t_e$ the same long time diffusion coefficient is obtained independent of the starting configuration, compare Fig. 5.1. Remarkably, the effect of particle collisions on the slowing down of the MSD is the same at different t_e. Therefore the MSD obtained at different t_e can be superimposed within the statistical error by simple time shifts (see Fig. 5.4*b*). The implication is that D_l can be factorized in terms of the short time diffusion coefficient (D_s) and D_{hs}:

$$D_l(t_e, \phi) = D_s(t_e, \phi) \cdot D_{hs}(\phi) \tag{5.5}$$

At short times, i.e. before bond breaking becomes significant and before the particles collide, the MSD is determined by free diffusion of the clusters. Consequently, D_s can be calculated from the size distribution of the clusters ($N(m)$) which is a function of t_e and ϕ:

$$D_s(t_e, \phi) = \sum_m \frac{m \cdot N(m) \cdot D(m)}{N} \tag{5.6}$$

where $D(m)$ is the average free diffusion coefficient of clusters with aggregation number m. If a percolating network is present we need to consider only the sol fraction

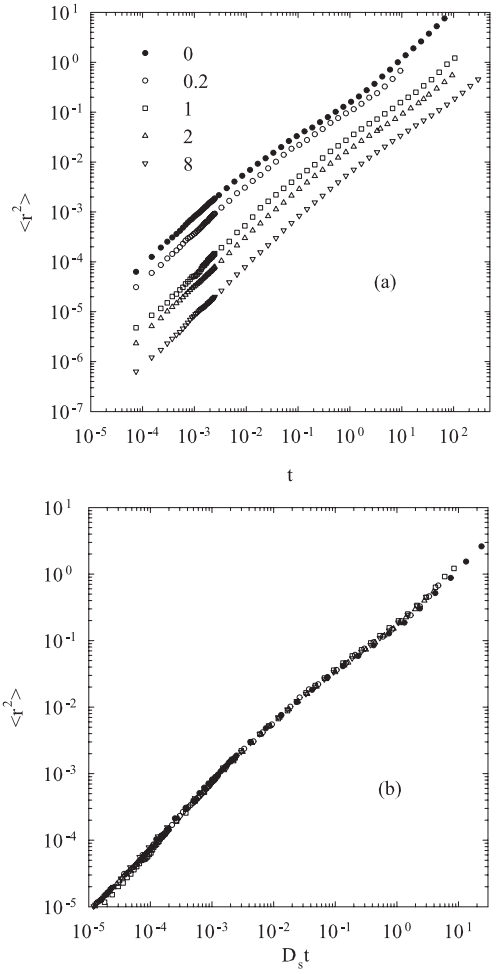

Figure 5.4: MSD for equillibriated systems (a) at $\phi = 0.49$ for different t_e. Fig. 4b shows a mastercurve obtained by plotting the same data as a function of $D_s t$.

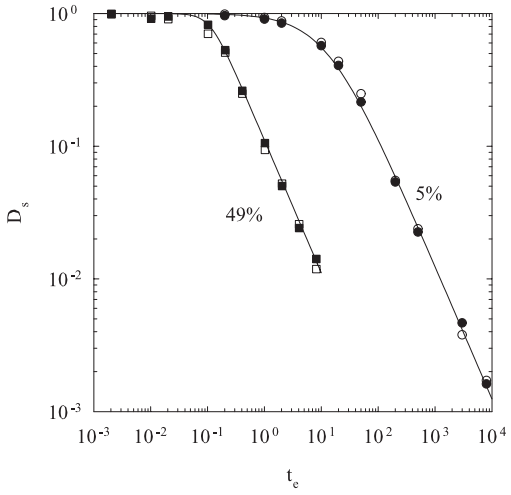

Figure 5.5: The short time diffusion coefficient as a fuction of t_e for $\phi = 0.49$ (squares) and $\phi = 0.05$ (circles) . Closed and open symbols represent simulation results and calculations using Eq. (5.6).

of mobile clusters (F):

$$D_s = \frac{F}{m_n} \cdot \frac{\sum_m^{sol} m \cdot N(m) \cdot D(m)}{\sum_m^{sol} N(m)} \tag{5.7}$$

where m_n is the number average aggregation number of the sol fraction. In the absence of hydrodynamic interactions $D(m) \propto m^{-1}$ so that $D_s \propto m_n^{-1}$. For the more realistic case of non-draining clusters $D(m)$ is inversely proportional to the radius of the clusters so that D_s decreases more weakly with increasing m_n.

Figure 5.5 shows D_s as a function of t_e for $\phi = 0.49$ and $\phi = 0.05$. We have calculated D_s from the cluster size distribution using Eq. (5.6) and D_l was calculated using Eq. (5.5). Comparison with the simulation results, see Fig (5.5), demonstrates that the effect of attraction on D_s is indeed fully determined by the cluster size distribution. Initially, D_l decreases with increasing t_e, because m_n increases until at a critical value of t_e (t_e^*) a percolating network is formed of immobile particles. t_e^* is 0.43 and 180 for $\phi = 0.49$ and $\phi = 0.05$, repectively. At the percolation threshold the weight average aggregation number diverges [73], but m_n and thus D_l remain finite. The maximum value of m_n is obtained at the percolation threshold, beyond which it decreases with increasing volume fraction. Beyond the percolation threshold the sol fraction decreases much more strongly with increasing attraction than m_n so that D_l continues to decrease. However, it is obvious that D_l will become zero only if $F = 0$, i.e. at infinite attraction strength. At large values of t_e, D_l decreases linearly with increasing t_e. As expected, at lower volume fractions stronger attraction is needed to cause significant slowing down.

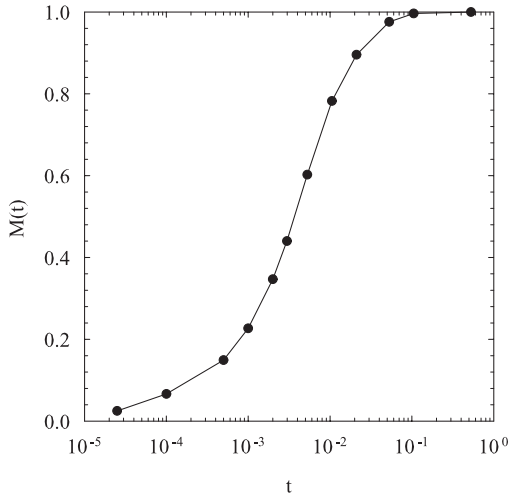

Figure 5.6: Fraction of mobile particles as a fuction of time for an equillibrated system at $t_e = 2$ and $\phi = 0.49$. The solid line is a guide to the eye.

The MSD shown in Fig. 5.4 represent an average over all particles, and do not show how the displacement of the particles is distributed. In the absence of attraction the probability distribution that a particle has moved a distance r^2 at a given time ($P(r^2)$) is given by:

$$P(r^2, t) = \frac{2\pi}{(4\pi Dt)^{3/2}} r \exp(-\frac{r^2}{4Dt}) \tag{5.8}$$

because each particle is equivalent. However, in the presence of attraction the displacement is highly heterogeneous, because the particles belong to clusters of different sizes. We have illustrated this for $\phi = 0.49$ at $t_e = 2$. In this case almost all of the particles belong to the gel fraction and cannot move until their bonds are broken. Thus at short times the displacement is highly heterogeneous with a large fraction of particles that do not move at all and a small fraction of sol particles (F) that diffuse freely until they collide. With increasing time, more and more of the sol particles collide with the percolating network and stop moving, while more and more gel particles break lose and start diffusing. Fig 5.6 shows how the fraction of mobile particles that has moved after a time t ($M(t)$) increases with increasing t.

Figure 5.7 compares $P(r^2)$ at different times with the distribution that would have been found for same $\langle r^2 \rangle$ if all particles had been equivalent. Note that the area under the curves is equal to $M(t)$. The heterogeneity of the displacement decreases with increasing time until for $t \gg t_e$ all particles have formed and broken bonds many times so that $M(t) = 1$ and $P(r^2)$ is given by Eq. 5.8 . Similar observations were made at $\phi = 0.05$.

Figure 5.7 resembles the results presented by Puertas et al. [170]. However, they used molecular dynamics simulations for which bound particles move freely as long as the displacement does not involve breaking of bonds, as will be discussed below. For

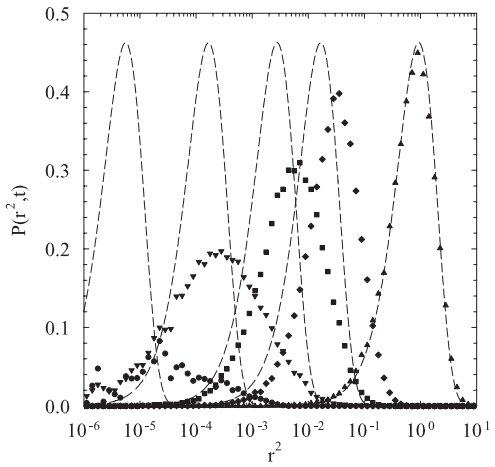

Figure 5.7: Probability distribution of r^2 at different times 0.001 (circle), 0.3 (triangledown), 0.5 (square), 3 (diamond) and 167 (triangle) for $\phi = 0.49$ and $t_e = 2$. The solid lines represent the distributions for freely diffusing spheres with the same average MSD, see Eq. 5.8.

this reason they observed a peak situated at a small r that represents the displacement of bound particles. A second peak was found at larger values of r representing the sol fraction and moved to longer distances with increasing time. The amplitude of this peak increased with increasing time as more and more particles break their bonds.

Finite interaction range

The effect of finite interaction range was tested for $\varepsilon = 0.1$ and $\varepsilon = 0.5$. We found also for this case that D_l could be factorized into D_s and D_{hs}, see Eq. 5.5, and that the effect of attraction on D_l is fully determined by the free diffusion of the clusters. However, the dynamic heterogeneity that was important for the zero range interaction disappeared rapidly with increasing interaction range especially at higher concentrations, because monomers and clusters can move only a short distance before they interact. Individual particles exchange rapidly between different clusters including the gel fraction, at least for $\alpha = 1$. Therefore each particle explores more rapidly the different dynamics of the system.

Recently, it was shown that the cluster distribution in equilibrium is similar for the two interaction ranges if compared at the same values of the second virial coefficient, at least for ϕ up to 0.2 [54]. We therefore expect that D_s is the same at the same B_2. Fig. 5.8 shows D_s as a function of B_{att} for 3 different volume fractions with $\varepsilon = 0.5$ and $\varepsilon = 0.1$. As mentioned in the introduction, for lower volume fractions the slowing down of D_s can be studied only over a limited range before phase separation occurs. As expected, D_s decreases with increasing B_{att} and the decrease is more important

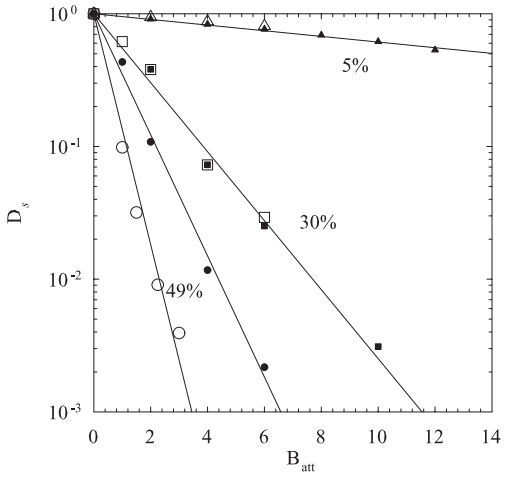

Figure 5.8: The short time diffusion coefficient at $\phi = 0.49$ (circles), $\phi = 0.3$ (squares) and $\phi = 0.05$ (triangles) for two different interaction ranges $\varepsilon = 0.5$ (closed) and $\varepsilon = 0.1$ (open) as a function of B_{att}. The solid lines are guide to the eye.

at higher concentrations. Again no sign of critical slowing down of the MSD was observed. For $\varepsilon = 0.5$ and $\varepsilon = 0.1$ the dependence of D_s on B_{att} was similar for $\phi = 0.05$ and 0.3, but for $\phi = 0.49$ it was stronger for $\varepsilon = 0.1$ than for $\varepsilon = 0.5$. At high volume fraction B_2 is no longer the main parameter that determines the cluster size distribution because higher order interaction becomes important.

Recently, Foffi et al. [76] reported a simulation study of the effect of the interaction range on D_l for hard spheres with a square well interaction. Molecular dynamics simulations were used that gave the same equilibrium structures as with the method used here. However, molecular dynamics simulations gives different dynamics so that absolute values of D_l cannot be compared with the results presented here. Nevertheless, they also found that the MSD of particles was independent of the interaction range if compared at the same value of B_2 and they argued that D_l was the same because the number of bonds and the bond life-time was determined by B_2. We expect that deviations will be found also with this method at higher concentrations and larger interaction ranges when higher order interaction becomes important.

5.1.4 Discussion

There are two causes for the decrease of D_l in a system of attractive hard spheres. The first one is collisions with other spheres. This effect of crowding increases with increasing volume fraction and leads to strong decrease of D_l near $\phi \approx 0.58$ that can be described to some extent by mode coupling theory, as mentioned in the Introduction. The second cause is bond formation, which leads to the formation of transient clusters and gels. This effect increases with increasing attraction. The diffusion at short times

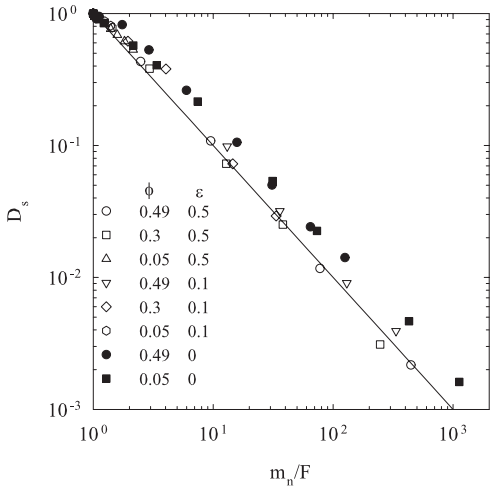

Figure 5.9: The short diffusion coefficient as a function m_n/F for different volume fractions (ϕ) and interaction ranges (ε) as indicated in the figure . The solid line represents $D_s = m_n/F$.

is not influenced by collisions so that in the absence of attraction D_s is equal to the free diffusion of the particles. The decrease of D_s with increasing attraction is caused solely by cluster formation and can be calculated from the cluster size distribution. Since for any finite interaction there is a finite fraction of free particles and clusters, D_s only becomes zero when the interaction is infinitely strong. The decrease of D_s with increasing interaction strength is mainly determined by m_n/F, see Fig. 5.9 and it is dominated by the decrease of the sol fraction for strong attraction when m_n is close to unity.

The subsequent decrease of the diffusion coefficient from D_s to D_l at long times is caused by crowding. An important observation is that the slowing down caused by crowding is independent of the attraction strength for $\alpha = 1$. The reason is that by definition for reversible DLCA the reversibility is expressed as soon as collisions occur and the memory of the connectivity is lost. Consequently, diffusion is slowed down by attraction, but does not become zero as long as the attraction is finite. The situation is different for reversible RLCA in which case the collisions occur between long-lived clusters and between the clusters and the percolating network. For given attraction strength D_s is the same for reversible DLCA and RLCA, but for RLCA the ratio D_l/D_s decreases with decreasing bond formation probability. This situation will be explored elsewhere.

The results presented here apparently contradict molecular dynamics simulations that showed critical slowing down at finite interaction strength [63, 69]. The main difference between our simulation method and molecular dynamics is that rigid bonds are formed so that only cluster motion is possible. In the molecular dynamics simulations bound particles are still allowed to diffuse freely as long as no bonds are

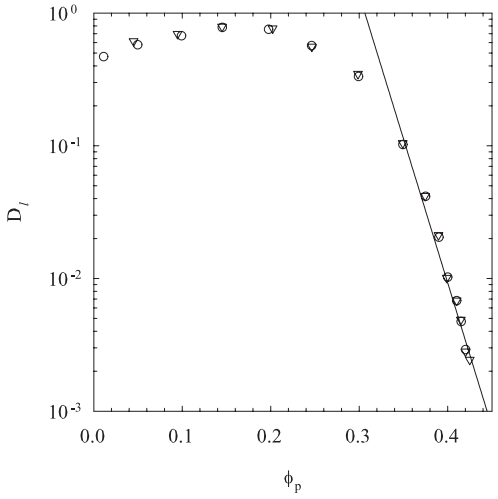

Figure 5.10: Long time self diffusion coefficient as a fuction of (ϕ_p) for 2 different values of ϕ_p^G (0.4265 (circles) and 0.4519 (triangles)) from [69].The solid lines represents $D_l \propto \exp(-50\phi_p)$.

broken. The implication is that D_s is equal to the free particle diffusion independent of the interaction strength. Consequently D_l is faster and D_l is even larger than D_{hs} for weak attraction. We have included bond flexibility in the simulations with finite interaction strength by allowing free diffusion for bound particles as long as it does not lead to bond breaking. Details of these simulations will be reported elsewhere. Here, we only mention that including bond flexibility increases D_l. It is clear, that allowing more freedom for movement does not lead to a critical slowing down of the diffusion at a finite interaction range so that the apparent contradiction with molecular dynamics simulations persists. But, a close look at the molecular dynamics simulation results shows that they can also be interpreted in terms of a power law decrease. For instance, Puertas et al. [69] simulated hard spheres with a short range depletion interaction caused by the addition of polymers. In Fig. 5.10 we have replotted D_l as a function of the polymer volume fraction ($\phi_p \propto -u$) for two different particle volume fractions. The authors interpreted the data in terms of Eq.5.2. At each concentration the smallest values of D_l deviated from this expression, which was attributed to "hopping". It is clear, however, from Fig. 5.9 that the decrease of $\ln D_l$ at large ϕ_p can also be described as a power law even for the smallest value of D_l implying that $D_l = 0$ only at infinite attraction.

Very recently, Zaccarelli et al. [65] made a detailed study of the dynamics in attractive hard sphere systems with limited valence (3 and 4) using molecular dynamics simulations. They observed that for strong attraction the variation of $\ln D_l$ could be described by a power law in terms of u at least for $\phi \leq 0.55$ implying that arrest only occurred at infinite attraction. On the other hand they could describe D_l as

a function of ϕ in terms of Eq. 5.1. ϕ_c was almost constant when increasing the attraction and only for strong attraction did they find a weak decrease of ϕ_c, but the extrapolation was uncertain in this case. The authors used the expression reversible gel for systems that arrested at $u \to -\infty$ ($T \to 0$) and glass (attractive or repulsive) for systems that arrested at $\phi \to \phi_c$. The expression attractive glass was introduced to describe the arrest that occurs for a given volume fraction at a finite attraction energy. It is clear from the present study that attractive glasses in this sense are only formed for irreversible aggregation.

5.1.5 Conclusion

Reversible cluster aggregation of hard spheres leads to equilibrium systems containing transient clusters and, above a critical interaction strength, a transient percolating network. If the aggregation is diffusion limited and the bonds are rigid, then the effect of attraction on D_l is decoupled from the effect of crowding. The latter is equal to that of non-interacting hard spheres, while the former is fully determined by the cluster size distribution. The self diffusion coefficient of the spheres decreases with increasing attraction, but becomes zero only for irreversible aggregation, contrary to predictions from mode coupling theory. Therefore attractive glasses in the sense of systems that are dynamically arrested by a finite interaction energy do not exist.

Chapter 6

The influence of bond-rigidity and cluster diffusion on the self-diffusion of hard spheres with square-well interaction.

[6.1] S. Babu, J. C. Gimel, T. Nicolai and C. De Michele, *submitted* (2007)

6.1 The influence of bond-rigidity and cluster diffusion on the self-diffusion of hard spheres with square-well interaction.

Abstract

Hard spheres interacting through a square-well potential were simulated using two different methods: Brownian Cluster Dynamics (BCD) and Event Driven Brownian Dynamics (EDBD). The structure of the equilibrium states obtained by both methods were compared and found to be almost identical. Self diffusion coefficients (D) were determined as a function of the interaction strength. The same values were found using BCD or EDBD. Contrary to EDBD, BCD allows one to study the effect of bond rigidity and hydrodynamic interaction within the clusters. When the bonds are flexible the effect of attraction on D is relatively weak compared to systems with rigid bonds. D increases first with increasing attraction strength, and then decreases for stronger interaction. Introducing intra-cluster hydrodynamic interaction weakly increases D for a given interaction strength. Introducing bond rigidity causes a strong decrease of D which no longer shows a maximum as function of the attraction strength.

6.1.1 Introduction

Suspensions of particles with attraction exhibit equilibrium states as well as non-equilibrium states like gels or glasses that evolve very slowly [13, 17, 59, 171]. Numerical simulations were found to be useful for the understanding of the structure and the dynamics of such systems [17, 172]. The advantage of simulations is that large scale phenomena may be related to the microscopic trajectories of the particles. In recent years computer simulations have yielded valuable insight not only into equilibrium properties such as cluster size distributions and structure factors, but also into the evolution of the system during phase separation [54, 63, 76] and gelation [27, 72, 73, 170, 173].

Often Monte Carlo methods are used to study structural properties at equilibrium and molecular dynamics to study dynamics and kinetics [79, 80]. Monte-Carlo methods allow one to study relatively large systems and generally require less computer time to obtain equilibrium states. A main draw back of classical Monte Carlo methods is that the definition of time is usually unphysical so that the evolution of the system towards equilibrium cannot be compared to that of real systems. Molecular dynamics simulate the particle displacement more realistically, but the system size and time scales that can be simulated with the current generation of computers are still relatively small.

The simplest model of interacting fluids is an ensemble of hard spheres that interact through a square well potential. Here we compare two different methods to simulate this model system: Brownian Cluster Dynamics (BCD) and Event Driven Brownian Dynamics (EDBD) [83]. With BCD clusters are constructed by forming bonds between spheres within each others interaction range with a given probability. With this method it is possible to account for hydrodynamic interaction within the clusters, though not between the clusters. It is also possible to study the influence of bond rigidity on the dynamics. This is important because in real systems bonds may be more or less rigid. With EDBD hydrodynamic interaction is ignored and the bonds are inherently completely flexible. We will show here that for reversibly aggregating systems bond rigidity has no influence on the structure of the steady state, but has a huge effect on the dynamics.

In the following we will first describe the two simulation methods. Then we compare the structure factors and the cluster size distributions of homogenous equilibrium states. We will show that almost the same structures are obtained at steady state with both methods. The main part of paper deals with the self diffusion coefficient as a function of the interaction strength. We compare the results obtained by the two simulation methods and discuss the influence of bond flexibility and intra-cluster hydrodynamic interaction.

6.1.2 Simulation method

We simulate hard spheres interacting through a square well potential characterized by a well depth u and a well width ϵ using BCD and EDBD. Both simulation methods start with an ensemble of N_{tot} randomly distributed spheres with diameter equal to unity in a box of size L so that the volume fraction is defined as $\phi = (\pi/6)N_{tot}/L^3$.

Event Driven Brownian Dynamics. This method was described in detail in the literature [83] and we only resume here the principal features. Initially a random velocity is assigned to each sphere from a Gaussian distribution with average squared velocity $< v^2 >= 3kT/M$, where k is Boltzmann's constant, T is the absolute temperature and M is the mass of the particle. Events are defined as occurrences when the sphere is at a distance unity or $1+\epsilon$ from another sphere, i.e. when spheres touch, or cross the interaction range. All spheres are moved over a distance $r = v\Delta t$, where Δt is sufficiently small so that the motion is Brownian over the relevant length scales, i.e. the interaction range and the average distance between the nearest neighbors.

The velocity of the spheres involved in the event are changed while conserving the energy and the momentum. When the event is a collision the spheres will bounce elastically in opposite directions. When the sphere enters a well its velocity is increased because the potential energy is decreased. When the sphere tries to leave a well it either bounces back elastically or it exits with a lower velocity. The change in the velocity and the probability to exit the well depend on u.

The mean squared displacement of a single sphere is given by: $< r^2 >= n(\Delta t)^2 < v^2 >$, where n is the number of simulation steps and Δt is equal to the maximum time step. If time is defined as $t \equiv n/(\Delta t)^2$ then the free diffusion coefficient of a single sphere is equal to: $D_0 = kT/(2M)$. In this paper the unit of energy is the thermal energy. We note that in the literature often u is fixed at unity and T is varied.

Brownian Cluster Dynamics. Spheres are considered to be in contact when they are within each others interaction range, i.e. when the center to center distance is smaller than $1 + \epsilon$. In the so-called cluster formation step, spheres in contact are bound with probability P. Alternatively, bonds are formed with probability α and broken with probability β, so that the $P = \alpha/(\alpha + \beta)$. In the latter case one can vary the kinetics of the aggregation from diffusion limited ($\alpha = 1$) to reaction limited ($\alpha \to 0$) with the same P and thus the same degree of reversibility. Clusters are defined as collections of bound spheres and monomers are clusters of size one. After this procedure N_c clusters are formed. We mention that more complex interaction potentials can be simulated by making P a function of the distance between two spheres.

The ratio of the number of bound (ν_b) to free contacts (ν-ν_b) is given by the Boltzmann distribution: $\nu_b/(\nu - \nu_b) = \exp(-\Delta H)$, where ΔH is the enthalpy difference between bound and free contacts. The formation of ν_b randomly distributed bonds over ν contacts leads to a decrease of the free energy equal to u per contact. This decrease may be written as the sum of the decrease of the enthalpy and the gain of the entropy: $\nu \cdot u = \nu_b \Delta H - T\Delta S$. The latter is determined by the number of ways

ν_b bonds can distributed over ν contacts: $T\Delta S = \ln(\nu!/[\nu_b!(\nu-\nu_b)!])$. Noticing that P=$\nu_b/\nu$, we can express P in terms of u:

$$P = 1 - \exp(u) \tag{6.1}$$

The cluster construction step is followed by one of three different movement steps that each simulates a different type of cluster dynamics.

BCD1. N_{tot} times a sphere is randomly selected and an attempt is made to move it a distance s in a random direction. The movement is accepted if it does not lead to overlap with any other sphere in the system and if it does not lead to the separation of bound spheres beyond the interaction range. Again it is important to choose the step size s sufficiently small so that the motion is Brownian over the relevant length scales. We have found that the results on the equilibrium structure were independent of the step size if s was at least five times smaller than the interaction range and at least three times smaller than the average distance between nearest neighbors [54, 81].

The mean squared displacement of a single sphere is given by: $< r^2 >= ns^2$ where n is again the number of simulation steps. Time was defined as $t \equiv n/s^2$, so that the free diffusion coefficient of single spheres is equal to: $D_0 = 1/6$.

BCD2 N_c times a cluster is randomly selected. An attempt is made to move the whole cluster over a distance s/d in a random direction with d the diameter of the cluster. By definition this cooperative movement never leads to bond breaking. The movement is refused if it leads to overlap of any of the spheres in the clusters with other spheres in the system. The free diffusion coefficient of single spheres is thus still 1/6, but the free diffusion coefficient of clusters is $1/(6d)$.

BCD3 This movement step is a combination of the previous two. First the movement step BCD1 is executed and the displacement of the centers of mass of each cluster is calculated. Then each cluster is given an additional displacement in the same direction so that the total displacement of the center of mass is the same as would be obtained by the movement step of BCD2. Again displacements are refused if they lead to overlap. As for movement step BCD2, the free diffusion coefficient of single spheres is 1/6, and that of larger clusters is $1/(6d)$. A lower degree of flexibility can be simulated by performing movement step BCD1 with a lower frequency than movement step BCD2.

The methods EDBD, BCD1 and BCD3 simulate systems with flexible bonds, while BCD2 simulates systems with rigid bonds. Using EDBD and BCD1 the effective friction coefficient of clusters is proportional to their aggregation number (so-called Rouse dynamics)[174], while for BCD2 and BCD3 it is proportional to their radius (so-called Zimm dynamics)[163]. It is, of course, straightforward to modify BCD2 to simulate systems with rigid bonds in which the friction coefficient is proportional to their aggregation number. This has not been done here, because in reality hydrodynamic interaction causes the free diffusion coefficient of clusters in solution to be inversely proportional to their radius [175]. The movement steps of EDBD and BCD1 are similar and one expects that diffusion coefficients obtained by these methods are close.

BCD may be considered a Monte Carlo type simulation, but if one is interested only in the structural properties at equilibrium it is more efficient to use other Monte-Carlo techniques that do not yield realistic kinetics or dynamics. BCD does not fulfill the condition of detailed balance, but does lead to a steady state independent of the starting configuration, which shows that it fulfills the condition of balance [176]. The same steady state is reached for each of the three movement steps with one exception: BCD2 does not lead to crystallization. The reason is that the pathway to form crystals is extremely unlikely when the bonds are rigid. BCD2 is therefore an excellent method to explore the properties of attractive spheres while avoiding crystallization [54].

6.1.3 Results and discussion

Equilibrium structure

The strength of the attraction is determined by the well width and the well depth. However, the equilibrium structure obtained at different ϵ is close if u is chosen such that the second virial coefficient is the same, especially if ϵ is small[54, 60]. B_2 may be written as the sum of a repulsive (excluded volume) part and an attractive part: $B_2 = B_{rep} - B_{att}$, with

$$B_{rep} = 4$$
$$B_{att} = 4\frac{P}{(1-P)}\left((1+\epsilon)^3 - 1\right)$$

where the unit of B_2 is the volume of a sphere.

As mentioned in the introduction strong attraction between the spheres leads to phase separation, while weak attraction leads to a homogeneous equilibrium state containing a distribution of transient clusters. All the three movement procedures of BCD leads to the same homogeneous equilibrium state, so for the structural properties we do not differentiate between the three methods. We have characterized these states in terms of the static structure factor ($S(q)$) and the cluster size distribution.

The structure factor at $q \to 0$ is inversely proportional to the compressibility and can be expressed in terms of a virial expansion at small volume fractions: $1/S(0) = 1+2B_2\phi+3B_3\phi^2$. For hard spheres interacting with a square well potential the second and third virial coefficients have been calculated analytically [161]. Figure(6.1) shows a comparison of $1/S(0)$ as a function of ϕ obtained from BCD simulations with the values calculated using the virial expansion. There is good agreement up to $\phi = 0.1$ beyond which higher order virial terms become important.

Figure(6.2) compares $S(q)$ obtained with BCD and EDBD at several conditions. Within the uncertainty range the same structures were observed with the two methods.

The cluster size distribution represents a more precise characterization. Clusters of bound spheres can be formed by connecting spheres in contact with probability

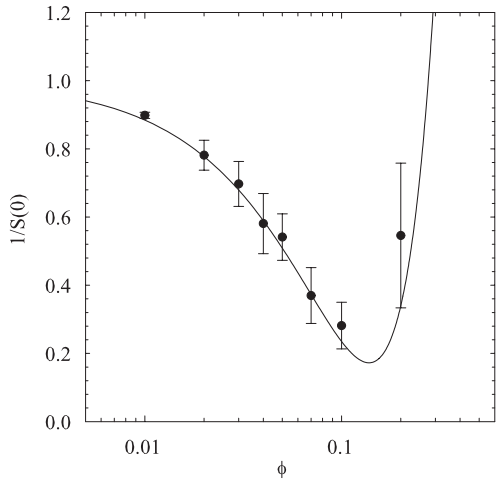

Figure 6.1: Concentration dependence of the compressibility for equilibrium systems at $\epsilon = 0.5$ for $B_2 = -6$ obtained by BCD. The solid line represents a calculation using the second and third virial coefficients, see text. The error bars represent the 95% confidence based on the results of 8 simulations.

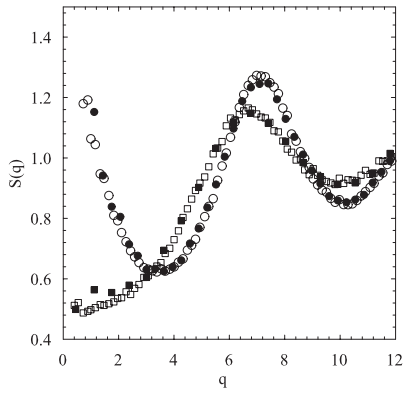

Figure 6.2: Comparison of the structure factor of equilibrium systems at $\phi = 0.15$ and $\epsilon = 0.1$ obtained by BCD (filled symbols) and EDBD (open symbols) with $B_2 = 2$ (squares) or $B_2 = -2$ (circles).

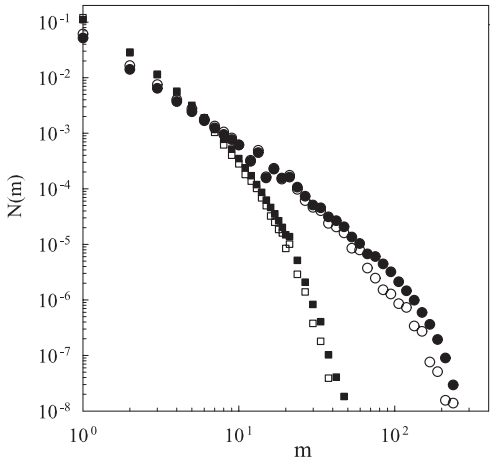

Figure 6.3: Comparison of the cluster size distribution of equilibrium systems at $\phi = 0.15$ and $\epsilon = 0.1$ obtained by BCD (filled symbols) and EDBD (open symbols) with $B_2 = 2$ (squares) or $B_2 = 0$ (circles).

$P = 1 - \exp(u)$ as defined above. A detailed analysis of these cluster size distributions has been reported elsewhere. Here, we have analysed the size distribution of clusters formed by connecting all contacts in order to facilitate comparison between BCD and EDBD. Figure(6.3) shows a comparison of $N(m)$ i.e. the average density of clusters consisting of m spheres at $\phi = 0.15$ and $\epsilon = 0.1$ for two values of B_2: 2 and 0. The width of the distribution increases with increasing u until at a critical value a system spanning transient network of spheres in contact is formed. There is a very small, but systematic difference between the cluster size distributions obtained with BCD and EDBD. Slightly larger clusters are formed with BCD. Nevertheless, we may conclude from these examples and similar comparisons at other conditions that the equilibrium structures obtained by BCD and EDBD are almost the same.

Diffusion

It can be shown that random displacement with constant step size as done with BCD leads to Brownian diffusion at distances much larger than the step size [41, 177]. For a proper comparison of the dynamic properties of BCD and EDBD simulations one has to ensure that the time scales and the free diffusion coefficients are the same, which can be done by choosing $\Delta t = s$ and $kT/M = 1/3$. Figure(6.4) shows a comparison of the average mean square displacement of hard spheres obtained from BCD and EDBD at ϕ=0.3. In both simulations $< r^2 >$ becomes proportional to t and the diffusion coefficient can be calculated as $D =< r^2 > /6t$. Figure(6.5) shows that the same ϕ dependence of D is obtained by the two methods within the uncertainty of the simulations. D decreases with increasing volume fraction due to steric hindrance and the diffusion slows down critically at the so-called glass transition, which has

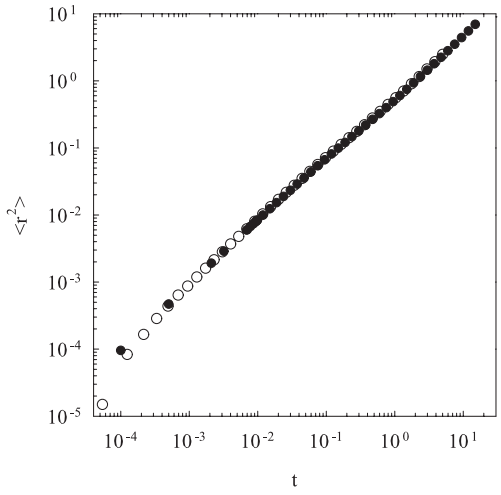

Figure 6.4: Comparison of the mean square displacement of non-interacting hard spheres obtained by BCD (filled symbols) and EDBD (open symbols).

been the subject of intensive investigation [14, 15].

When we introduce attraction between the spheres we need to consider cooperative cluster motion and bond flexibility. EDBD allows only one type of motion, but using BCD one can choose between different movement steps.

We have simulated the mean square displacement of spheres using EDBD and BCD with the three different movement steps described above. In each case diffusive motion was observed for large t and the diffusion coefficient could be determined. BCD1 and EDBD simulate the same situation and therefore the results should be the same. Figure(6.6) shows an example of the dependence of D on the step size obtained using BCD1. It appears that the exact value of D is more sensitive to the step size than the static structure factor or the cluster size distribution since the latter did not depend significantly on the step size for $s < 0.5$. The value extrapolated to $s = 0$ is the same as the value found with EDBD within the simulation error. Similar results were obtained at different volume fractions and interaction strengths. The fact that these very different simulation methods lead to the same results, strengthens confidence in both methods. In terms of computational efficiency both methods are equivalent.

A comparison of the dependence of D on B_{att} obtained with BCD using the 3 different movement steps is shown in fig.(6.7) for two different volume fractions (0.15 and 0.49) and two different well widths (0.1 and 0.5). The range of B_{att} that can be explored is limited by the liquid-liquid or liquid-crystal phase separation that occurs at strong attraction. The values of D shown in fig.(6.7) were obtained at a single value of s, but for a few examples the effect of s was determined, which showed that they were about 10% smaller than the values extrapolated to $s = 0$.

D decreases strongly with increasing attraction when the bonds are rigid (BCD2).

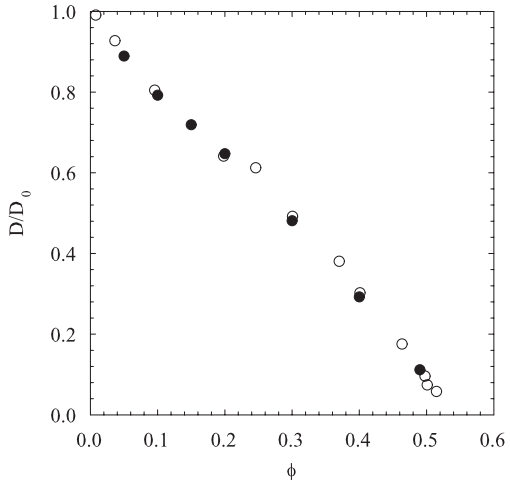

Figure 6.5: Comparison of the decrease of the diffusion coefficient with increasing volume fraction for non-interacting hard spheres obtained with BCD (filled symbols) and EDBD (open symbols)[83].

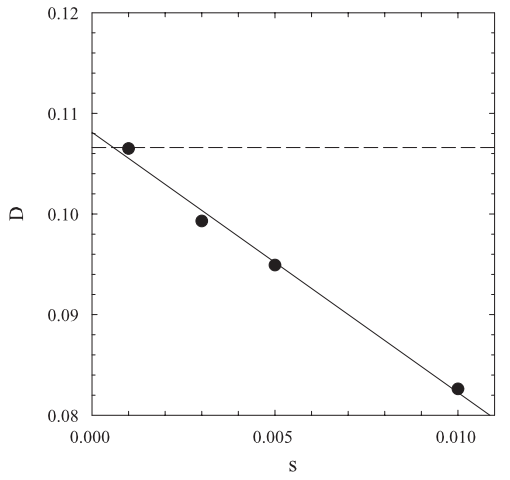

Figure 6.6: Dependence of the diffusion coefficient on the step size simulated using BCD1 ($\phi = 0.49$, $B_{att} = 6$, $\epsilon = 0.1$, filled symbols). The dashed line represents the result from EDBD. We note that at $\phi = 0.49$ the average distance between randomly distributed spheres is 0.014[8, 25].

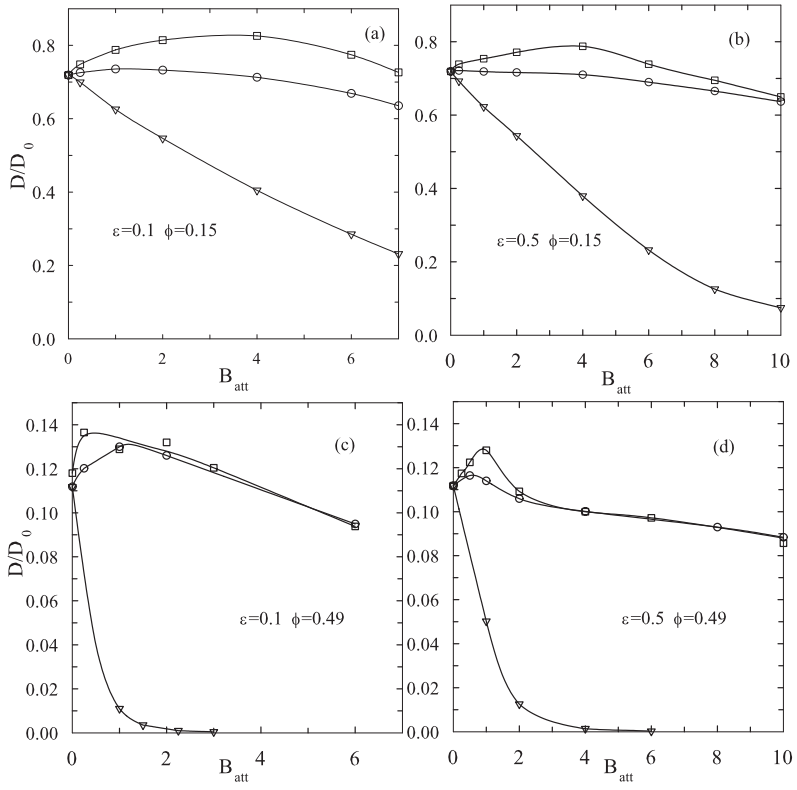

Figure 6.7: Variation of the diffusion coefficient with increasing attraction obtained from BCD1 (circles), BCD2 (triangles), and BCD3 (squares) at two different volume fractions and two different interaction widths. The interaction strength is expressed in terms of the attractive part of the second virial coefficient.

In this case the displacement of bound spheres is equal to that of the center of mass of the clusters to which they belong. The size of the clusters increases rapidly with increasing attraction and beyond a critical value a transient (bond) percolating network is formed. Spheres that are part of the network are immobile until the bonds that tie them to the network are broken. A detailed study of the diffusion coefficient of square well fluids forming rigid bonds using BCD2 has been reported recently [77]. It was shown that D decreases with increasing B_{att} following a power law for large B_{att} and only becomes zero when the bonds are irreversible, i.e. $B_{att} \to \infty$.

In comparison, the influence of attraction on D is weak when the bonds are flexible, i.e. using EDBD, BCD1 or BCD3. The difference between methods BCD1 (EDBD) and BCD3 is that for the latter clusters move faster (Zimm dynamics) so that D is slightly larger. The effect increases with increasing cluster size and is expected to be maximal close to the percolation threshold. The values of B_{att} at the bond percolation thresholds are about 6 at $\phi = 0.15$ for both well widths, while at $\phi = 0.49$ they are 0.5 and 1.2 for $\epsilon = 0.1$ and 0.5, respectively. The difference between the two methods decreases for larger B_{att} when most spheres belong to the percolating network that has no center of mass movement. The few remaining free spheres are mostly monomers so that the movement steps BCD1 and BCD3 become equivalent.

Regardless of the method, the effect of attraction on D is qualitatively different if the bonds are flexible, because in that case bound spheres can move freely within the interaction range. D increases weakly with increasing attraction until it reaches a maximum beyond which it decreases. The relative amplitude of the increase is very small for the volume fractions studied here, but becomes important at higher volume fractions [14]. It is at the origin of the so-called reentrant glass transition of interacting spheres as a function of the attraction strength [69, 148]. The influence of attraction on the critical slowing down of hard spheres has attracted a lot of attention in the recent past and has been investigated for square well fluids using EDBD simulations [63].

The appearance of a maximum diffusion coefficient can be qualitatively understood by considering two opposing effects. On one hand, attraction causes clustering of particles so that more space is created in which monomers and clusters can diffuse freely, leading to faster diffusion of the spheres. On the other hand, bonds restrict the motion of spheres and the long time diffusion of bound spheres is equal to the center of mass diffusion of the clusters to which they belong. The restriction becomes more important as the average bond life time increases.

When the attraction is weak the average bond life time is still small so that the effect of restriction is weak and the effect of creating more free space dominates leading to an increase of D. With increasing B_{att} the clusters become larger and the average bond life time increases until the effect of increasing restriction of the movement becomes more important than the effect of increasing free volume so that D decreases. These features are independent of the volume fraction and the well width. The effect of attraction on the diffusion coefficient remains small in the single phase regime if the bonds are flexible at least for $\phi < 0.5$.

6.1.4 Summary

BCD and EDBD simulations of hard spheres interacting with a square well potential lead to steady states that have almost the same structure factor and the cluster size distribution.

EDBD assumes flexible bonds and ignores hydrodynamic interaction. The values of the self diffusion coefficient obtained by EDBD are very close to those obtained with BCD if the same assumptions are used. A weak maximum of D is found as a function of the interaction strength caused by the opposing effects of increasing free volume and increasing bond life time.

The effect of intra-cluster hydrodynamics (Zimm dynamics) and bond rigidity can be explored with BCD. Introducing rigid bonds leads to a strong decrease of D with increasing attraction and suppresses the maximum. Introducing intra-cluster hydrodynamics to the system with flexible bonds weakly increases D at a given interaction strength.

Chapter 7

Diffusion limited cluster aggregation with irreversible flexible bonds

[7.1] S. Babu, J. C. Gimel and T. Nicolai *in preparation* (2007)

7.1 Diffusion limited cluster aggregation with irreversible flexible bonds

Abstract

Irreversible diffusion limited cluster aggregation (DLCA) of hard spheres was simulated using Brownian cluster dynamics. Bound spheres were allowed to move freely within a specified range, but no bond breaking was allowed. The structure and size distribution of the clusters was investigated before gelation. The pair correlation function and the static structure factor of the gels were determined as a function of the volume fraction and time. Bond flexibility led to local densification of the clusters and the gels, with a certain degree of order. At low volume fractions densification of the clusters occurred during their growth, but at higher volume fractions it occurred mainly after gelation. At very low volume fractions, the large scale structure (fractal dimension), size distribution and growth kinetics of the clusters was found to be close to that known for DLCA with rigid bonds. Restructuring of the gels continued for long times, indicating that aging processes in systems with strong attraction do not necessarily involve bond breaking. The mean square displacement of particles in the gels was determined. It is shown to be highly heterogeneous and to increase with decreasing volume fraction.

7.1.1 Introduction

Strong attraction between particles in solution leads to aggregation. The kinetics of this aggregation process depends on the probability that a bond is formed when two particles collide. Two limiting cases are diffusion limited cluster aggregation (DLCA) if bonds are formed at each collision and reaction limited cluster aggregation (RLCA) if the probability to form a bond is very small. Irreversible aggregation has been studied in detail both experimentally [1, 36, 85, 86, 178, 179] and using computer simulations [3, 4, 23–27, 31, 180–182]. The structure of clusters formed by random aggregation is self similar and characterized by a fractal dimension (d_f), which relates the radius of gyration (R_g) to the aggregation number (m): $m \propto R_g^{d_f}$. The number of clusters with aggregation number m can be described by a power law: $N(m) \propto m^{-\tau}$. As long as the clusters are on average far apart (flocculation) one finds $d_f = 1.8$ and $\tau = 0$ for DLCA and $d_f = 2.1$ and $\tau = 1.5$ for RLCA [37].

With time the clusters grow and the cumulated volume occupied by the clusters ($V_{cum} = \sum N(m) \cdot 4\pi R_g^3/3$) increases so that the average free space between the aggregates decreases. When V_{cum} approaches the volume of the system the aggregates start to interpenetrate. The aggregation process of highly interpenetrated clusters can be described by the percolation model and leads to gelation. For percolating clusters $d_f = 2.5$ and $\tau = 2.2$ [35]. The cross-over between flocculation and percolation occurs at a characteristic aggregation number (m_c) and radius of gyration (R_c), that decrease with increasing particle volume fraction (ϕ) [23, 25, 27].

Computer simulations of irreversible DLCA and RLCA have been done so far for hard spheres that form rigid bonds at contact [25, 26, 114, 182]. In this case the aggregated particles are on average bound to two other particles, because ternary collisions are not possible. However, in reality the bonds may be flexible, i.e. they may freely rotate. One example is the much studied aggregation of spheres in the presence of other smaller particles through a depletion interaction [59, 183–187]. Another example is the aggregation of emulsion droplets with a slippery layer [36]. The latter experiment has motivated computer simulations of irreversible diffusion limited aggregation (DLA) with flexible bonds [181]. The difference between DLA and DLCA is that during the former individual particles are allowed to diffuse until they collide with a single cluster [37], while during the latter all particles in the systems diffuse and collide to form many clusters. DLA leads to a self similar cluster with $d_f = 2.5$. In ref. [181] the DLA simulation was modified to include free diffusion of the particle on the surface of the particle to which it is bound and was called slippery DLA. Real random aggregation processes are, of course, better described by DLCA.

Here we report on a simulation study of DLCA with finite interaction range in which the relative motion of bound particles is unhindered as long they remain within each others range. If the interaction range is very small compared to the radius of the particles this method could be called slippery DLCA, but here we will use the expression flexible DLCA for all interaction ranges. Flexible DLCA (or RLCA) should represent realistically the experimental systems mentioned above in the limiting case

that the attraction energy is much larger than the thermal energy. The results of flexible DLCA will be compared to those obtained by DLCA with rigid bonds.

7.1.2 Simulation method

The simulation method used here is called Brownian Cluster Dynamics (BCD). A detailed description of the method and a comparison with molecular dynamics were reported elsewhere [188]. Briefly, clusters are formed by connecting spheres within each others interaction range with probability P. Particles are chosen randomly and moved a step size s in a random direction unless it leads to overlap or breaks a bond. The centre of mass displacement of the clusters is calculated and the clusters are moved cooperatively in the same direction so that the total displacement is inversely proportional to their radius, unless it leads to overlap. BCD is equivalent to molecular dynamics if the cooperative cluster displacement is omitted as long as s is sufficiently small. Systems with rigid bonds are simulated by performing only the cooperative cluster movements and not the individual particle displacements within the clusters. The equilibrium state obtained by molecular dynamics and BCD is the same, but the dynamics depend strongly on whether the bonds are rigid or flexible.

Irreversible DLCA is simulated by setting $P = 1$. The simulation is started with N_{tot} randomly distributed spheres with unit diameter in a box of size L so that $\phi = N_{tot}/L^3(\pi/6)$. The unit of time is set equal to the time needed for an isolated sphere to diffuse a distance equal to its diameter. E.g. for spheres with diameter $1\mu m$ in water at $20°C$ the time unit is 0.4 seconds. The box size was varied up to $L = 100$ and all the results shown here were not influenced by finite size effects unless specified.

7.1.3 Results

In the following we show mainly results obtained with the interaction range fixed at $\epsilon = 0.1$, but we will briefly discuss the effect of varying the range.

Kinetics

It is well known that in the flocculation regime, i.e. $V_{cum} \ll L^3$ the cluster growth during DLCA can be described by the kinetic equations introduced by Smolechowski [39–41]:

$$\frac{\mathrm{d}N(m)}{\mathrm{d}t} = \frac{1}{2}\sum_{i+j} K(i,j)N(i)N(j) - \sum_{j} K(m,j)N(m)N(j) \tag{7.1}$$

Where $K(i,j)$ is the so-called kernel that expresses the rate constant at which a cluster with aggregation number i collides with a cluster with aggregation number j:

$$K(i,j) = 4\pi\left(R_{col,i} + R_{col,j}\right)\left(D_i + D_j\right) \tag{7.2}$$

with D the diffusion coefficient of the clusters and R_{col} their collision radius. D is inversely proportional to the hydrodynamic radius (R_h) of the clusters. For large clusters both R_{col} and R_h are proportional to R_g [175]. In fact, the growth kinetics of DLCA can be well described by eq(7.1) using a constant kernel equal to $K(1,1)$. It follows that the time dependence of the weight (m_w) averaged aggregation number can be written as:

$$m_w = 1 + K(1,1)t\phi \tag{7.3}$$

In our simulations the particle diameter is unity and the diffusion coefficient of the individual spheres is 1/6 so that $K(1,1) = 4\pi/3$. The ratio of the weight and the number (m_n) averaged aggregation numbers becomes two for large m_w. These results have been confirmed using BCD with rigid bonds, but only if ϕ was very low. In [25] the interaction range was zero. Increasing the interaction range increases the collision radius and therefore $K(1,1)$, but the effect is small for $\epsilon = 0.1$. For $\phi > 0.01$ it is difficult to observe the flocculation regime because the crossover to the percolation regime occurs already when m_w is still relatively small. The growth of m_w accelerates when V_{cum} approaches L^3 and m_w diverges at the gel time (t_g). This change of the growth kinetics between flocculation at short times and percolation close to t_g has also been observed experimentally [112].

Figure(7.1a) compares the increase of $m_w - 1$ as a function of time for DLCA with rigid and with flexible bonds at different volume fractions, while fig.(7.1b) shows the evolution of the polydispersity index (m_w/m_n). The size of the clusters at the start of the simulation depends on the interaction range and the volume fraction, because more particles are within each others range if ϵ or ϕ are larger. For large ϵ and ϕ the system percolates immediately, i.e. when the spheres are still randomly distributed, as was discussed in detail in [164]. The percolation threshold decreases with increasing ϕ and is 0.27 for $\epsilon = 0.1$.

At $\phi = 0.01$ the increase of m_w with time was linear and m_w/m_n was close to two as expected for the flocculation regime. The results were similar for rigid and flexible DLCA, but rigid DLCA showed the influence of a transition to the percolation regime sooner. The gel point was not reached for this volume fraction during the simulation which took several weeks of computer time. For $\phi > 0.08$ the flocculation regime was not observed and the growth of both the size and the polydispersity of the clusters accelerated until they diverged at t_g. The growth of the clusters and gelation was somewhat faster for flexible DLCA. At $\phi = 0.05$ the increase of m_w was initially slightly faster during flexible DLCA, but then the growth became almost linear over a short period of time while the polydispersity index remained constant. After this period the increase of m_w and m_w/m_n accelerated until the gel was formed. During rigid DLCA the slowing down of the aggregation was not observed so that gelation at this volume fraction was faster than for flexible DLCA. The growth rate at different volume fractions can be understood by considering the structure of the clusters as will be discussed below.

Figure(7.2) shows $N(m)$ for $m_w = 100$ obtained at different volume fractions.

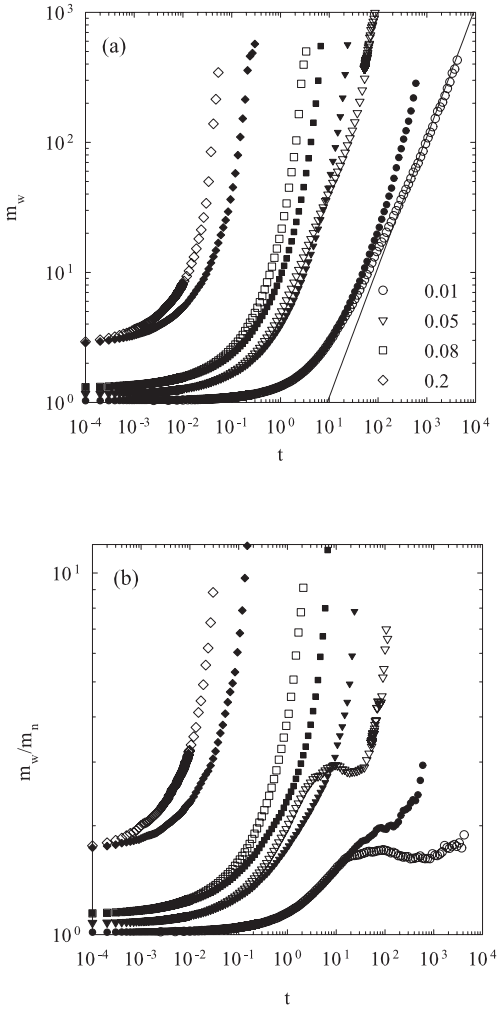

Figure 7.1: (a) $m_w - 1$ is plotted as a function of time t obtained from rigid DLCA (filled symbols) and flexible DLCA (open symbols) for $\epsilon = 0.1$ at different ϕ as indicated in the figure. The solid line has a slope of 1. (b) The polydispersity index is plotted as a funtion of t for different ϕ.

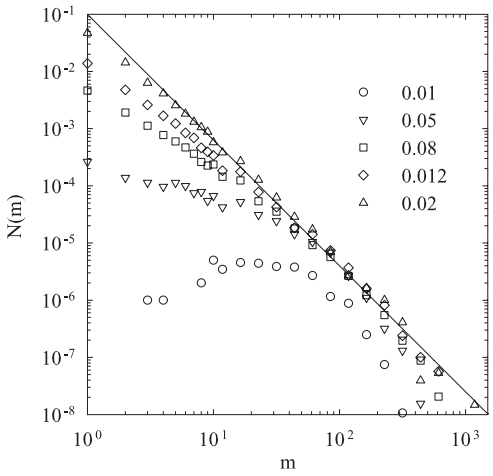

Figure 7.2: Cluster size distribution is plotted as a function of the aggregation number m obtained from flexible DLCA for $\epsilon = 0.1$ at different ϕ as indicated in the figure. The solid line has a slope of -2.2.

At the lowest concentration we observed a bell shape as is also observed for rigid DLCA in the flocculation regime [25, 189]. At higher volume fractions $N(m)$ followed approximately the power law decay expected for the percolation regime: $N(m) \propto m^{-2.2}$. We note that the cut-off function of the size distribution of percolating clusters has a Gaussian shape [110, 180]. More extensive simulations on even larger boxes will be needed to test whether $N(m)$ obtained from flexible DLCA has exactly the same functional form as for rigid DLCA or static percolation.

Aggregation leads to an increase of the number of bonds per particle (z). In fig.(7.3a) the average number of bonds per particle ($< z >$) is plotted as a function of time. As mentioned above, the starting value of $< z >$ is larger for larger ϕ because more randomly distributed spheres are within each others interaction range. At low volume fractions, $< z >$ increased during rigid DLCA until it stagnated at a value close to 2, while at large ϕ the increase of $< z >$ was small because almost all the particles were already part of the final structure at the start of the aggregation. During flexible DLCA $< z >$ increased sharply at first, but when it had reached a value around 7 further growth of $< z >$ became very slow. Contrary to the case of rigid DLCA, $< z >$ continued to increase over the whole duration of the simulation even after all spheres were attached to the network indicating that restructuring of the system occurred. This process was very slow and may be called ageing. For $\phi > 0.08$ most of the restructuring happened after the gel point and continued even when the sol fraction had become very small.

In fig.(7.3b) are plotted the values of $< z >$ at the end of the simulation as a function of the volume fraction. $< z >$ has a minimum at $\phi \approx 0.2$, the origin of which will be discussed below. The distribution of z at long times only weakly

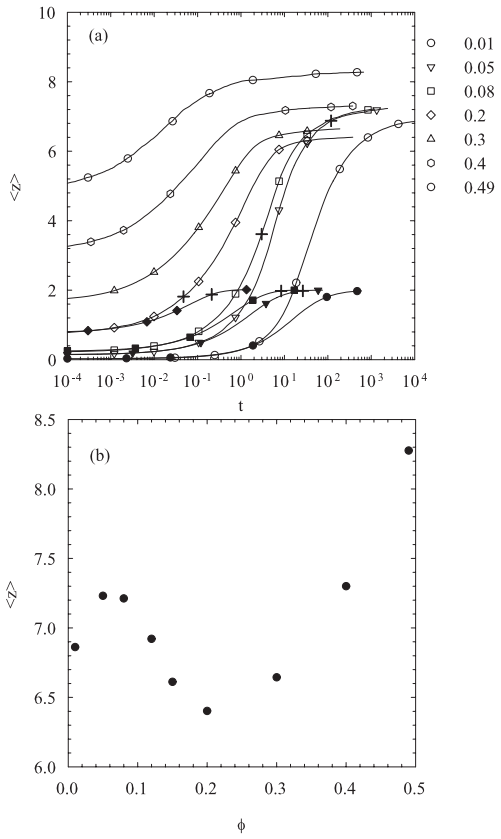

Figure 7.3: (a) The average number of neighbor obtained from rigid DLCA (filled symbols) and flexible DLCA (open symbols) for $\epsilon = 0.1$ is plotted as a function of time for different ϕ as indicated in the figure crosses indicate the gel time. (b) $< z >$ at the end of the simulation for flexible DLCA with $\epsilon = 0.1$ is plotted as a function of ϕ.

depended on the volume fraction for $\phi < 0.3$. It was approximately Gaussian with a half width of 4. It started at $z = 3$ and peaked close to $< z >$. Very few particles had $z = 12$ showing that no crystallisation had occurred. At higher volume fractions the distribution shifted to larger z.

Cluster structure

During rigid DLCA the cluster configuration is determined by random collisions and the clusters cannot rearrange once they are formed. Therefore rigid DLCA yields in the flocculation regime clusters with the same average radius of gyration for a given aggregation number independent of time. This is not the case for flexible DLCA where the particles in the clusters rearrange until a maximum of bonds are formed without breaking any existing bond. In this way the density of the clusters increases with

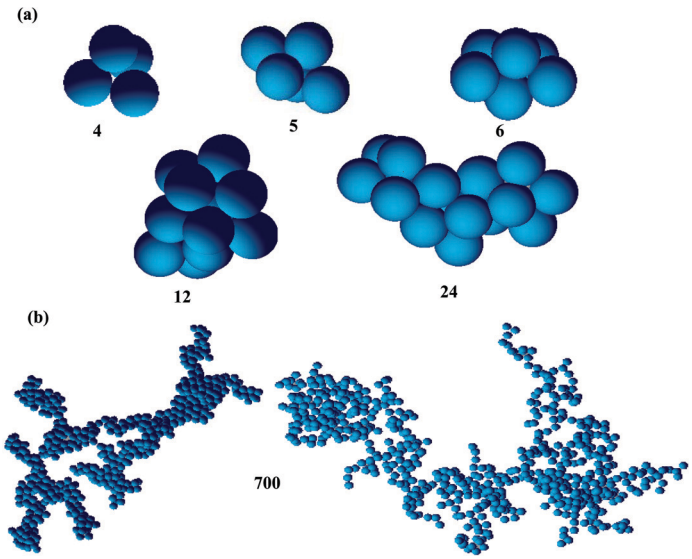

Figure 7.4: (a)Images of clusters with different aggregation numbers formed by flexible DLCA with $\epsilon = 0.1$. (b) Comparison of a cluster formed by flexible DLCA (left) and by rigid DLCA (right) with aggregation number 700.

time. At very low volume fractions the growth rate was slower than the restructuring time so that at each moment the cluster configuration had reached the steady state, while at high volume fractions the gel was formed quicker than the time needed to restructure. Therefore the value of $< z >$ at the gel point were close to the final value for $\phi < 0.05$, but much lower at large ϕ, see fig.(7.3a).

Figure(7.4a) shows images of clusters formed during flexible DLCA at very low volume fractions. The configuration of clusters up to $m = 6$ was unique contrary to clusters formed by rigid DLCA. For $m = 7$ one configuration was observed in 90% of the cases, but one other configuration was also possible. With increasing aggregation number more different configurations were found. Large clusters were generally elongated strands that branched when m exceeded about 20. The randomly branched structures resembled clusters formed by rigid DLCA, except that the strands were much thicker than the single particle diameter, see fig.(7f.4b). The basic unit of all larger clusters formed by flexible DLCA was a tetrahedron and for $m \geq 4$ particles with less than 3 neighbours were not observed. The fact that the tetrahedron is the basic structural unit does not imply however that tetrahedra were formed first and subsequently aggregated to form larger clusters as was suggested in [36]. At all stages of the aggregation we observed all aggregation numbers with no preference for multiples of 4.

As mentioned in the introduction, the large scale structure of clusters formed by rigid DLCA in the flocculation regime is self similar with $d_f = 1.8$. In fig.(7.5a) a comparison is shown of the dependence of m on R_g between clusters formed by flexible DLCA and by rigid DLCA at $\phi = 0.01$. In both cases $m = a \cdot R_g^{1.8}$, but the prefactor

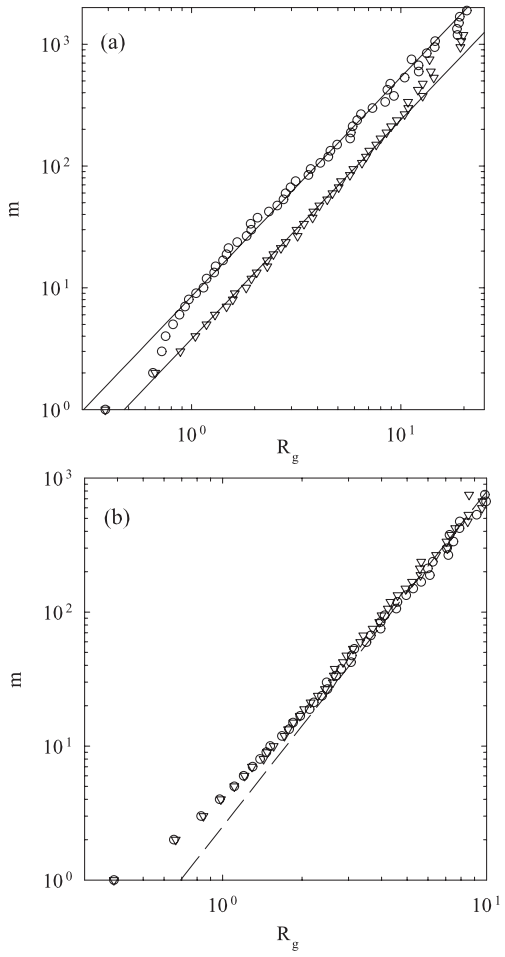

Figure 7.5: The aggregation number is plotted as function of R_g for both rigid DLCA (triangles) and flexible DLCA (circles) at (a) $\phi = 0.01$ and (b) $\phi = 0.2$ with $\epsilon = 0.1$. The solid lines and the dashed line have slopes of -1.8 and -2.5 respectively.

was larger for flexible DLCA ($a = 8.5$) than for rigid DLCA ($a = 3.8$) because the local structure of clusters is denser. Figure(7.5b) shows the dependence of m on R_g for clusters formed at $\phi = 0.2$ close to the gel point. The structure of the clusters was almost the same for flexible and rigid DLCA because not much restructuring had yet occurred before the gel was formed. For larger clusters $m \propto R_g^{2.5}$ as predicted by the percolation theory. At intermediate volume fractions the density of the clusters increased with time for flexible DLCA and the transition between flocculation and percolation shifted to larger values of m with decreasing ϕ.

The structure of the clusters at higher volume fractions was the same for rigid and flexible DLCA, yet the growth rate was faster for flexible DLCA. This can be explained by the fact that neighbouring fractal clusters have a larger probability to

bind when they are flexible than when they are rigid. It is likely that in the case of rigid clusters rotation would also accelerate the growth during the percolation regime. At low volume fractions both the collision radius and the hydrodynamic radius of clusters formed during flexible DLCA were smaller for a given aggregation number. Apparently, both effects compensated to give similar growth kinetics for flexible and rigid DLCA. However, the percolation regime was reached at larger m during flexible DLCA than during rigid DLCA. Densification of the clusters during flexible DLCA explains why the growth rate at $\phi = 0.05$ was initially faster and at later times slower than for rigid DLCA. Initially, the growth was faster due to flexibility, but later densification rendered the clusters smaller so that the transition to the percolation regime was delayed.

Gel structure

The gel structure can be characterized by the pair correlation function ($g(r)$) or its Fourier transform the static structure factor ($S(q)$). $g(r)$ represents the average number concentration of particles at a distance r from any given particle and reaches the number concentration of the system ($C = \phi 6/\pi$) at large r. An extensive study of gels formed by rigid DLCA was reported in [25, 26]. It was shown that pair correlation functions of gels at low volume fractions had distinct features at small r followed by a power law decay ($g(r) \propto r^{(d_f-3)}$ with $d_f = 1.8$) for $r > 3$. $g(r)$ had a weak minimum at a characteristic value r_{min} close to the correlation length of the concentration fluctuations before it reached C. The correlation length decreased with increasing volume fraction, and became of the order of a few particle diameters for $\phi > 0.05$. As a consequence, the fractal structure did not exist at higher volume fractions.

$g(r)$ showed a delta peak at $r = 1$ representing the contribution of the two nearest neighbours and increased continuously to 0.18 at $r = 2$ starting from a low value close to $r = 1$. At low volume fractions the main contribution to $g(r)$ in this range came from the bound next-nearest neighbours. Their contribution stopped at $r = 2$ which caused a discontinuous drop of $g(r)$. A small inflection of $g(r)$ was observed at $r = 3$ marking the influence of the second shell and at larger r the power law decay started. The local structure of the gels was identical for small volume fractions ($\phi < 0.05$) but changed at higher volume fractions because positional correlations between randomly distributed spheres at $t = 0$ were no longer negligible.

Figure.(7.6a) shows pair correlation functions of gels obtained by flexible DLCA at different volume fractions. The values of $g(r)$ within the interaction range were much larger than for $r > 1 + \epsilon$ and are shown separately in fig.(7.6b). There is a discontinuity in $g(r)$ at $r = 1 + \epsilon$, i.e. the maximum distance between a pair of bonded particles. This discontinuity is a consequence of the square well interaction and is not seen for a continuous potential such as the Lennart-Jones potential. For $r > 1 + \epsilon$, peaks can be seen indicating a high degree of local order that was absent for rigid DLCA. The maxima at $r = 1.7 - 1.8$ and $r = 2 - 2.2$ are characteristic for the tetrahedral structure with a bond length between 1 and 1.1. If this structure

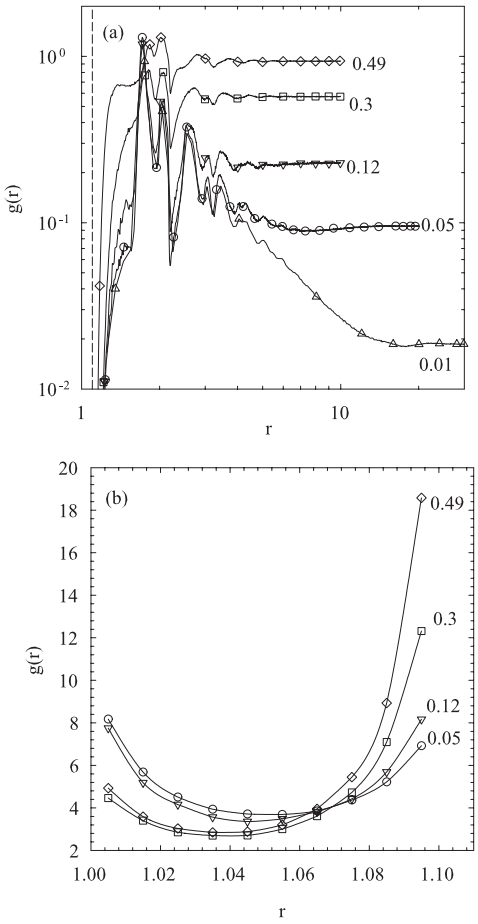

Figure 7.6: (a) The pair correlation function is plotted for different ϕ for $\epsilon = 0.1$ as indicated in the figure. The dashed line indicate the interaction range 1.1. (b) Zoom of $g(r)$ between $1 < r < 1 + \epsilon$.

is extended in a regular linear fashion it leads to the so-called Bernal spiral. Small peaks at larger distances indicate that the order persists to some extent but for $r > 5$ the structure became self similar.

At even larger distances a very weak minimum was observed at small volume fractions similar to that found for rigid DLCA, but at a given volume fraction it was situated at larger r values for flexible DLCA. At a given volume fraction, the correlation length of the gel is larger for flexible DLCA because the structure is locally denser. For the same reason the crossover between flocculation and percolation occurred at larger R_g. It was shown in [26] for rigid DLCA, that the correlation length and R_c are close.

Bonded nearest neighbours can be situated at any distance within the interaction range, i.e. between 1 and 1.1 in the present case, but fig(7.6b) shows that the distance was not uniformly distributed. In fact there was a preference for distances close to 1

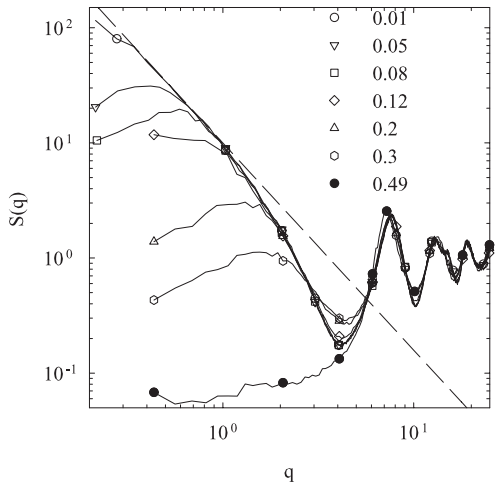

Figure 7.7: The structure factor is plotted for ϵ at different ϕ as indicated in the figure. The solid lines are guide to the eye and dashed line have a slope of 1.8. For clarity we have kept only few symbols.

or $1 + \epsilon$, which means that some bonds were compressed and others stretched. The local structure was independent of the volume fraction for $\phi < 0.1$, because it is mainly determined by the aggregation process of particles that were initially outside each others range. At higher volume fractions a significant number of particles were in contact before the aggregation process started. The restructuring was thus more constrained and leading to less local order. The split between the peaks at $r = 1.7$ and 2 became less distinct and resembled more closely the split peak observed for super cooled liquids.

The corresponding structure factors are shown in fig.(7.7) for different volume fractions. At small q a maximum was found at a value (q_{max}) that increased with increasing concentration. For rigid DLCA it was shown that the position of maximum is inversely proportional to that of the minimum of the pair correlation function $q_{max} \propto 3/r_{min}$ [26]. Over a narrow q-range $S(q)$ decreased with increasing q following a power law, which is expected for self similar structures: $S(q) \propto q^{-d_f}$. The data are compatible with $d_f = 1.8$, see the solid line in fig.(7.7), but for a precise determination of the fractal dimension even smaller volume fractions need to be investigated. At large q-values $S(q)$ oscillated around unity.

Figure(7.8) compares the structure factors of stable gels formed by flexible and rigid DLCA at $\phi = 0.05$. The maximum has a much larger amplitude and is situated at smaller q-values for gels formed by flexible DLCA and the oscillations at large q are stronger. The reason is that the local density of the gels is higher and therefore the correlation length is larger. At this volume fraction a large scale fractal structure can be observed if the gels are produced by flexible DLCA, but not if they are produced by rigid DLCA.

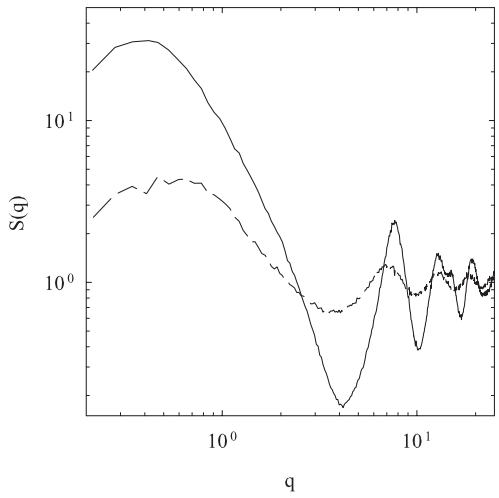

Figure 7.8: The structure factor obtained from flexible DLCA (solid lines) and rigid DLCA (dashed line) for $\phi = 0.05$ and $\epsilon = 0.1$.

Structural evolution

The evolution of $g(r)$ and $S(q)$ as a function of time during rigid DLCA was shown in [26]. With time the maximum of $S(q)$ shifted to lower q and increased in amplitude, while the minimum of $g(r)$ shifted to larger r, because the correlation length increased. During rigid DLCA the structure is fixed as soon as the bonds are formed, but this is not the case for flexible DLCA. We illustrate this point by showing the evolution of the structure at $\phi = 0.08$ during flexible DLCA. At this volume fraction the local structure is not yet influenced by correlation between the randomly distributed spheres.

$g(r)$ is plotted in fig(7.9) at different times. At the start of the aggregation, $g(r)$ was constant within the bond range, i.e. $1 < r < 1.1$, and equal to C. With time the number of bonds increased, but $g(r)$ remained constant in the range even when the gel was formed. At longer times, however, $g(r)$ became larger at $r = 1$ and $r = 1.1$, implying that in order to maximize the number of bonds under constraint, many bonds needed to be either stretched or compressed during restructuring of the gel. The peaks at $r = 1.7$ and $r = 2$ appeared already before the gel point indicating that some tetrahedral structure had been formed without bond stretching or compression. The characteristic minimum of $g(r)$ at r_{min} developed slowly and moved to longer distances.

Figure(7.10) shows the corresponding evolution of the structure factor. The shift of the maximum to lower q and the increase of its amplitude are caused by an increase of the correlation length. The amplitude of the oscillations at high q-values increased due to local densification. At low volume fractions the pair correlation function and the structure factor changed very little after the gel point because the aggregation was

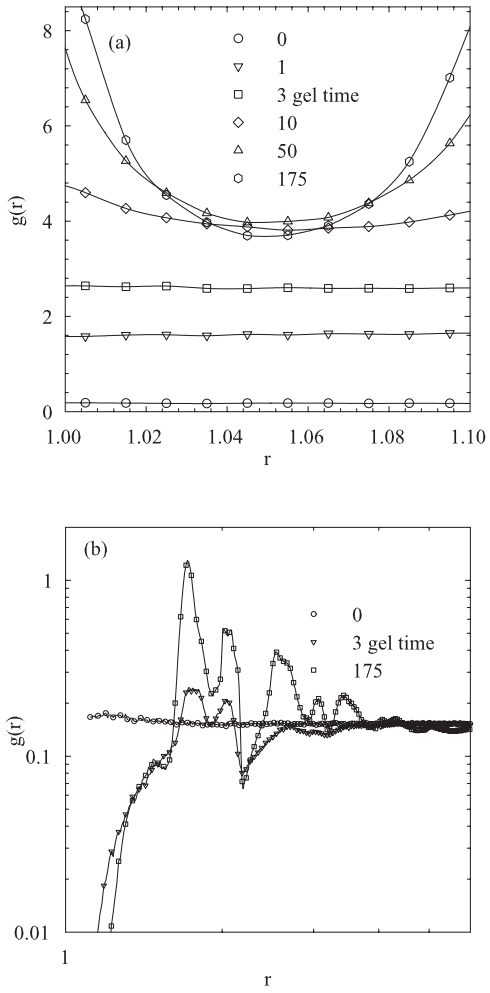

Figure 7.9: (a) $g(r)$ is plotted as a funtion of distance for $\phi = 0.08$ and $\epsilon = 0.1$ between $1 < r < 1 + \epsilon$ at different times as indicated in the figure. (b) $g(r)$ is plotted for $r > 1 + \epsilon$ for the same system at different times as indicated in the figure.

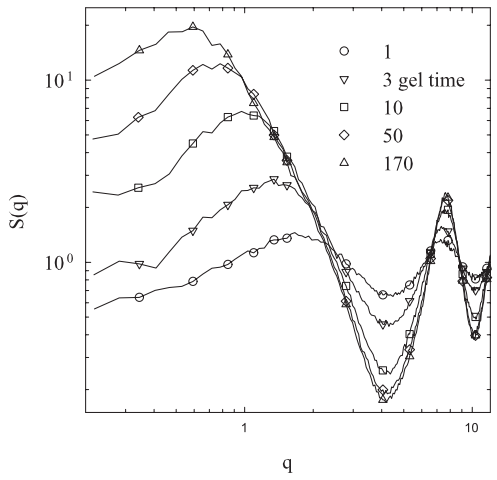

Figure 7.10: The $S(q)$ is plotted for $\phi = 0.08$ and $\epsilon = 0.1$ for different times as indicated in the figure.

sufficiently slow so that the clusters had time to restructure before they percolated. At high volume fractions gels were formed very rapidly and the structure at the gel point resembled that of gels formed by rigid DLCA. In this case, the distinguishing features of the flexible DLCA gels developed after the gel point. At long times the structural changes became increasingly slow, but they did not stop completely during the simulation time.

Dynamics

For rigid DLCA the mean squared displacement (MSD) of the spheres in the gels is, of course, zero. However, in flexible DLCA gels the spheres have a significant mobility, which can be characterised by measuring the MSD as a function of time. It is important to distinguish displacements due to restructuring from displacements due to flexibility. The displacement due to restructuring can be probed by measuring the average total MSD from the start of the aggregation process. The total MSD as a function of time increases rapidly at first followed by a very week increase when all particles are part of the gel.

One can characterise the flexibility of the gels by measuring the MSD over a period of time during which restructuring is negligible, i.e. for gels that have aged for a long time. Alternatively, one can stop further bond formation and thus further restructuring. This is, of course, easier to do in simulations than in experiments on real systems. Figure(7.11a) shows the MSD of spheres in gels at the latest simulation time, when all particles were part of the percolating network. Initially, free diffusion was observed over very short distances. Then the average MSD slowed down and finally stagnated at a value $< r^2 >= \delta^2$. δ^2 increased with decreasing concentration,

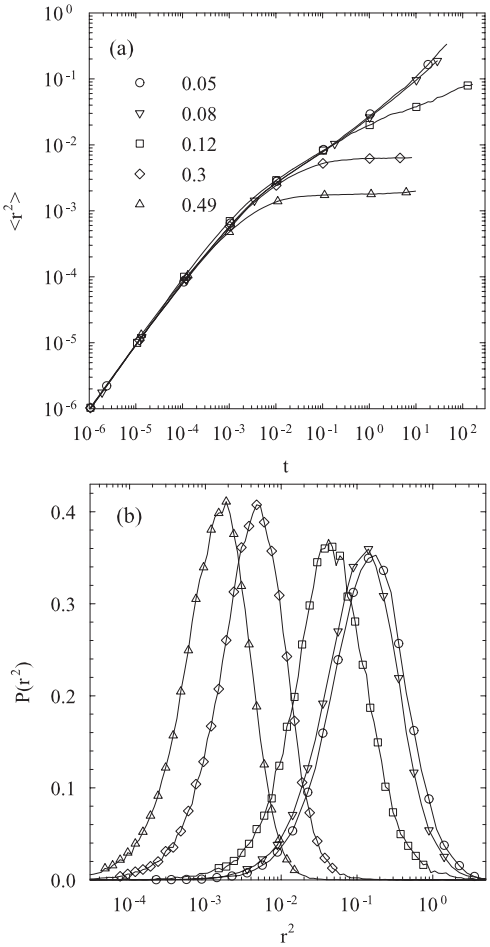

Figure 7.11: (a) The MSD of spheres in aged gel is plotted as a funtion of time for different ϕ as indicated in the figure. (b) The corresponding distribution of r^2 at the longest time.

but we could not properly observe δ^2 at low volume fractions because the times scales involved were too large.

If the displacement of the particles is caused by Brownian motion, the distribution of r^2 (or the self part of the van Hove correlation function $P(r^2)$) can be described by a Gaussian function. Figure(7.11b) shows $P(r^2)$ when the average was close to δ^2. It is clear that the displacement was highly heterogeneous as might be expected from the heterogeneous structure of the gels.

The self part of the intermediate scattering function was found to fully decay at scattering wave vectors $q \gg 1/\delta$, while it showed a plateau at long delay times for smaller q at a value that increased with decreasing q. This is, of course, a direct consequence of the restricted MSD of the particles, see below.

Effect of the interaction range.

For rigid DLCA the effect of increasing the interaction range is twofold. In the first place, as mentioned above, the collision radius of the spheres is increased by a factor $1+\epsilon$. As a consequence the clusters are larger and the aggregation is faster. In the second place, the concentration of bonds between the randomly distributed spheres at the start of the aggregation is larger. The latter effect becomes important when the average distance between nearest neighbours (Δ) is smaller than $1+\epsilon$ ($\Delta < 1.1$ for $\phi > 0.2$). The percolation threshold of randomly distributed spheres decreases with increasing ϵ was discussed in [164]. However, as long as Δ is much larger than $1+\epsilon$, i.e. at small volume fractions, the effect of the interaction range on the structure of the clusters and the gels is small and the fractal dimension remains the same.

For flexible DLCA the same effects are present, but in addition the system has a larger degree of freedom to increase the number of bonds by restructuring if ϵ is larger. As a consequence the value of $< z >$ of the gels increases with increasing ϵ. For $\epsilon = 0.5$ we found $< z > \approx 9.5$ after long times at low volume fractions. The larger degree of freedom effect could be seen even for pentamers and hexamers where all spheres are bound to all other spheres. A qualitatively different local structure is formed when ϵ is larger than 0.41 because the tetrahedral configuration is no longer the basic unit. Figure(7.12) shows a comparison of the structure factor at $\phi = 0.05$ for $\epsilon = 0.1$ and $\epsilon = 0.5$. The maximum is situated at larger q for $\epsilon = 0.5$ and has a smaller amplitude, indicating that the correlation length is smaller if ϵ is larger. The second maximum is situated at smaller q indicating that the local structure (the strand thickness) is larger and the oscillations at high q have a lower amplitude indicating less order. The comparison shows that when the interaction range is larger then the gels are more homogeneous with thicker strands and less local order. The effect of the interaction range on the structure is small for small ϵ and we expect that using a smaller interaction range than 0.1 will have little influence on the structure.

7.1.4 Discussion

Experimentally, structures similar to those found in the present simulations of flexible DLCA have been reported for mixtures of hard spheres and polymers in which an effective attraction between the spheres is induced by depletion of the polymers [183]. If the concentration of polymers is high the attraction may become so strong that the aggregation is irreversible on the time scale of observation. In this case no significant evolution of the structure is observed after gelation. We note that in experiments matters are sometimes complicated by electrostatic interaction.

Recently, experiments on aggregating emulsion droplets were reported where the bonds were claimed to be truly irreversible, but bound droplets were free to move along the interface [36]. The structure factor obtained from the experiments was compared to results of flexible DLA simulations [181]. Many of the features that distinguish the structure of clusters formed by rigid DLCA from those formed by

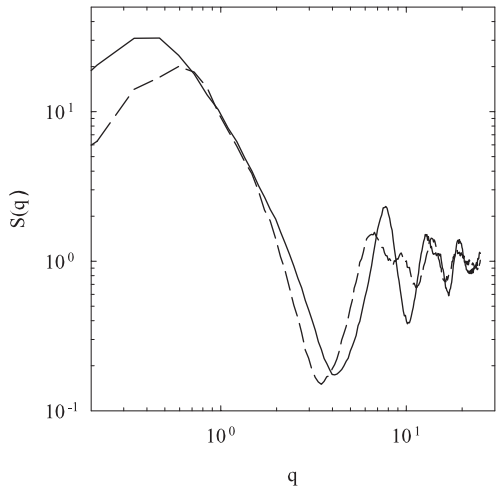

Figure 7.12: The $S(q)$ for $\epsilon = 0.1$ (solid line) and $\epsilon = 0.5$ (dashed line) at $\phi = 0.05$.

flexible DLCA have also been observed in simulations of rigid and flexible DLA with zero interaction range (note that the expressions classic and slippery were used in [181] to refer to rigid and flexible, respectively). Also in DLA, flexible bonds caused the formation of thicker strands with a local tetrahedral configuration. As for DLCA, the fractal dimension of DLA clusters was the same for flexible and rigid bonds. The distribution of z was similar for flexible DLA and DLCA, and the structure factor showed prominent oscillations at high q-values in both cases.

In fig.(7.13) the structure factor obtained from flexible DLCA ($\epsilon = 0.1$) is compared to that obtained from flexible DLA ($\epsilon = 0$) and experiments. The experimental structure factor was obtained by dividing the scattering data of the system with the particle form factor of the droplets. The latter was obtained experimentally before the aggregation had started and was assumed to be not influenced by interaction. As mentioned above, the aggregation process is more realistically described by DLCA, which results in a smaller fractal dimension ($d_f = 1.8$) than obtained by DLA ($d_f = 2.5$). Nevertheless, the results from the two types of simulations are remarkably close at large q-values, indicating that almost the same local structure is formed. This is perhaps not surprising if one considers that local restructuring occurred in both cases until the maximum number of bonds was formed under almost the same constraints. The simulations reproduced the position of the peak at $q = 7.5$ seen in the experiments, but the amplitude was somewhat smaller (notice that the experimental data have been shifted upward for the comparison with the simulation results in figure 4 of [181]). The upturn at low q-values started at larger q in the simulations than in the experiments. However, one should be careful when drawing conclusions on the basis of the deviation at low q-values, because the experimental results are very sensitive to the exact shape of the particle form factor in this q-range.

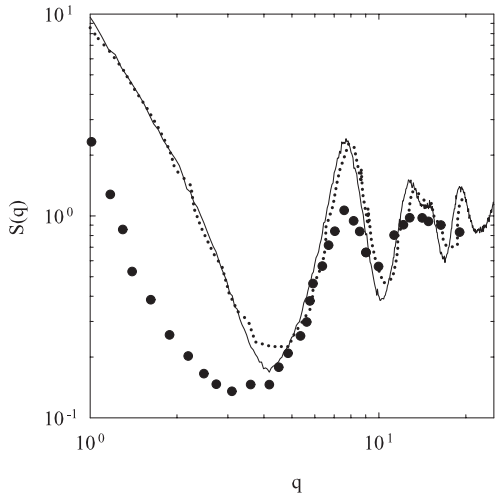

Figure 7.13: Comparison of $S(q)$ between flexible DLCA (solid line), slippery DLA [181](dotted line) and experiment [36] (closed circle).

As far as we are aware, flexible DLCA with strictly irreversible bonds has not been simulated before, but the present results may be compared with molecular dynamics simulations of reversible DLCA in the limit of very strong attraction. Foffi et al. [63] studied the structure and dynamics of spheres with a square well interaction with width $\epsilon = 0.005$ and two different well depths: -2 and -20 kT. The interaction strengths may also be expressed in terms of the second virial coefficient [161]: $B_2 = -44$ and $B_2 = -2.9 \cdot 10^7$, in units of the particle volume. At both interaction strengths the systems are far below the binodal of the liquid-liquid phase separation. Crystallisation was avoided by using a bidisperse distribution of spheres with slightly different sizes. At smaller interaction strength the system slowly coarsened with time, but at $B2 = -2.9 \cdot 10^7$ the bonds may be considered irreversible on the time scale of the simulation. This situation is thus comparable to flexible DLCA.

The features of the gels obtained by Foffi et al. were very close to the ones reported here. Unfortunately, the authors did not show pair correlation functions, which would allow a more detailed comparison of the local structure. But the images of the clusters and the static structure factors of the gels resemble closely those shown here. The distribution of the bond coordination number was almost the same as the one found in this study, but $< z >$ was a bit smaller which can be explained by the narrower interaction range. Foffi et al. also observed a minimum of $< z >$ at volume fractions close to 25%, which they speculated to be related to the critical point of the liquid-liquid phase separation. We believe that the minimum is caused by a combination of opposing effects. At very low volume fractions the clusters can restructure while they grow, but with increasing volume fraction the growth rate increases and much of the restructuring has to occur after the percolation threshold. This increases the

constraints on the restructuring and thus lowers $< z >$ with increasing ϕ. At high volume fractions, however, the number of bonds increases due to crowding even for randomly distributed spheres. This leads to an increase of $< z >$ with increasing ϕ. The latter effect is more important when ϵ is larger, which explains the stronger increase of $< z >$ found in the present study.

Foffi et al. argued that the gel was formed by *a phase separation process interrupted by attractive glass transition*. The same idea has also been put forward by others [59, 69, 75, 187, 190–192]. It is clear, that gelation occurs only for interaction strengths where the equilibrium state would be phase separated and therefore one might indeed call the gel formation an interrupted phase separation. However, the suggested origin of the interruption is debatable. The concept of attractive glass was introduced to account for the slowing down of the dynamics at high concentrations with increasing attraction. Even if attractive glass formation would be a useful concept for hard spheres with a narrow interaction range at high volume fractions it is not clear what it means in the context of the arrested state at low concentrations. Many particles are situated at the surface of the network strands and cannot be in a glassy state. These surface particles can escape from their neighbours by breaking all the bonds. This process inevitably leads to coarsening. The arrest is only inferred if the observation time is shorter than the time needed for surface particles to escape. We have done preliminary simulations that showed that the rate of coarsening decreased with decreasing B_2 following a power law and is simply too slow at $B2 = -2.9 \cdot 10^7$ to observe on the time scale probed by Foffi et al..

The results presented here may also be compared with earlier Brownian dynamics simulations of colloidal gels formed by monodisperse spheres by d'Arjuzon et al.[193]. In those simulations the spheres interacted with a continuous potential that was steeply repulsive at contact and attractive over a range of 0.1. The shape of the potential was chosen to be close to that of depletion interaction. Above a certain interaction strength the spheres crystallised [98], but when the interaction was very strong crystallisation was no longer observed for the duration of the simulation. A detailed study was done of the dynamics of this system at a single volume fraction $\phi = 0.3$ and a minimum interaction potential of $-8kT$. For this interaction strength the life time of the bonds near the potential minimum is very long compared to the duration of the simulation. However, stretched bonds were still rapidly broken and reformed, because the potential goes zero at the outer limit of the interaction range. In spite of the different shape of the potential and the reversibility of stretched bonds many features of this simulation are similar to those reported here for strictly irreversible aggregation with the same bond range. It was also found that $< z >$ increased rapidly at first followed by a very slow increase. A similar distribution of the bond coordination number was found at long times and $g(r)$ showed similar features notably the two peaks indicating tetrahedral structure. The MSD of spheres in the gel and also the distribution of displacements at $\phi = 0.3$ were similar to those reported here. The authors argued that displacements larger than one particle diameter were due to particles breaking of the network. It is clear from the present simulations,

however, that even in irreversibly bound gels large scale mobility is possible due to cooperative motion. It is probable that at lower volume fractions the maximum displacement is determined by the correlation length of the gels. We note that in a recent simulation study of more open gels formed by restricting the bond angles and thus avoiding the formation of dense strands, it was also noted that the MSD displacement can be quite large due to cooperative motion [194].

D'Arjuzon et al. studied the self-intermediate scattering function in detail and found a fast decay towards a plateau followed by a slow decay to zero. The value of the plateau was shown to be directly related to δ. The relaxation time of the slow decay increased with increasing waiting time and became very slow. Preliminary calculations showed similar behaviour for the square well system studied here. The similarities between the two systems indicate that the reversibility of stretched bonds is not an essential feature. We believe that in both systems the aging is caused by the formation of more (strong) bonds under the constraint that existing (strong) bonds cannot break at least for the duration of the simulation.

Lodge and Heyes [99] studied spheres interacting with a Lennart-Jones potential with varying interaction range and depth using Brownian dynamics simulations. A similar shape of the pair correlation function was found if the range was narrow and the interaction strong. However, they also observed a peak at a smaller distance indicating that some crystallisation had occurred. The authors studied the phase separation kinetics up to $t = 40$ in the time units used here. The kinetics was very slow in the case of strong attraction and may thus also be called aging. In fact the time dependence of the peak position shown in fig.(7.10) is close to that obtained by Lodge and Heyes using a Lennart-Jones potential with a narrow interaction range. This indicates again that when the interaction is strong, the breaking of bonds is not important for the aging process at least in the early stages.

7.1.5 Conclusion

Irreversible DLCA with flexible bonds causes locally densification, but on large length scales the structure is the same as for DLCA with rigid bonds. The fractal dimension of clusters formed in very dilute systems is 1.8 in both cases. Locally the systems have a tetrahedral structure and show a certain degree of order that is independent of the volume fraction for $\phi < 0.1$. At higher volume fraction the order is less distinct and similar to that of super cooled liquids.

The system tries to maximize the number of bonds under the constraint of no bond breaking. The increase of the bond coordination number is fast at first, but it becomes progressively slower. The slow restructuring (aging) of the gels continues for very long times. At low volume fractions most of the local densification occurs while the clusters are formed, but at high volume fractions ($\phi > 0.1$) the restructuring occurs mainly after gelation.

At very low volume fractions the growth rate of the clusters during flexible DLCA is the same as for rigid DLCA and can be understood in terms of Smolechowski's

kinetic equations. At high volume fractions the growth rate is somewhat faster, because flexibility increases the collision rate.

Gels formed at low volume fractions show a large degree of flexibility. The average MSD stagnates at a value that increases with decreasing volume fraction. However, the MSD of the particles is highly heterogeneous reflecting the fractal structure of the gels.

Many features that appeared during irreversible flexible DLCA closely resemble simulations and experiments reported in the literature on spheres with a strong but finite attractive interaction. For the interpretation of these studies it is essential to consider whether the effect of bond breaking is significant during the time of observation.

Chapter 8

Tracer diffusion in colloidal gels

[8.1] S. Babu, J. C. Gimel and T. Nicolai *accepted J. Phys. Chem. B* (2007)

8.1 Tracer diffusion in colloidal gels

Abstract

Computer simulations were done of the mean square displacement (MSD) of tracer particles in colloidal gels formed by diffusion or reaction limited aggregation of hard spheres. The diffusion coefficient was found to be determined by the volume fraction accessible to the spherical tracers (ϕ_a) independent of the gel structure or the tracer size. In all cases, critical slowing down was observed at $\phi_a \approx 0.03$ and was characterized by the same scaling laws reported earlier for tracer diffusion in a Lorentz gas. Strong heterogeneity of the MSD was observed at small ϕ_a and was related to the size distribution of pores.

8.1.1 Introduction

Irreversible aggregation of colloidal particles such as proteins [195], clay [86] or oil droplets [88] in solution often leads to the formation of a percolating structure that can resist stress. Recently, the colloidal gel[196, 197] formation has been studied in detail for diffusion limited cluster aggregation of hard spheres using off-lattice computer simulations [25, 26]. The gels have locally a self-similar structure characterized by a fractal dimension and are homogeneous beyond a characteristic length scale that decreases with increasing volume fraction of the particles (ϕ).

The transport properties of tracer particles in colloidal gels obviously depend on the volume fraction of the gels that is accessible to the centre of mass of the particles (ϕ_{a}). The accessible volume, or porosity, depends on the size of the tracers; if the tracers are very small compared to the colloids, ϕ_{a} is close to $1-\phi$ [46], but it decreases for a given ϕ with increasing size of the tracers. Consequently, the long time diffusion coefficient (D) of the tracers decreases with increasing ϕ or tracer size and goes to zero at a critical value of ϕ_{a}. When the accessible volume is small it consists of randomly branched pores that can be of finite size or else percolate through the system.

It has long been known that transport close to the dynamical arrest can be described in terms of diffusion on a percolating network [45]. The geometrical and transport properties of percolation have been investigated extensively on lattices using computer simulations [48, 51, 198]. The diffusion coefficient of particles was found to go to zero at the percolation threshold following a power law: $D \propto \varepsilon^{\mu}$, where $\varepsilon = (\phi_{\mathrm{a}} - \phi_{\mathrm{a}}^{\mathrm{c}})/\phi_{\mathrm{a}}^{\mathrm{c}}$ is the relative distance of the accessible volume fraction to the threshold value ($\phi_{\mathrm{a}}^{\mathrm{c}}$). Close to the threshold the mean square displacement (MSD) of the tracers becomes sub-diffusive meaning that the MSD has a power law dependence on time: $\langle r^2 \rangle \propto t^k$ with $k < 1$ [45, 49].

In standard lattice simulations the probability to move between neighbouring sites of the network is constant. However, in real systems the pores have a broad continuous range of channel diameters and therefore the local mobility of tracers varies in space. In order to account for this effect, the lattice model was extended to include a power law distribution of probabilities to move between sites [198]. If the exponent of this power law is less than unity, the mobility over large distances is dominated by the lowest probability, which decreases with increasing distance. For this reason μ and k are reduced to an extent that depends on the exponent. Two different estimates of μ and k were given for the case of randomly distributed overlapping spherical obstacles, i.e. obstacles forming a so-called Lorentz gas, leading to slightly different values of μ and k: 2.38 and 0.36 [198] or 2.88 and 0.32 [48].

Recently, detailed off-lattice simulations were reported on the tracer diffusion in porous media formed by a Lorentz gas at different densities very close to the percolation threshold [49]. The aim was to verify the adequacy of the extended lattice model for this system. Anomalous diffusion was observed at the threshold and the exponents μ and k were found to be consistent with the predictions by Machta et al [48]. The critical value of the accessible volume fraction was $\phi_{\mathrm{a}}^{\mathrm{c}} = 0.0298$ close

to values found with other simulations [51] and in experiments on real systems [52].

However, a Lorentz gas of overlapping spherical obstacles is not a realistic model for particle gels. Here we investigate the transport in particle gels formed by irreversible aggregation of hard spheres using computer simulations. Two limiting cases are gels formed by diffusion limited aggregation (DLCA) in which a rigid bond is formed at each collision and reaction limited aggregation (RLCA) in which the bond formation probability goes to zero. Irreversible aggregation leads to the formation of self-similar aggregates with a fractal dimension 1.8 for DLCA and 2.1 for RLCA [1]. When the aggregates have grown to the extent that they fill up the space they connect into a system spanning structure. Such gels can actually be made and the diffusion of tracer particles in such systems can be determined experimentally using e.g. confocal laser scanning microscopy [199] or pulsed field gradient NMR [200]. In order to investigate the effect of spatial correlation caused by aggregation, we also studied tracer self-diffusion in systems of frozen randomly distributed hard spheres (FHS).

8.1.2 Simulation method

Gels were simulated by irreversible cluster-cluster aggregation starting from a random distribution of hard spheres with unit diameter until all particles are connected, see ref 4 for details. The diffusion of tracers was simulated by small displacements in a random direction. If the displacement led to overlap the movement was either refused or truncated at contact. For small MSD the step size was chosen sufficiently small so that reducing it further had no significant effect on the results. For large MSD larger step sizes were chosen to speed up the displacement. This did not influence the relative time dependence of the MSD, but did result in the wrong absolute values. The correct absolute values were recovered by superposition at smaller MSD with simulations using small step sizes. In a few cases we used a small step size up to large MSD to verify that this procedure gave the correct results.

The time unit was chosen as the time needed for a tracer to diffuse over its diameter at infinite dilution, which is about $0.4s$ for a particle with a diameter of $1\mu m$ in water at room temperature. Simulations were done in a box with length 50 using periodic boundary conditions. We checked for finite size effects by varying the box size, and all results shown here are not influenced by finite size effects. We averaged over several hundred paths of randomly inserted tracers and 10 independent system configurations. ϕ_{a} was calculated as the probability that a tracer could be randomly inserted without overlap.

8.1.3 Results and discussion

We present first results for the case that the tracer particles have the same diameter as the obstacle particles, after which we discuss the effect of varying the tracer size. In Fig. 8.1 the dependence of ϕ_{a} is plotted as a function of ϕ for randomly distributed

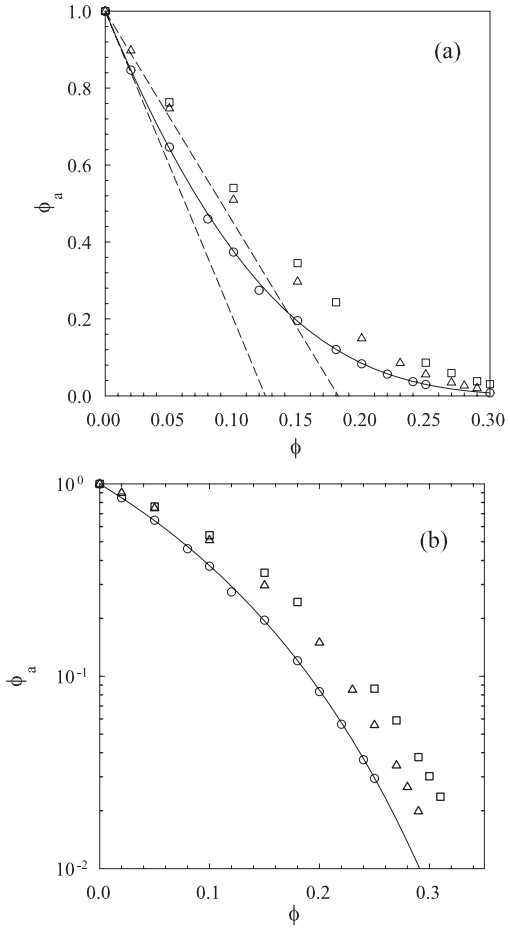

Figure 8.1: (a)The accessible volume fraction as a function of ϕ for tracer spheres in FHS (cirlce), DLCA (triangle) and RLCA (square) gels of spheres with the same diameter as the tracers. The dashed lines represent the limiting low concentration behaviour, see text. (b)Shows the same data on a logarithmic scale for $\phi_{\rm a}$. The solid line represents values calculated using the Carnahan-Starling equation.

hard spheres and gels formed by DLCA and RLCA. In the latter case, ϕ_a increased with decreasing bond formation probability, but the variation became negligible below 10^{-4}, which we have taken as the RLCA limit. For a given concentration, ϕ_a is larger for RLCA gels than for DLCA gels which in turn is larger than for the hard sphere system. Gels have a larger ϕ_a, because the particles are connected and therefore have a larger fraction of overlapping excluded volume. ϕ_a is larger for RLCA than DLCA, because RLCA clusters are denser. For non-interacting hard spheres ϕ_a is directly related to the chemical potential (μ_{cs}): $\phi_a = \phi \exp(-\mu_{cs})$ [21], and can be calculated using the so-called Carnahan-Starling equation [201] for μ_{cs}, see solid line in Fig 8.1. For randomly distributed hard spheres the initial dependence of ϕ_a on ϕ is given by: $\phi_a = 1 - \phi(1+b)^3$, where b is the size ratio of the tracers over the obstacles [46]. For gels the initial dependence can be estimated by assuming that the gels consist of strands of touching spheres: $\phi_a = 1 - \phi(1 + 3b + 1.5b^2)$. The dashed lines in Fig 8.1 show that these estimates are only valid for small ϕ_a.

Images of the accessible volume in DLCA gels at different ϕ are shown in Fig. 8.2. At low volume fractions (Fig. 8.2*a*), almost all pores percolate through the system (*yellow*), but with increasing ϕ (Figs 8.2*b* and 8.2*e*) the fraction of finite pores increases until above a critical value (ϕ^c) (Fig. 8.2*d*) there is no longer a percolating pore. For clarity, we have shown the percolating pore separately in Figs 8.2*c* and 8.2*f*.

The MSD averaged over all tracers is shown in Fig. 8.3 for DLCA gels at different ϕ. The results are similar to those obtained by Höfling et al [49] for the Lorentz gas. Initially, the tracers diffuse freely until they hit the obstacles. Then the displacement of tracers is anomalous until $\langle r^2 \rangle$ exceeds a characteristic value (ξ^2) after which it becomes again diffusional with a reduced diffusion coefficient. ξ represents the correlation length of the percolating pores and diverges at the threshold. The correlation length of the pores depends also on the tracer size, see below, and is not related to the correlation length of the gels. The latter decreases with increasing volume fraction and is only a few particle diameters for $\phi > 0.05$ [26]. The tracers in finite size pores are trapped and do not contribute to $\langle r^2 \rangle$ at long times. For $\phi > \phi_c$, all the tracers are trapped and $\langle r^2 \rangle$ stagnates at twice the averaged squared radius of gyration of the pores ($\langle R_g^2 \rangle$). This follows from the fact that the average distance a tracer has moved in a finite size pore at $t \to \infty$ is the same as the average distance between two randomly placed tracers.

In Fig. 8.4, the dependence on ϕ of the long time diffusion coefficient relative to the free diffusion coefficient (D) is compared for DLCA and RLCA gels and frozen random hard spheres. For a given volume fraction, D is close for the two gels, but is smaller for FHS. We note that for systems of freely moving obstacles D decreases much more slowly with increasing ϕ [77, 166]. D goes to zero at ϕ_c equal to 0.248 ± 0.003, 0.279 ± 0.001 and 0.295 ± 0.005, for FHS, DLCA and RLCA, respectively. The error bars indicated the highest fraction where we observed long time diffusion and the lowest fraction where we observed stagnation of MSD

The same results are plotted as a function of ϕ_a in Fig. 8.5. For comparison

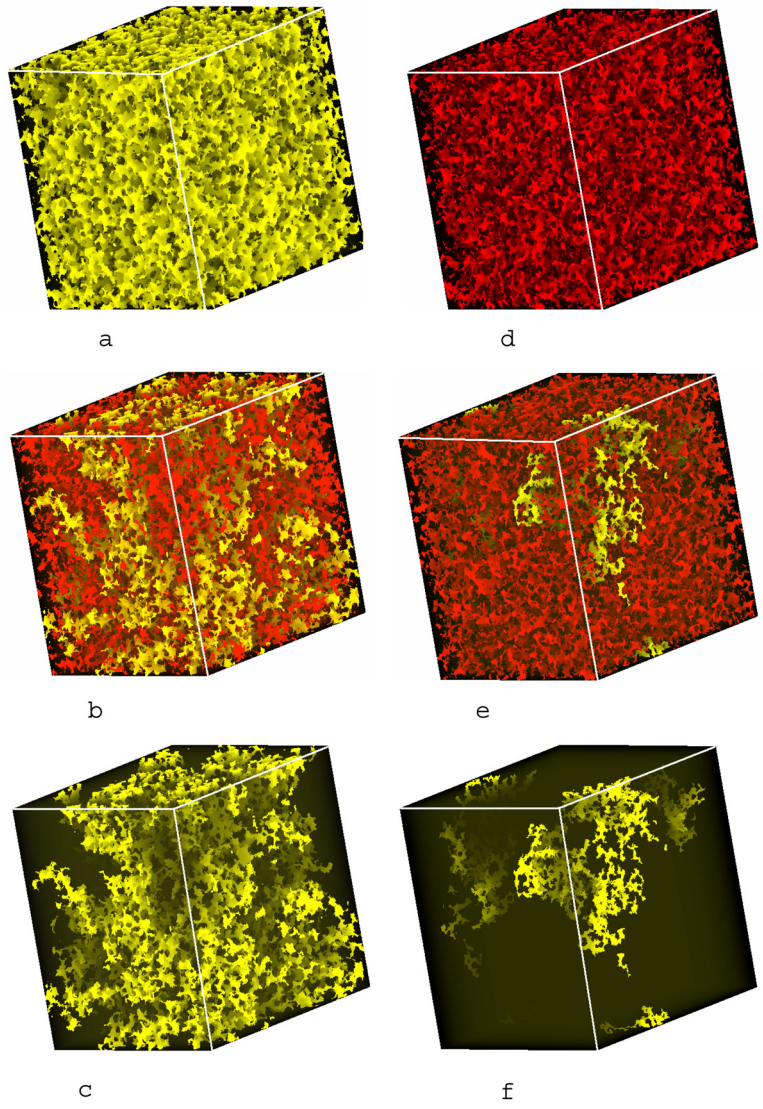

Figure 8.2: Images of the accessible volume for DLCA gels at different values of ϕ_a. Percolating and isolated pores are indicated in yellow and red, respectively. For clarity figures 2*c* and 2*f* show just the percolating pore of systems shown in figures 2*b* and 2*e*, respectively.

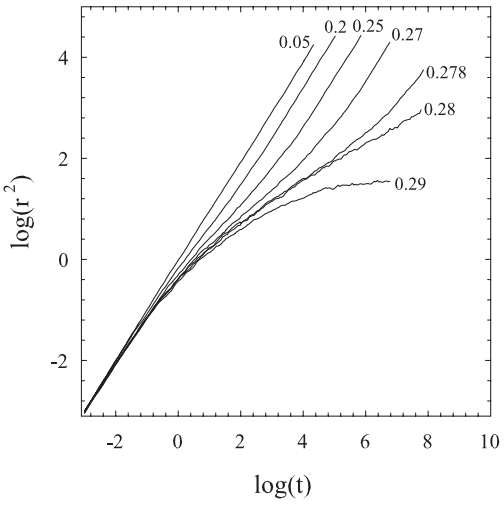

Figure 8.3: MSD of tracer spheres in DLCA gels of spheres with the same diameter as the tracers at different ϕ, indicated in the figure.

we have included in Fig. 8.5 results obtained for the Lorentz gas [49]. Here, and in ref 11, only the diffusion of tracers in the pores is considered. Other results for the Lorentz gas were obtained in the context of the conductivity that is proportional to point tracer diffusion [46, 202]. In these earlier simulations the average was taken over all tracers including the immobile ones placed in the obstacles so that D is reduced by a factor $\phi_{\rm a}$. After correction, these results are close to the results shown in Fig. 8.5. Experimental results derived from conductivity measurements on fused spherical glass beads in water [52] are close to the simulation results. When $\phi_{\rm a}$ approches unity D should decrease as $\sqrt{\phi_{\rm a}}$ [8]. The full dependence can be described approximately by the following empirical equation which has the predicted limiting behavior for $\phi_{\rm a} \to 1$ and $\phi_{\rm a} \to \phi_{\rm a}^{\rm c}$:

$$D = \sqrt{\phi_{\rm a}} \left[\frac{\phi_{\rm a} - \phi_{\rm a}^{\rm c}}{\phi_{\rm a}(1 - \phi_{\rm a}^{\rm c})} \right]^{\mu} \tag{8.1}$$

with $\phi_{\rm a}^{\rm c} = 0.03$ and $\mu = 2.8$ see solid lines in Fig. 8.5.

It appears that $\phi_{\rm a}$ is the parameter that determines the diffusion coefficient for all these different systems; the variation of $\phi_{\rm a}$ for a given D is less than 20%. In each case D goes to zero at a critical value ($\phi_{\rm a}^{\rm c}$) close to 0.03, but the actual value of $\phi_{\rm a}^{\rm c}$ is not universal as noted earlier by Rintoul [51]. The inset of Fig. 8.5 shows the data plotted as a function of the distance to the percolation threshold ε. For the Lorentz gas we have used the precise value of ϕ_a^c calculated by Rintoul: $\phi_{\rm a}^{\rm c} = 0.0301 \pm 0.0003$. For the other systems we do not have the same precision, but we found that the data superimpose close to $\phi_{\rm a}^{\rm c}$ if we choose $\phi_{\rm a}^{\rm c} = 0.029$ for FHS, $\phi_{\rm a}^{\rm c} = 0.02655$ for DLCA gels and $\phi_{\rm a}^{\rm c} = 0.033$ for RLCA gels.

The dependence of D close to the percolation threshold is compatible with a power

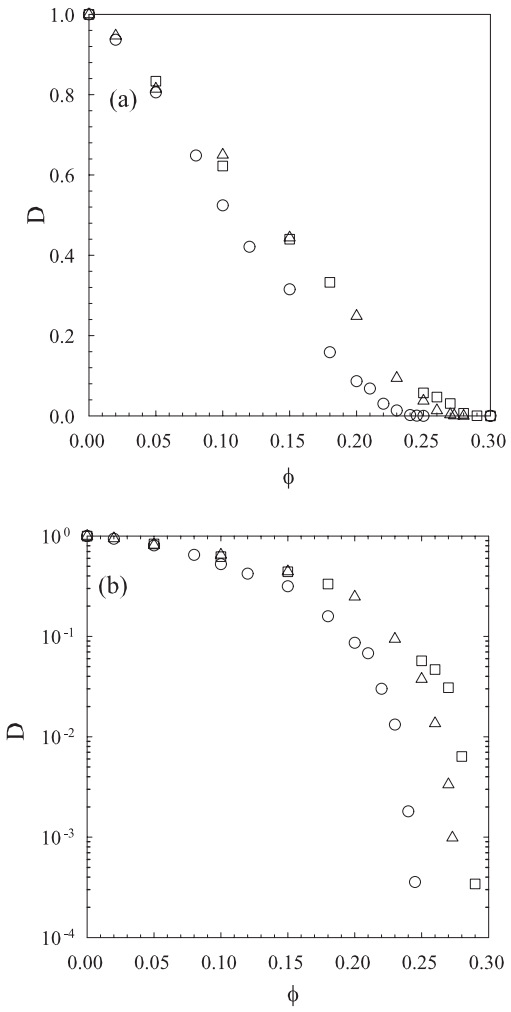

Figure 8.4: (a) Relative diffusion coefficient of tracer spheres as a function of ϕ in FHS (circle), DLCA (triangle) and RLCA (square) gels of spheres with the same diameter as the tracers,(b) shows the same data on a logarithmic scale for D.

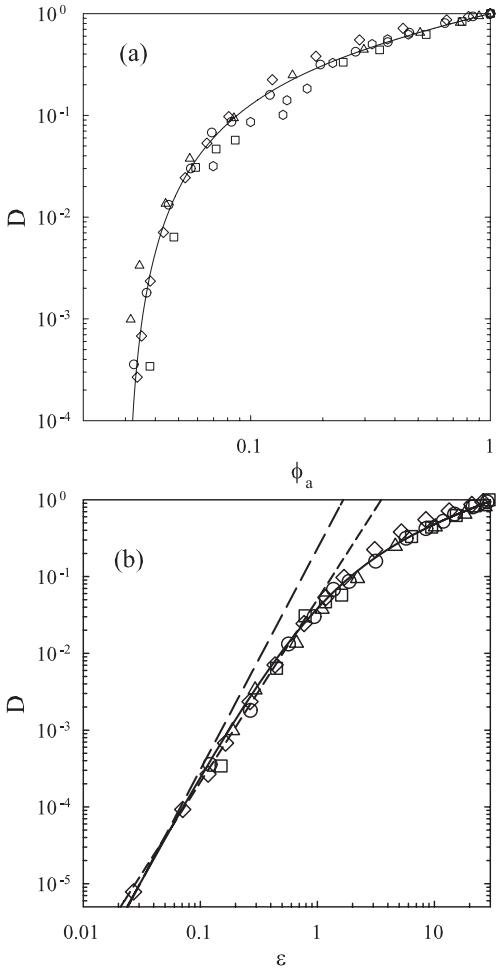

Figure 8.5: Relative diffusion coefficient of tracer spheres as a function of ϕ_a in FHS (circle), and DLCA (triangle) and RLCA (square) gels of spheres with the same diameter as the tracers. The results for the Lorentz gas [49] (diamond) and experiments [52] (hexagon) are also shown for comparison. The solid line represents Eq. 8.1 where we have used $\phi_a^c = 0.03$ and $\mu = 2.8$. These values were chosen to obtain visually a good description of the data. (b) Shows the same data plotted as a function of $\varepsilon = (\phi_a - \phi_a^c)/\phi_a^c$ on a logarithmic scale. The straight lines in the (b) represent the predicted power law dependences from ref [198] (2.38, short dashed) and ref [48] (2.88, long dashed).

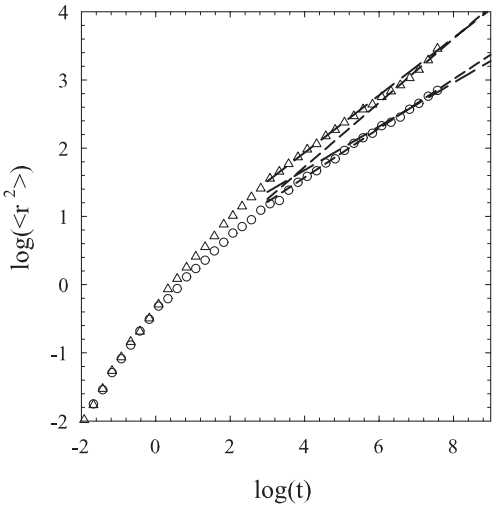

Figure 8.6: Comparison of the MSD of tracers in a DLCA gel at the percolation threshold of the accessible volume placed anywhere in the accessible volume (circle) or just in the percolating pore (triangle). The straight lines represent the predicted power law dependences in the system and in the percolating pore from [198] (short dashed) and [48] (long dashed).

law: $D \propto \varepsilon^{\mu}$. However, there is considerable uncertainty in the value of the exponent due to the strong correlation between $\phi_{\mathrm{a}}^{\mathrm{c}}$ and μ. For instance, Höfling et al. [49] fixed μ at 2.88 predicted by Machta et al. [48] and found in this way $\phi_{\mathrm{a}}^{\mathrm{c}} = 0.0298$. Fixing $\phi_{\mathrm{a}}^{\mathrm{c}}$ at 0.0301 we find $\mu = 2.5$ using the same data. In fact predictions for μ from ref[198] and ref[48] are both compatible with the data, see Fig. 8.5, and we are not in the position to decide which, if any, is correct. Nevertheless, μ is clearly larger than the value 1.88 obtained from lattice simulations of diffusion in percolating systems [45].

The power law exponent, k, of the anomalous MSD at the threshold is related to μ as [45]: $k = 2(\nu - \beta/2)/(2\nu + \mu - \beta)$, where β characterizes the dependence of the volume fraction of the percolating pores ($\phi_{\mathrm{a}}^{\mathrm{p}}$) close to the threshold: $\phi_{\mathrm{a}}^{\mathrm{p}} \propto \varepsilon^{\beta}$ and ν characterizes the divergence of the correlation length: $\xi \propto \varepsilon^{-\nu}$. If one only considers the displacement of tracers in the percolating pore the exponent is larger: $k' = 2\nu/(2\nu+\mu-\beta)$. Fig. 8.6 compares the average MSD at the percolation threshold of tracers placed anywhere in the accessible volume with that of tracers placed in the percolating pore. Utilizing the values for $\nu = 0.88$ and $\beta = 0.41$ obtained from lattice simulations [35] gives $k = 0.36$ and $k' = 0.47$ for $\mu = 2.38$ and $k = 0.32$ and $k' = 0.42$ for $\mu = 2.88$. The latter appear to describe the data better, but unfortunately, accurate determination of the limiting power law behaviour is largely beyond the current computer capacities, given the fact that the limiting power law behaviour of the cluster size distribution is not yet observed even for lattice simulations with a box

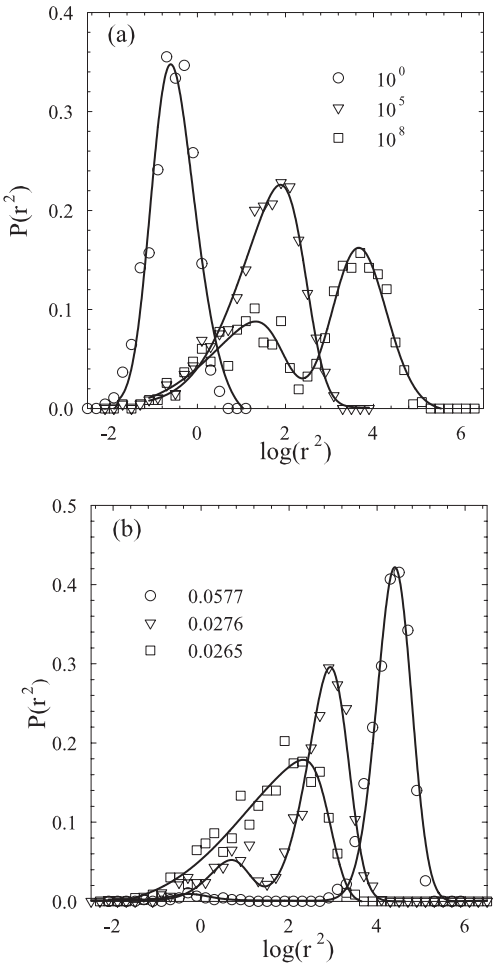

Figure 8.7: Distribution of the MSD of tracers in a DLCA gel for a fixed $\phi_a = 0.0276$ close to the percolation threshold at different times (a) and for a fixed $t = 10^6$ at different ϕ_a (b), as indicated in the figure. The solid lines are guides to the eye.

size of 1023 [110].

The displacement of tracers is highly heterogeneous close to the percolation threshold and can be characterized in terms of the probability distribution that tracers have moved a distance r^2 at time t ($P(r^2)$). For $\phi_a > \phi_a^c$, we need to distinguish between the fraction (ϕ_a^p) of tracers in the percolating pore and the fraction ($1 - \phi_a^p$) in finite size pores. $P(r^2)$ of tracers in the percolating pores is Gaussian if the MSD is much larger than ξ^2 and $\langle r^2 \rangle$ increases linearly with time. On the other hand, $P(r^2)$ of tracers trapped in a finite size pore becomes independent of t and $\langle r^2 \rangle$ stagnates at $2\langle R_g^2 \rangle$. Therefore $P(r^2)$ splits up into two peaks: one representing tracers in the percolating pore that displaces linearly with t and another representing tracers in finite size pores that stagnates, with amplitudes ϕ_a^p and $(1 - \phi_a^p)$, respectively. The split-up is illustrated in Fig.8.7*a* where $P(r^2)$ is shown at three times for a DLCA gel just above the percolation threshold ($\phi_a = 0.0276$). At the shortest time the MSD is still much smaller than ξ^2, and one observes a single distribution. The split-up starts when $\langle r^2 \rangle \approx \xi^2$ and is clearly visible at the longest time when $\langle r^2 \rangle$ is much larger than ξ^2. Fig. 8.7*b* shows the distributions at $t = 10^6$ for three values of ϕ_a. At $\phi_a = 0.0265$, i.e. smaller than ϕ_a^c, only one peak is observed representing the pore size distribution, which is broad close to the threshold. At $\phi_a = 0.056$ almost all accessible volume percolates and a narrow peak is seen that shifts to larger r^2 with time. For $\phi_a = 0.032$, i.e. just above ϕ_a^c, both peaks representing freely diffusing and trapped tracers are observed.

The same features were found when ϕ_a was varied by varying the tracer size at constant obstacle volume fraction. As mentioned above, ϕ_a decreases with increasing tracer size starting from $\phi_a = 1 - \phi$ for point tracers see inset of Fig. 8.8. Examples of the dependence of D on ϕ_a are given in Fig. 8.8 for different tracer diameters between 0.1 and 1 for gels and FHS at fixed volume fractions. Diffusion coefficients obtained at other volume fractions showed the same universal behaviour. For the Lorentz gas there is a strict equivalence between the diffusion of point tracers and finite size tracers at the same ϕ_a [46]. Similar equivalence exists between finite size tracers in FHS and point tracers in randomly distributed semi-penetrable spheres. It was found, for a limited range of ϕ_a, that D was the same for a given ϕ_a for tracers with different sizes in FHS [46]. Fig. 8.8 shows that the effect of tracer size on D is essentially determined by ϕ_a also for gels, but the relationship is not exact.

8.1.4 Conclusion

The most important result of the simulations presented here is that the diffusion coefficient in a system of immobile non-interacting obstacles is determined by the volume that is accessible to the tracers independent of the tracer size. We have found this to be true for two different gel structures, but also for frozen hard spheres and for the Lorentz gas. This point has so far not been considered in existing theories on tracer diffusion in gels.

The tracer diffusion becomes zero at a critical value of accessible volume $\phi_a^c \approx 0.03$

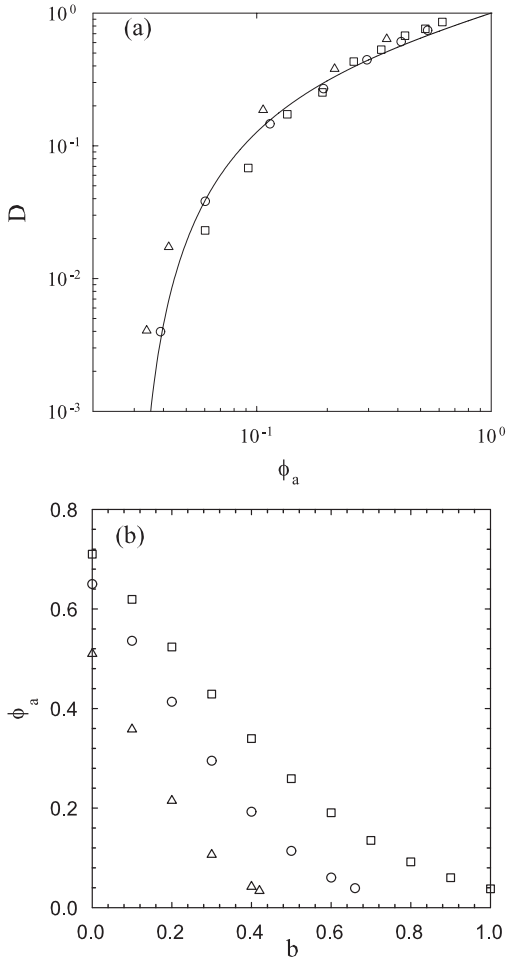

Figure 8.8: Relative diffusion coefficient of tracer spheres with different diameters between 0.1 and 1 as a function of ϕ_{a} in FHS at $\phi = 0.35$ (circle), a DLCA gel at $\phi = 0.49$ (triangle) and a RLCA gel at $\phi = 0.29$ (square) formed by spheres of unit diameter. The solid line is the same as in Fig. 8.5. (b) Shows the dependence of ϕ_{a} on the tracer diameter.

that is almost the same for gels and frozen hard spheres. The dependence of D on ϕ_a close to ϕ_a^c can be described in terms of a power law dependence on the distance to ϕ_a^c. The MSD at ϕ_a^c is anomalous and increases as a power law with time with an exponent less than unity. The exponents of the two power law relationships are related and are consistent with the percolation model.

In principle the diffusion coefficient can be predicted with reasonable accuracy if the gel structure is known and ϕ_a can be calculated. Unfortunately, the reverse case, i.e. deducing the gel structure from a measurement of the diffusion coefficient is not as straightforward because the relation between ϕ_a and the structure is not direct. Nevertheless, the validity of postulated gel structures may be tested by measuring diffusion coefficients of tracers with different size.

A different relation between D and ϕ_a is expected when the bonds between the obstacle particles are flexible or when they interact with the tracers. These effects can be tested with the same simulation method and will be reported in the future.

Chapter 9

Conclusion

The present thesis has mainly explored the non equilibrium phenomena of interacting spheres with the help of computer simulations. The simulation technique is called Brownian Cluster Dynamics. We were able to study the effect of co-operative cluster diffusion that is neglected in molecular dynamics simulation. At low concentrations, cluster diffusion does play a significant role while at high concentrations the cluster motion can be neglected.

One of the main issues that have been addressed in this thesis is the slowing down of dynamics as we increase the attraction between particles. Using rigid bonds and making the interaction range zero we were able to completely suppress phase separation. The self diffusion of spheres slows down with increasing attraction. but shows complete arrest only at infinite attraction i.e. truly irreversible systems. Increasing the attraction has two effects: one is the increase of the life time of the bonds and the other is the increase of the free space as particles cluster and share common excluded volume. The increase of free space dominates when the attraction is small causing an increase of the diffusion coefficient compared to that of a hard sphere fluid. This effect causes the repulsive glass line to shift towards higher volume fractions. As we increase the attraction the bond life time increases leading to bigger clusters and eventually percolation. With further increase of the attraction more spheres become part of the percolating network until almost no particles are free. However as long as the system is reversible at some point monomers break free and will diffuse till they collide with the network. Thus the origin of slow dynamics at low concentration is due to the formation of long living bonds in the percolating network and not to a glass transition.

When the accessible volume of frozen gels was calculated we observed that they contained more accessible volume than random hard spheres see *chapter* 8. The tracer diffusion in these systems is a universal function of the accessible volume independent of the structure of the obstacles and the size of the tracers. The reason is that the accessible space has the same structure irrespective of the structure of the obstacles and the tracer size. One might be tempted to extend this observation for frozen systems to explain the diffusion coefficient for mobile hard spheres. The accessible volume (ϕ_a) of random hard spheres is related to their chemical potential and has been calculated up to close packing (64%) by Torquato [8]. ϕ_a goes to zero only at random close packing. In fig9.1 we have plotted the diffusion coefficient of random hard spheres as a function of the accessible volume. The dependence of D on ϕ_a can be described by the following relation.

$$D = \phi_a^{\gamma} \exp\left[-\left(\frac{\phi_a^*}{\phi_a}\right)^{\zeta}\right] \tag{9.1}$$

where $\phi_a^* = 2 \cdot 10^{-11}$, $\gamma = 0.13$ and $\zeta = 0.2$. It not clear why a power law behavior is seen with a stretched exponential cut off but perhaps these observations can lead to the devolpment of a theory. The advantage of using the accessible volume as a parameter is that it gives a direct relationship between thermodynamics and dynamics

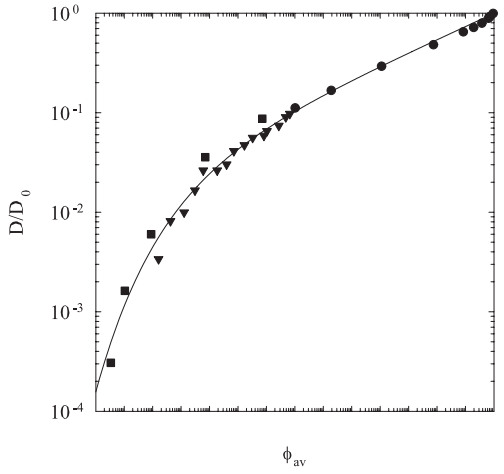

Figure 9.1: The diffusion coefficient for random hard spheres obtained from simulations [77](circle) [84] (triangle) and [74] (square) is plotted as a function of accessible volume available to the center of mass of a sphere. The solid line represents a fit to eq(9.1).

for hard sphere fluids.

The formation of rigid bonds with finite interaction range causes liquid-liquid phase separation. The transition from nucleation and growth to spinodal decomposition is observed to be a continuous phenomenon making it impossible to trace out unambiguously a spinodal for colloidal systems as was suggested earlier by Binder [62]. Introducing flexibility in reversible aggregation of attractive spheres without long range repulsion drives crystallization. Preliminary results showed that the kinetics of crystallization slows down abruptly above a critical interaction strength. However, the coarsening process of the meta stable liquid-liquid phase separation is still observed and slows down more progressively with increasing attraction.

When the aggregation is irreversible and the bonds are flexible the system forms a network of thick strands that resembles the intial stage of phase separation. The evolution of the system continue for a long time even after all the particles are part of the network. Aging is thus not a necessary sign of reversibility.

After some time the evolution is no longer visible. This stagnation of the evolution has been observed in experiments and simulation of strongly attractive spheres. It has been explained as phase separation interrupted by attractive glass formation. Indeed the core of dense domain may be glassy but it is not clear why the particles at the surface should also be immobile. Our results on irreversible aggregation with flexible bonds shows that every particle is part of a tetrahedron, i.e. the particles have at least 3 bonds. The particles with few bonds are at the surface and can escape if their their bonds are broken almost simultaneously. These results lead us to the conclusion that coarsening is slowed down by bond formation but never completely arrested if

the attraction is finite.

For all the experiments where people have observed the formation of thick strands and local ordering without further coarsening, most likely the aggregation was irreversible on the time scale of the experiments.

Future work

So far we have only tried to mimic the squarewell potential with BCD. However one can simulate continuous potentials by making the probability to form or break bonds dependent on the distance. The cluster construction step remains essentially the same but for the acceptance of the movement of the clusters we have to check the energy difference following the Metropolis rule.

Random or patchy interactions which is believed to mimic protein interaction and can be quite easily be introduced in BCD. The effect of cooperative cluster motion on the kinetics of such systems still remains to be explored.

For the tracer diffusion we have considered only frozen systems with only hard sphere repulsive interaction between the tracer and the system. In real experiment the obstcales are flexible and also the tracer can interact with the obstacles on the basis of a more complex potential. The study of these effects is importanat for instance in medicine where the transport of drugs in tissues can be modeled as diffusion of tracers in disordered media.

Bibliography

[1] D. A. Weitz and J. S. Huang. Limits of the fractal dimension for irreversible kinetic aggregtaion of gold colloids. *Physical Review Letters*, 54(13):1416–1419, 1985.

[2] Jean Christophe Gimel, Dominique Durand, and Taco Nicolai. Structure and distribution of aggregates formed after heat-induced denaturation of globular proteins. *Macromolecules*, 27:583–589, 1994.

[3] Max Kolb, Robert Botet, and Rmi Jullien. Scaling of kinetically growing clusters. *Physical Review Letters*, 51:1123–1126, 1983.

[4] Paul Meakin. Formation of fractal clusters and networks by irreversible diffusion-limited aggregation. *Physical Review Letters*, 51(13):1119–1122, 1983.

[5] Valerie J. Anderson and Henk N. W. Lekkerkerker. Insights into phase transition kinetics from colloid science. *Nature*, 416:811–815, 2002.

[6] Fabrice Lafleche, Dominique Durand, and Taco Nicolai. Association of adhesive spheres formed by hydrophobically end-capped peo. 1. influence of the presence of single end-capped peo. *Macromolecules*, 36:1331–1340, 2003.

[7] R. Tuinier, J. Rieger, and C. G. de Kruif. Depletion-induced phase separation in colloid-polymer mixtures. *Advances in Colloid and Interface Science*, 103:1–31, 2003.

[8] Salvatore Torquato. *Random heterogeneous materials. Microstructure and macroscopic properties.* Springer, New York, 2002.

[9] William G. Hoover and Francis H. Ree. Melting transition and communal entropy for hard spheres. *Journal of Chemical Physics*, 49(8):3609–3617, 1968.

[10] P. N. Pusey and W. van Megen. Phase behaviour of concentrated suspensions of nearly hard colloidal spheres. *Nature*, 320:340–342, 1986.

[11] M. D. Rintoul and S. Torquato. Computer simulations of dense hard-sphere systems. *Journal of Chemical Physics*, 105(20):9258–9265, 1996.

[12] M. D. Rintoul and S. Torquato. Erratum: "computer simulations of dense hard-sphere systems." [j. chem. phys 105, 9258 (1996)]. *Journal of Chemical Physics*, 107(7):2698, 1997.

[13] W. van Megen, T. C. Mortensen, S. R. Williams, and J. Muller. Measurement of the self-intermediate scattering function of suspensions of hard spherical particles near the glass transition. *Physical Review E*, 58(5):6073–6085, 1998.

[14] Emanuela Zaccarelli, Giuseppe Foffi, Kenneth A. Dawson, S. V. Buldyrev, Francesco Sciortino, and Piero Tartaglia. Confirmation of anomalous dynamical arrest in attractive colloids: a molecular dynamics study. *Physical Review E*, 66:041402–1–14, 2002.

[15] Th. Voigtmann, A. M. Puertas, and M. Fuchs. Tagged-particle dynamics in a hard-sphere system: mode-coupling theory analysis. *Physical Review E*, 70:061506–1–19, 2004.

[16] I. Tokuyama, M. Oppenheim. On the theory of concentrated hard-sphere suspensions. *Physica A*, 216(1-2):85–119, 1995.

[17] Francesco Sciortino and Piero Tartaglia. Glassy colloidal systems. *Advances in Physics*, 54(6-7):471–524, 2005.

[18] Kenneth A. Dawson, Aonghus Lawlor, Paolo de Gregorio, Gavin D. McCullagh, Emanuela Zaccarelli, and Piero Tartaglia. Universality behaviour in "ideal" dynamical arrest transitions of a lattice glass model. *Physica A*, 316:115–134, 2002.

[19] Aonghus Lawlor, Dan Reagan, Gavin D. McCullagh, Paolo de Gregorio, Piero Tartaglia, and Kenneth A. Dawson. Universality in lattice models of dynamic arrest: introduction of an order parameter. *Physical Review Letters*, 89:245503–1–4, 2002.

[20] P. N. Pusey, Wilson C. K. Poon, S. M. Ilett, and P. Bartlett. Phase behaviour and structure of colloidal suspensions. *Journal of Physics. Condensed Matter*, 6:A29–A36, 1994.

[21] Daan Frenkel and Berend Smit. *Understanding molecular simulation. From algorithms to applications.*, volume 1 of *Computational science series.* Academic Press, San Diego, 2002.

[22] Tamas Vicsek. *Fractal growth phenomena.* World scientific, Singapore, 1989.

[23] Jean Christophe Gimel, Dominique Durand, and Taco Nicolai. Transition between flocculation and percolation of a diffusion-limited cluster-cluster aggregation process using three-dimensional monte carlo simulation. *Physical Review B*, 51(17):11348–11357, 1995.

[24] Jean Christophe Gimel, Taco Nicolai, and Dominique Durand. 3d monte carlo simulations of diffusion limited cluster aggregation up to the sol-gel transition: structure and kinetics. *Journal of Sol-Gel Science and Technology*, 15(2):129–136, 1999.

[25] Manuel Rottereau, Jean Christophe Gimel, Taco Nicolai, and Dominique Durand. Monte-carlo simulation of particle aggregation and gelation: I growth, structure and size distribution of the clusters. *European Physical Journal E*, 15:133–140, 2004.

[26] Manuel Rottereau, Jean Christophe Gimel, Taco Nicolai, and Dominique Durand. Monte-carlo simulation of particle aggregation and gelation: Ii pair correlation function and structure factor. *European Physical Journal E*, 15:141–148, 2004.

[27] Silvia Diez Orrite, S. Stoll, and P. Schurtenberger. Off-lattice monte carlo simulations of irreversible and reversible aggregation processses. *Soft Matter*, 1:364–371, 2005.

[28] Agustin E. Gonzalez, M. Lach-hab, and Estela Blaisten-Barojas. On the concentration dependence of the cluster-fractal dimension in colloidal aggregation. *Journal of Sol-Gel Science and Technology*, 15:119–127, 1999.

[29] Anwar Hasmy and Rmi Jullien. Percolation in cluster-cluster aggregation processes. *Physical Review E*, 53(2):1789–1794, 1996.

[30] Paul Meakin. Reaction-limited cluster-cluster aggregation in dimensionalities 2-10. *Physical Review A*, 38(9):4799–4814, 1988.

[31] G. Odriozola, Arturo Moncho-Jorda, A. Schmitt, J. Callejas-Fernandez, R. Martinez-Garcia, and Roque Hidalgo-Alvarez. A probabilistic aggregation kernel for computer-simulated transition from dlca to rlca. *Europhysics Letters*, 53:797–803, 2001.

[32] Marco Lattuada, Hua Wu, Anwar Hasmy, and Massimo Morbidelli. Estimation of fractal dimension in colloidal gels. *Langmuir*, 19:6312–6316, 2003.

[33] Agustin E. Gonzalez and Guillermo Ramirez-Santiago. Scaling of the structure factor in fractal aggregation of colloids: computer simulations. *Journal of Colloid and Interface Science*, 182:254–267, 1996.

[34] D. A. Weitz and M. Oliveria. Fractal structures formed by kinetic aggregation of aqueous gold colloids. *Physical Review Letters*, 52(16):1433–1436, 1984.

[35] Dietrich Stauffer and Amnon Aharony. *Introduction to percolation theory*. Taylor & Francis, London, second edition edition, 1992.

[36] J. N. Wilking, S. M. Graves, C. B. Chang, K. Meleson, M. Y. Lin, and T. G. Mason. Dense cluster formation during aggregation and gelation of attractive slippery nanoemulsion droplets. *Physical Review Letters*, 96:015501–1–4, 2006.

[37] Paul Meakin. Aggregation kinetics. *Physica Scripta*, 46:295–331, 1992.

[38] Marco Lattuada, Hua Wu, and Massimo Morbidelli. A simple model for the structure of fractal aggregates. *Journal of Colloid and Interface Science*, 268:106–120, 2003.

[39] M. von Smoluchowski. Drei vortrge ber diffusion, brownsche molekularebewegung und koagulation von kolloidteilchen. *Z. Phys.*, 17:585, 1916.

[40] M. von Smoluchowski. Versuch einer mathematischen theorie der koagulations kinetic kolloider lsugen. *Z. Phys. Chem.*, 92:129, 1917.

[41] S. Chandrasekhar. Stochastic problems in physics and astronomy. *Reviews of Modern Physics*, 15(1):1–89, 1943.

[42] G. Odriozola, A. Schmitt, Arturo Moncho-Jorda, J. Callejas-Fernandez, R. Martinez-Garcia, R. Leone, and Roque Hidalgo-Alvarez. Constant bond breakup probability model for reversible aggregation processes. *Physical Review E*, 65:031405–1–8, 2002.

[43] P. G. J. van Dongen and M. H. Ernst. Comment on "large-time behavior of the smoluchowski equations of coagulation". *Physical Review A*, 32(1):670–672, 1985.

[44] Matthias Thorn, Michael L. Broide, and Markus Seesselberg. Fluctuations in discrete fragmentation processes studied by stochastic simulations. *Physical Review E*, 51(5):4089–4094, 1995.

[45] Shlomo Havlin and Daniel Ben-Avraham. Diffusion in disordered media. *Advances in Physics*, 36(6):695–798, 1987.

[46] In Chan Kim and S. Torquato. Diffusion of finite-sized brownian particles in porous media. *Journal of Chemical Physics*, 96(2):1498–1503, 1992.

[47] Sujin Babu, Jean-Christophe Gimel, and Taco Nicolai. Tracer diffusion in colloidal gels. *accepted Journal of Physical Chemistry B*, 2007.

[48] Jonathan Machta and Steven M. Moore. Diffusion and long-time tails in the overlapping lorentz gas. *Physical Review A*, 32(5):3164–3167, 1985.

[49] Felix Hofling, Thomas Franosch, and Erwin Frey. Localization transition of the tree-dimensional lorentz model and continuum percolation. *Physical Review Letters*, 96:165901–1–4, 2006.

[50] C. Bruin. A computer experiment on diffusion in the lorentz gas. *Physica*, 72:261–286, 1974.

[51] M. D. Rintoul. Precise determination of the void percolation threshold for two distributions of overlapping spheres. *Physical Review E*, 62(1):68–72, 2000.

[52] James N. Roberts. Grain consolidation and electrical conductivity in porous media. *Physical Review B*, 31(9):5990–5997, 1985.

[53] In Chan Kim and S. Torquato. Determination of the effective conductivity of hetergeneous media by brownian motion simulation. *Journal of Applied Physics*, 68(8):3892–3903, 1990.

[54] Sujin Babu, Jean-Christophe Gimel, and Taco Nicolai. Phase separation and percolation of reversibly aggregating spheres with a square-well attraction potential. *Journal of Chemical Physics*, 125(19):184512–1–10, 2006.

[55] Fernando Del Rio, Edgar Avalos, Rodolfo Espindola, Luis F. Rull, George Jackson, and Santiago Lago. Vapour-liquid equilibrium of the square-well fluid of variable range via hybrid simulation approach. *Molecular Physics*, 100(15):2531–2546, 2002.

[56] J. Richard Elliott and Liegi Hu. Vapor-liquid equilibria of square-well spheres. *Journal of Chemical Physics*, 110(6):3043–3048, 1999.

[57] Lourdes Vega, Enrique de Miguel, Luis F. Rull, George Jackson, and Ian A. McLure. Phase equilibria and critical behavior of square-well fluids of variable width by gibbs ensemble monte carlo simulation. *Journal of Chemical Physics*, 96(3):2296–2305, 1992.

[58] Giuseppe Foffi, Gavin D. McCullagh, Aonghus Lawlor, Emanuela Zaccarelli, and Kenneth A. Dawson. Phase equilibria and glass transition in colloidal systems with short-ranged attractive interactions: application to protein crystallization. *Physical Review E*, 65:031407–1–17, 2002.

[59] K. N. Pham, S. U. Egelhaaf, P. N. Pusey, and Wilson C. K. Poon. Glasses in hard spheres with short-range attraction. *Physical Review E*, 69:011503–1–13, 2004.

[60] M. G. Noro and Daan Frenkel. Extended corresponding-states behavior for particles with variable range attractions. *Journal of Chemical Physics*, 113(8):2941–2944, 2000.

[61] Jean Christophe Gimel, Taco Nicolai, and Dominique Durand. Monte carlo simulation of transient gel formation and break-up during reversible aggregation. *European Physical Journal E*, 5:415–422, 2001.

[62] Kurt Binder and Dietrich Stauffer. Statistical theory of nucleation, condensation and coagulation. *Advances in Physics*, 25(4):343–396, 1976.

[63] G. Foffi, C. De Michele, Francesco Sciortino, and Piero Tartaglia. Arrested phase separation in a short-ranged attractive colloidal system: A numerical study. *Journal of Chemical Physics*, 122:224903–1–13, 2005.

[64] Giuseppe Foffi, Emanuela Zaccarelli, Francesco Sciortino, Piero Tartaglia, and Kenneth A. Dawson. Kinetic arrest originating in competition between attractive interactions and packing force. *Journal of Statistical Physics*, 100:363–376, 2000.

[65] Emanuela Zaccarelli, Ivan Saika-Voivod, Sergey V. Buldyrev, A. J. Moreno, Piero Tartaglia, and Francesco Sciortino. Gel to glass transition in simulation of a valence-limited colloidal system. *Journal of Chemical Physics*, 124:124908–1–14, 2006.

[66] Cristiano de Michele, Simone Gabrielli, Piero Tartaglia, and Francesco Sciortino. Dynamics in the presence of attractive patchy interactions. *Journal of Physical Chemistry B*, 110:8064–8079, 2006.

[67] Emanuela Bianchi, Julio Largo, Piero Tartaglia, Emanuela Zaccarelli, and Francesco Sciortino. Phase diagram of patchy colloids: toward empty liquids. *Physical Review Letters*, 97:168301–1–4, 2006.

[68] Antonio M. Puertas, Matthias Fuchs, and Michael E. Cates. Dynamical heterogeneities close to a colloidal gel. *Journal of Chemical Physics*, 121(6):2813–2822, 2004.

[69] Antonio M. Puertas, Matthias Fuchs, and Michael E. Cates. Simulation study of nonergodicity transitions: gelation in colloidal systems with short-range attractions. *Physical Review E*, 67:031406–1–13, 2003.

[70] S. Mossa, Francesco Sciortino, Piero Tartaglia, and Emanuela Zaccarelli. Ground-state clusters for short-range attractive and long-range repulsive potentials. *Langmuir*, 20:10756–10763, 2004.

[71] Francesco Sciortino, Stefano Mossa, Emanuela Zaccarelli, and Piero Tartaglia. Equilibrium cluster phases and low-density arrested disordered states: The role of short-range attraction and long-range repulsion. *Physical Review Letters*, 93(5):055701–1–4, 2004.

[72] Emanuela Del Gado and Walter Kob. Structure and relaxation dynamics of a colloidal gel. *Europhysics Letters*, 72(6):1032–1038, 2005.

[73] Sujin Babu, Manuel Rottereau, Taco Nicolai, Jean Christophe Gimel, and Dominique Durand. Flocculation and percolation in reversible cluster-cluster aggregation. *European Physical Journal E*, 19:203–211, 2006.

[74] B. Doliva and A. Heuer. Cooperativity and spatial correlations near the glass transition: computer simulation results of hard spheres and disks. *Physical Review E*, 61(6):6898–6908, 2000.

[75] Kenneth A. Dawson, Giuseppe Foffi, Matthias Fuchs, Wolfgang Gotze, Francesco Sciortino, M. Sperl, Piero Tartaglia, Th. Voigtmann, and Emanuela Zaccarelli. Hihger-order glass-transition singularities in colloidal systems with attractive interactions. *Physical Review E*, 63:011401–1–17, 2000.

[76] Giuseppe Foffi, Cristiano De Michele, Francesco Sciortino, and Piero Tartaglia. Scaling of dynamics with the range of interaction in short-range attractive colloids. *Physical Review Letters*, 94:078301–1–4, 2005.

[77] Sujin Babu, Jean-Christophe Gimel, and Taco Nicolai. Self-diffusion of reversibly aggregating spheres. *Journal of Chemical Physics*, 127:054503–1–7, 2007.

[78] Pablo I. Hurtado, Ludovic Berthier, and Walter Kob. Heterogeneous diffusion in a reversible gel. *Physical Review Letters*, 98:135503–1–4, 2007.

[79] D. C. Rapaport. *The art of computer simulations*. Cambridge University Press, London, 1997.

[80] M. P. Allen and D. J. Tildesley. *Computer simulation of liquids.* Clarendon Press, Oxford, 1987.

[81] Manuel Rottereau, Jean Christophe Gimel, Taco Nicolai, and Dominique Durand. Influence of the brownian step size in off-lattice monte carlo simulations of irreversible particle aggregation. *European Physical Journal E*, 18(1):15–19, 2005.

[82] J.-P. Hansen and I. R. McDonald. *Theory of simple liquids.* Academic Press, London, 1986.

[83] A. Scala, Th. Voigtmann, and C. De Michele. Event-driven brownian dynamics for hard spheres. *Journal of Chemical Physics*, 126:134109–1–10, 2007.

[84] Robin J. Speedy. Diffusion in the hard sphere fluid. *Molecular Physics*, 62(2):509–515, 1987.

[85] Marina Carpineti, F. Ferri, Marzio Giglio, E. Paganini, and U. Perini. Salt-induced fast aggregation of polystyrene latex. *Physical Review A*, 42(12):7347–7354, 1990.

[86] Taco Nicolai and Sthane Cocard. Structure of gels and aggregates of disk-like colloids. *European Physical Journal E*, 5:221–227, 2001.

[87] C. G. de Kruif, Marion A. M. Hoffmann, Marieke E. van Marle, Peter J. J. M. van Mil, Sebastianus P. F. M. Roefs, Marleen Verheul, and Nel Zoon. Gelation of proteins from milk. *Faraday Discussions*, 101:185, 1995.

[88] S. H. Chen, J. Rouch, Francesco Sciortino, and Piero Tartaglia. Static and dynamic properties of water-in-oil microemulsions near the critical and percolation points. *Journal of Physics. Condensed Matter*, 6:10855–10883, 1994.

[89] Anwar Hasmy, Marie Foret, Jacques Pelous, and Rmi Jullien. Small-angle neutron-scattering investigation of short-range correlations in fractal aerogels: Simulations and experiments. *Physical Review B*, 48:9345–9353, 1993.

[90] Marco Lattuada, Peter Sandkuhler, Hua Wu, Jan Sefcik, and Massimo Morbidelli. Aggregation kinetics of polymer colloids in reaction limited regime: experiments and simulations. *Advances in Colloid and Interface Science*, 103:33–56, 2003.

[91] Max Kolb and Hans J. Herrmann. The sol-gel transition modelled by irreversible aggregation of clusters. *Journal of Physics A: Mathematical and General*, 18:L435–L441, 1985.

[92] Anwar Hasmy and Rmi Jullien. Sol-gel process simulation by cluster-cluster aggregation. *Journal of Non-Crystalline Solids*, 186:342–348, 1995.

[93] Fereydoon Family, Paul Meakin, and John M. Deutch. Kinetics of coagulation with fragmentation: scaling behaviour and fluctuations. *Physical Review Letters*, 57(6):727–730, 1986.

[94] Max Kolb. Reversible diffusion-limited cluster aggregation. *Journal of Physics A: Mathematical and General*, 19:L263–L268, 1986.

[95] Wan Y. Shih, Ilhan A. Aksay, and Ryoichi Kikuchi. Reversible-growth model: cluster-cluster aggregation with finite binding energies. *Physical Review A*, 36(10):5015–5019, 1987.

[96] M. D. Haw, M. Sievwright, Wilson C. K. Poon, and P. N. Pusey. Cluster-cluster gelation with finite bond energy. *Advances in Colloid and Interface Science*, 62:1–16, 1995.

[97] Martin T. A. Bos and Joost H. J. van Opheusden. Brownian dynamics simulation of gelation and aging in interacting colloidal systems. *Physical Review E*, 53(5):5044–5050, 1996.

[98] K. Geoffrey Soga, John R. Melrose, and Robin C. Ball. Metastable states and kinetics of colloid phase separation. *Journal of Chemical Physics*, 110(4):2280–2288, 1999.

[99] J. F. M. Lodge and D. M. Heyes. Transient colloidal gels by brownian dynamics computer simulation. *Physical Chemistry Chemical Physics*, 1:2119–2130, 1999.

[100] Antonio Coniglio, Lucilla de Arcangelis, Emanuela del Gado, A. Fierro, and N. Sator. Percolation, gelation and dynamical behaviour in colloids. *Journal of Physics. Condensed Matter*, 16:S4831–S4839, 2004.

[101] S. A. Safran, Itzhak Webman, and Gary S. Grest. Percolation in interacting colloids. *Physical Review A*, 32(1):506–511, 1985.

[102] Jian-Min Jin, K. Parbhakar, L. H. Dao, and K. H. Lee. Gel formation by reversible cluster-cluster aggregation. *Physical Review E*, 54(1):997–1000, 1996.

[103] Takamichi Terao and Tsuneyoshi Nakayama. Sol-gel transition of reversible cluster-cluster aggregations. *Physical Review E*, 58:3490–3494, 1998.

[104] M. E. Cates, M. Fuchs, K. Kroy, Wilson C. K. Poon, and A. M. Puertas. Theory and simulation of gelation, arrest and yielding in attracting colloids. *Journal of Physics. Condensed Matter*, 16:S4861–S4875, 2004.

[105] Jean Christophe Gimel, Taco Nicolai, and Dominique Durand. Relation between aggregation and phase separation: Three-dimensional monte carlo simulations. *Physical Review E*, 66:061405–1–5, 2002.

[106] R. Wessel and R. C. Ball. Diffusion-limited aggregation at equilibrium. *Physical Review A*, 45(4):R2177–R2178, 1992.

[107] R. Wessel and R. C. Ball. Cluster-cluster aggregtaion with random bond breaking. *Journal of Physics A: Mathematical and General*, 26:L159–L163, 1993.

[108] Giorgio Parisi and Nicolas Sourlas. Critical behavior of branched polymers and the lee-yang edge singularity. *Physical Review Letters*, 46(14):871–874, 1981.

[109] M. H. Ernst and P. G. J. van Dongen. Scaling laws in aggregation: fragmentation models with detailed balance. *Physical Review A*, 36(1):435–437, 1987.

[110] Jean Christophe Gimel, Taco Nicolai, and Dominique Durand. Size distribution of percolating clusters on cubic lattices. *Journal of Physics A: Mathematical and General*, 33:7687–7697, 2000.

[111] Giovani Dietler, Claude Aubert, David S. Cannell, and Pierre Wiltzius. Gelation of colloidal silica. *Physical Review Letters*, 57(24):3117–3120, 1986.

[112] Hua Wu, Jianjun Xie, and Massimo Morbidelli. Kinetics of cold-set diffusion-limited aggregations of denaturated whey protein isolate colloids. *Biomacromolecules*, 6:3189–3197, 2005.

[113] Laurent Lobry, Norberto Micali, Francesco Mallamace, Ciya Liao, and Sow Hsin Chen. Interaction and percolation in the l64 triblock copolymer micellar system. *Physical Review E*, 60(6):7076–7087, 1999.

[114] Agustin E. Gonzalez. Universality of colloid aggregation in the reaction limit: the computer simulations. *Physical Review Letters*, 71(14):2248–2251, 1993.

[115] Anwar Hasmy, Eric Anglaret, Marie Foret, Jacques Pelous, and Rmi Jullien. Small-angle neutron-scattering investigation of long-range correlations in silica aerogels: simulations and experiments. *Physical Review B*, 50(9):6006–6016, 1994.

[116] M. D. Haw, Wilson C. K. Poon, and P. N. Pusey. Structure factors from cluster-cluster aggregation simulation at high concentration. *Physica A*, 208:8–17, 1994.

[117] Bert H. Bijsterbosch, Martin T. A. Bos, Eric Dickinson, Joost H. J. van Opheusden, and Pieter Walstra. Brownian dynamics simulation of particle gel formation: from argon to yoghurt. *Faraday Discussions*, 101:51–64, 1995.

[118] M. D. Haw, M. Sievwright, Wilson C. K. Poon, and P. N. Pusey. Structure and characteristic length scales in cluster-cluster aggregation simulation. *Physica A*, 217:231–260, 1995.

[119] Francesco Sciortino, Andrea Belloni, and Piero Tartaglia. Irreversible diffusion-limited cluster aggregation: the behaviour of the scattered intensity. *Physical Review E*, 52(4):4068–4079, 1995.

[120] Anwar Hasmy, Eric Anglaret, Romain Thouy, and Rmi Jullien. Fluctuating bond aggregation: numerical simulation of neutrally-reacted silica gels. *Journal de Physique I*, 7:521–542, 1997.

[121] A. M. Puertas, A. Fernandez-Barbero, and F. J. de las Nieves. Brownian dynamics simulation of diffusive mesoscopic particle aggregation. *Computer Physics Communications*, 121-122:353–357, 1999.

[122] A. Schmitt, G. Odriozola, Arturo Moncho-Jorda, J. Callejas-Fernandez, R. Martinez-Garcia, and Roque Hidalgo-Alvarez. Multiple contact kernel for diffusionlike aggregation. *Physical Review E*, 62(6):8335–8343, 2000.

[123] Anna A. Rzepiela, Joost H. J. van Opheusden, and Ton van Vliet. Brownian dynamics simulation of aggregation kinetics of hard spheres with flexible bonds. *Journal of Colloid and Interface Science*, 244:43–50, 2001.

[124] Hang Shing Ma, Rmi Jullien, and George W. Scherer. Dangling bond deflection model: growth of gel network with loop structures. *Physical Review E*, 65:041403–1–10, 2002.

[125] Paul Meakin. The effects of random bond breaking on diffusion limited cluster-cluster aggregation. *Journal of Chemical Physics*, 83(7):3645–3649, 1985.

[126] Wan Y. Shih, Jun Liu, Wei-Heng Shih, and Ilhan A. Aksay. Aggregation of colloidal particles with a finite interparticle attraction energy. *Journal of Statistical Physics*, 62(5/6):961–984, 1991.

[127] Takamichi Terao and Tsuneyoshi Nakayama. Reversible cluster-cluster aggregation and colloidal gels. *Progress of Theoretical Physics Supplement*, 138:354–359, 2000.

[128] G. Odriozola, A. Schmitt, J. Callejas-Fernandez, R. Martinez-Garcia, R. Leone, and Roque Hidalgo-Alvarez. Simulated reversible aggregation processes for different interparticle potentials: the cluster aging phenomenon. *Journal of Physical Chemistry. B, Materials, Surfaces, Interfaces & Biophysical*, 107:2180–2188, 2003.

[129] D. M. Heyes. Cluster analysis and continuum percolation of 3d square-well phases. mc and py solutions. *Molecular Physics*, 69(3):559–569, 1990.

[130] A. Rotenberg. Monte carlo equation of state for hard spheres in an attractive square well. *Journal of Chemical Physics*, 43(4):1198–1201, 1965.

[131] B. J. Alder, D. A. Young, and M. A. Mark. Studies in molecular dynamics. x. corrections to the augmented van der waals theory for the square well fluid. *Journal of Chemical Physics*, 56(6):3013–3029, 1972.

[132] Douglas Henderson, William G. Madden, and Donald D. Fitts. Monte carlo and hypernetted chain equation of state for the square-well fluid. *Journal of Chemical Physics*, 64(12):5026–5034, 1976.

[133] A. L. R. Bug, S. A. Safran, Gary S. Grest, and Itzhak Webman. Do interactions raise or lower a percolation threshold ? *Physical Review Letters*, 55(18):1896–1899, 1985.

[134] S. C. Netemeyer and Eduardo D. Glandt. Percolation behavior of the square-well fluid. *Journal of Chemical Physics*, 85(10):6054–6059, 1986.

[135] Gustavo A. Chapela, Sergio E. Martinez-Casas, and Carmen Varea. Square-well orthobaric densities via spinodal decomposition. *Journal of Chemical Physics*, 86(10):5683–5688, 1987.

[136] Y. C. Chiew and Y. H. Wang. Percolation and connectivity of the attractive square-well fluid: Monte carlo simulation study. *Journal of Chemical Physics*, 89(10):6385–6390, 1988.

[137] Eric Dickinson, Christer Elvingson, and Stephen R. Euston. Structure of simulated aggregates formed by reversible flocculation. *Journal of the Chemical Society. Faraday transactions II*, 85(7):891–900, 1989.

[138] David M. Heyes. Coordination number and equation of state of square-well and square-shoulder fluids: simulation and quasi-chemical model. *Journal of the Chemical Society, Faraday Transactions*, 87(20):3373–3377, 1991.

[139] Aleksey Lomakin, Neer Asherie, and George B. Benedek. Monte carlo study of phase separation in aqueous protein solutions. *Journal of Chemical Physics*, 104(2):1646–1656, 1996.

[140] Neer Asherie, Aleksey Lomakin, and George B. Benedek. Phase diagram of colloidal solutions. *Physical Review Letters*, 77(23):4832–4835, 1996.

[141] Nikolai V. Brilliantov and John P. Valleau. Thermodynamic scaling monte carlo study of the liquid-gas transition in the square-well fluid. *Journal of Chemical Physics*, 108(3):1115–1122, 1998.

[142] S. B. Kiselev, J. F. Ely, L. Lue, and J. R. Elliott. Computer simulations and crossover equation of state of square-well fluids. *Fluid Phase Equilbria*, 200:121–145, 2002.

[143] Giuseppe Foffi, Kenneth A. Dawson, Sergey V. Buldyrev, Francesco Sciortino, Emanuela Zaccarelli, and Piero Tartaglia. Evidence for an unusual dynamical-arrest scenario in short-ranged colloidal systems. *Physical Review E*, 65:050802–1–4, 2002.

[144] Emanuela Zaccarelli, G. Foffi, Kenneth A. Dawson, S. V. Buldyrev, Francesco Sciortino, and Piero Tartaglia. Static and dynamical correlation functions behaviour in attarctive colloidal systems from theory and simulation. *Journal of Physics: Condensed Matter*, 15:S367–S374, 2003.

[145] Pedro Orea, Yurko Duda, and Jos Alejandre. Surface tension of a square well fluid. *Journal of Chemical Physics*, 118(12):5635–5639, 2003.

[146] Pedro Orea, Yurko Duda, Volker C. Weiss, Wolffram Schrer, and Jos Alejandre. Liquid-vapor interface of square-well fluids of variable interaction range. *Journal of Chemical Physics*, 120(24):11754–11764, 2004.

[147] Giuseppe Foffi, Francesco Sciortino, Emanuela Zaccarelli, and Piero Tartaglia. Dynamical arrest in dense short-ranged attractive colloids. *Journal of Physics: Condensed Matter*, 16(38):S3791–S3806, 2004.

[148] Emanuela Zaccarelli, Francesco Sciortino, and Piero Tartaglia. Numerical study of the glass-glass transition in short-ranged attractive colloids. *Journal of Physics: Condensed Matter*, 16:S4849–S4860, 2004.

[149] Giuseppe Foffi, Emanuela Zaccarelli, Sergey V. Buldyrev, Francesco Sciortino, and Piero Tartaglia. Aging in short-ranged attractive colloids: a numerical study. *Journal of Chemical Physics*, 120(18):8824–8830, 2004.

[150] D. L. Pagan and J. D. Gunton. Phase behavior of shor-range square-well model. *Journal of Chemical Physics*, 122:184515–1–6, 2005.

[151] Mark A. Miller and Daan Frenkel. Competition of percolation and phase separation in a fluid of adhesive hard spheres. *Physical Review Letters*, 90(13):135702–1–4, 2003.

[152] Mark A. Miller and Daan Frenkel. Phase diagram of the adhesive hard sphere fluid. *Journal of Chemical Physics*, 121(1):535–545, 2004.

[153] R. J. Baxter. Percus-yevick equation for hard spheres with surface adhesion. *Journal of Chemical Physics*, 49(6):2770–2774, 1968.

[154] N. A. Seaton and Eduardo D. Glandt. Monte carlo simulation of adhesive disks. *Journal of Chemical Physics*, 84(8):4595–4601, 1986.

[155] N. A. Seaton and Eduardo D. Glandt. Aggregation and percolation in a system of adhesive spheres. *Journal of Chemical Physics*, 86(8):4668–4677, 1987.

[156] N. A. Seaton and Eduardo D. Glandt. Monte carlo simulation of adhesive spheres. *Journal of Chemical Physics*, 87(3):1785–1790, 1987.

[157] W. G. T. Kranendonk and Daan Frenkel. Simulation of the adhesive-hard-sphere model. *Molecular Physics*, 64(3):403–424, 1988.

[158] Sang Bub Lee. Numerical test of the percus-yevick approximation for continuum media of adhesive sphere model at percolation threshold. *Journal of Chemical Physics*, 114(5):2304–2311, 2001.

[159] M. A. Miller and Daan Frenkel. Simulating colloids with baxter's adhesive hard sphere model. *Journal of Physics. Condensed Matter*, 16:S4901–S4912, 2004.

[160] G. A. Vliegenthart and Henk N. W. Lekkerkerker. Predicting the gas-liquid critical point from the second virial coefficient. *Journal of Chemical Physics*, 112(3):5364–5369, 2000.

[161] Tera Kihara. Virial coefficients and models of molecules in gases. *Reviews of Modern Physics*, 25(4):831–843, 1953.

[162] S. Torquato. Mean nearest-neighbor distance in random packing of hard d-dimensional spheres. *Physical Review Letters*, 74(12):2156–2159, 1995.

[163] Bruno H. Zimm. Dynamics of polymer molecules in dilute solution: viscoelasticity, flow birefringence and dielectric loss. *Journal of Chemical Physics*, 24(2):269–278, 1956.

[164] Manuel Rottereau, Jean Christophe Gimel, Taco Nicolai, and Dominique Durand. 3d monte carlo simulation of site-bond continuum percolation of spheres. *European Physical Journal E*, 11:61–64, 2003.

[165] H. Sigurgeirsson and D. M. Heyes. Transport coefficients of hard sphere fluids. *Molecular Physics*, 101(3):469–482, 2003.

[166] Ichirou Moriguchi. Self-diffusion coefficient in dense hard sphere colloids. *Journal of Chemical Physics*, 106(20):8624–8625, 1997.

[167] B. Cichocki and K. Hinsen. Dynamic computer simulation of concentrated hard sphere suspensions. *Physica A*, 187:133–144, 1992.

[168] Emanuela Zaccarelli, S. V. Buldyrev, Emilia La Nave, A. J. Moreno, I. Saika-Voivod, Francesco Sciortino, and Piero Tartaglia. Model for reversible colloidal gelation. *Physical Review Letters*, 94:218301–1–4, 2005.

[169] Francesco Sciortino, Piero Tartaglia, and Emanuela Zaccarelli. One-dimensional cluster growth and branching gels in colloidal systems with short-range depletion attraction and screened electrostatic repulsion. *Journal of Physical Chemistry B*, 109:21942–21953, 2005.

[170] Antonio M. Puertas, Matthias Fuchs, and Michael E. Cates. Mode coupling and dynamical heterogeneity in colloidal gelation: simulation study. *Journal of Physical Chemistry B*, 109:6666–6675, 2005.

[171] Kenneth A. Dawson. The glass paradigm for colloidal glasses, gels, and other arrested states driven by attractive interactions. *Current Opinion in Colloid and Interface Science*, 7:218–227, 2002.

[172] E. Zaccarelli. Colloidal gels: equilibrium and non-equilibrium routes. *Journal of Physics: Condensed Matter*, 19:323101, 2007.

[173] Antonio M. Puertas, Emanuela Zaccarelli, and Francesco Sciortino. Viscoelastic properties of attractive and repulsive colloidal glasses. *Journal of Physics: Condensed Matter*, 17:L271–L277, 2005.

[174] P. E. Rouse. A theory of the linear viscoelastic properties of dilute solutions of coiling polymers. *Journal of Chemical Physics*, 21:1272–1280, 1953.

[175] Marco Lattuada, Hua Wu, and Massimo Morbidelli. Hydrodynamic radius of fractal clusters. *Journal of Colloid and Interface Science*, 268:96–105, 2003.

[176] Vasilios I. Manousiouthakis and Michael W. Deem. Strict detailed balance is unnecessary in monte carlo simulation. *The Journal of Chemical Physics*, 110(6):2753–2756, 1999.

[177] K. Kikuchi, M. Yoshida, T. Maekawa, and H. Watanabe. Metropolis monte carlo method as a numerical technique to solve the fokker-planck equation. *Chemical Physics Letters*, 185(3,4):335–338, 1991.

[178] M. Y. Lin, H. M. Lindsay, D. A. Weitz, R. Klein, R. C. Ball, and Paul Meakin. Universal diffusion-limited colloid aggregation. *Journal of Physics. Condensed Matter*, 2:3093–3113, 1990.

[179] M. Y. Lin, H. M. Lindsay, D. A. Weitz, R. C. Ball, R. Klein, and Paul Meakin. Universal reaction-limited colloid aggregation. *Physical Review A*, 41(4):2005–2020, 1990.

[180] Jean Christophe Gimel, Taco Nicolai, Dominique Durand, and Jean-Marie Teuler. Structure and size distribution of percolating clusters. comparison with gelling systems. *European Physical Journal B*, 12:91–97, 1999.

[181] Clair R. Seager and Thomas G. Mason. Slippery diffusion-limited aggregation. *Physical Review E*, 75(1):011406–4, 2007.

[182] Paul Meakin and Fereydoon Family. Structure and dynamics of reaction-limited aggregation. *Physical Review A*, 36(11):5498–5501, 1987.

[183] A. D. Dinsmore and D. A. Weitz. Direct imaging of three-dimensional structure and topology of colloidal gels. *Journal of Physics. Condensed Matter*, 14:7581–7597, 2002.

[184] Andrew I. Campbell, Valerie J. Anderson, Jeroen S. van Duijneveldt, and Paul Bartlett. Dynamical arrest in attractive colloids: The effect of long-range repulsion. *Physical Review Letters*, 94(20):208301–4, 2005.

[185] Peter J. Lu, Jacinta C. Conrad, Hans M. Wyss, Andrew B. Schofield, and David A. Weitz. Fluids of clusters in attractive colloids. *Physical Review Letters*, 96(2):028306–4, 2006.

[186] Nikoleta B. Simeonova, Roel P. A. Dullens, Dirk G. A. L. Aarts, Volkert W. A. de Villeneuve, Henk N. W. Lekkerkerker, and Willem K. Kegel. Devitrification of colloidal glasses in real space. *Physical Review E*, 73:041401–1–5, 2006.

[187] S. Manley, H. M. Wyss, K. Miyazaki, J. C. Conrad, V. Trappe, L. J. Kaufman, D. R. Reichman, and D. A. Weitz. Glasslike arrest in spinodal decomposition as a route to colloidal gelation. *Physical Review Letters*, 95(23):238302–4, 2005.

[188] S. Babu, Jean Christophe Gimel, Taco Nicolai, and Cristiano de Michele. The influence of bond-rigidity and cluster diffusion on the self-diffusion of hard spheres with square-well interaction. *0*, 0(0):0, 2007. submitted New Journal of Physics.

[189] G. Odriozola, R. Leone, A. Schmitt, J. Callejas-Fernandez, R. Martinez-Garcia, and Roque Hidalgo-Alvarez. Irreversible versus reversible aggregation: mean field theory and experiments. *Journal of Chemical Physics*, 121(11):5468–5481, 2004.

[190] A. M. Puertas, Matthias Fuchs, and Michael E. Cates. Comparative simulation study of collidal gels and glasses. *Physical Review Letters*, 88(9):098301–1–4, 2002.

[191] E. Zaccarelli, F. Sciortino, P. Tartaglia, G. Foffi, G. D. McCullagh, A. Lawlor, and K. A. Dawson. Competition between crystallization and glassification for particles with short-ranged attraction. possible applications to protein crystallization. *Physica A: Statistical Mechanics and its Applications*, 314(1-4):539–547, 2002.

[192] Frederic Cardinaux, Thomas Gibaud, Anna Stradner, and Peter Schurtenberger. Interplay between spinodal decomposition and glass formation in proteins exhibiting short-range attractions. *Physical Review Letters*, 99(11):118301–4, 2007.

[193] Rodolphe J. M. d Arjuzon, William Frith, and John R. Melrose. Brownian dynamics simulations of aging colloidal gels. *Physical Review E*, 67(6):061404, 2003.

[194] Emanuela Del Gado and Walter Kob. Length-scale-dependent relaxation in colloidal gels. *Physical Review Letters*, 98(2):028303–4, 2007.

[195] Taco Nicolai. Structure of self-assembled globular proteins. In Eric Dickinson and Martin E. Leser, editors, *Food colloids. Self-assembly and material sciences*, pages 35–56, Cambridge, 2007. The Royal Society of Chemistry.

[196] Wilson C. K. Poon and M. D. Haw. Mesoscopic structure formation in colloidal aggregation and gelation. *Advances in Colloid and Interface Science*, 73:71–126, 1997.

[197] Veronique Trappe and Peter Sandkuhler. Colloidal gels - low-density disordered solid-like state. *Current Opinion in Colloid and Interface Science*, 8:494–500, 2004.

[198] B. I. Halperin, Shechao Feng, and P. N. Sen. Differences between lattice and continuum percolation transport exponents. *Physical Review Letters*, 54(22):2391–2394, 1985.

[199] V. Prasad, D. Semwogerere, and Eric R. Weeks. Confocal microscopy of colloids. *Journal of Physics: Condensed Matter*, 19:113102–1–25, 2007.

[200] William S. Price. Protein association studied by nmr diffusometry. *Current Opinion in Colloid and Interface Science*, 11:19–23, 2006.

[201] Norman F. Carnahan and Kenneth E. Starling. Equation of state for noninteracting rigid spheres. *Journal of Chemical Physics*, 51(2):635–636, 1969.

[202] Jan. Tobochnik, David. Laing, and Gary. Wilson. Random-walk calculation of conductivity in continuum percolation. *Physical Review A*, 41(6):3052–3058, 1990.

Abstract

This thesis deals with the study of the structure and the dynamics of attractive spheres. For this purpose a new simulation technique called the Brownian cluster dynamics (BCD) was introduced. With BCD we can relax the system by cooperative cluster relaxation and can also study the effect of bond rigidity. The method was compared with Event Driven Brownian Dynamics simulations which gave the same static and dynamic properties. Using zero interaction range we were able to suppress phase separation and thereby to study the slow dynamics of strongly attracting spheres. The results disproves the existence of so-called attractive glasses at low volume fractions proposed in the literature. By introducing rigid bonds we suppressed crystallization for short range interaction which allowed us to study the kinetics of phase separation and more specifically the inter play between phase separation and gelation. As we distribute bonds between nearest neighbors we were able to trace out two kinds of percolation lines as a function of volume fraction and interaction strength: the bond percolation and the contact percolation. We also studied the effect of flexibility of bonds on irreversible aggregation. The structures created by flexibly bonded diffusion limited cluster aggregation were locally quite dense but they were fractal at large length scales. Tracer diffusion was studied in gels formed by irreversible aggregation of hard spheres. It was found that the diffusion coefficient is determined by the accessible volume, i.e. the volume available to the centre of mass of the tracer. We put forward a phenomenological equation connecting the diffusion coefficient and the accessible volume valid for different gel structures and tracer sizes.

Résumé

Ce travail de thèse porte sur l'étude des propriétés statiques et dynamiques de solutions de sphères dures attractives à courte portée. Pour ce faire, nous avons développé au laboratoire un algorithme original appelé Browian Cluster Dynamics (BCD). Avec cet algorithme, une assemblée de sphères dures attractives et browniennes peut être relaxée depuis une température infinie jusqu'à son état d'équilibre à une température donnée en suivant une trajectoire réaliste dans l'espace des phases. Cette technique est basée sur le mouvement coopératif diffusionnel des amas transitoires formés au cours de la réaction d'agrégation. Cela nous permet d'accéder au propriétés statiques, cinétiques et dynamiques du système, à tout instant, même loin de l'équilibre thermodynamique. De plus, la technique BCD permet de prendre en compte la rigidité des liens formés entre les sphères. En limitant la portée de l'interaction à une adhésion de contact, on a pu empêcher la séparation de phase et étudier ainsi les phénomènes de percolation et de transition vitreuse en diminuant la température. Ainsi nous avons pu montrer que les verres attractifs n'existent qu'à température nulle. En rendant les liens formés rigides, nous avons pu nous affranchir des phénomènes de cristallisation naturellement présents dans ce type de système et étudier la cinétique de séparation de phase de type liquide-liquide ainsi que les phénomènes de percolation dans la solution. L'introduction de la flexibilité des liens nous a permis d'étudier son influence sur le diagramme de phase (cristallisation) mais aussi sur les phénomnes d'agrégation irréversible. Cela nous a permis de comprendre la structure locale des amas formés au cours de certains processus d'agrégation irréversible au cours desquels les amas se restructurent par glissement des particules les constituant. Enfin, nous nous sommes intéressés aux propriétés de transport de matière dans les gels formés par agrégation irréversible. Pour cela nous avons étudié le mouvement brownien d'un traceur de taille variable dans des gels fabriqués à différentes concentrations et conditions d'agrégation. Nous avons pu établir une loi phénoménologique reliant le coefficient de diffusion du traceur au volume accessible à son centre de masse. La loi d'échelle gouvernant la transition entre diffusion et localisation du traceur est bien expliquée par la théorie de la percolation.